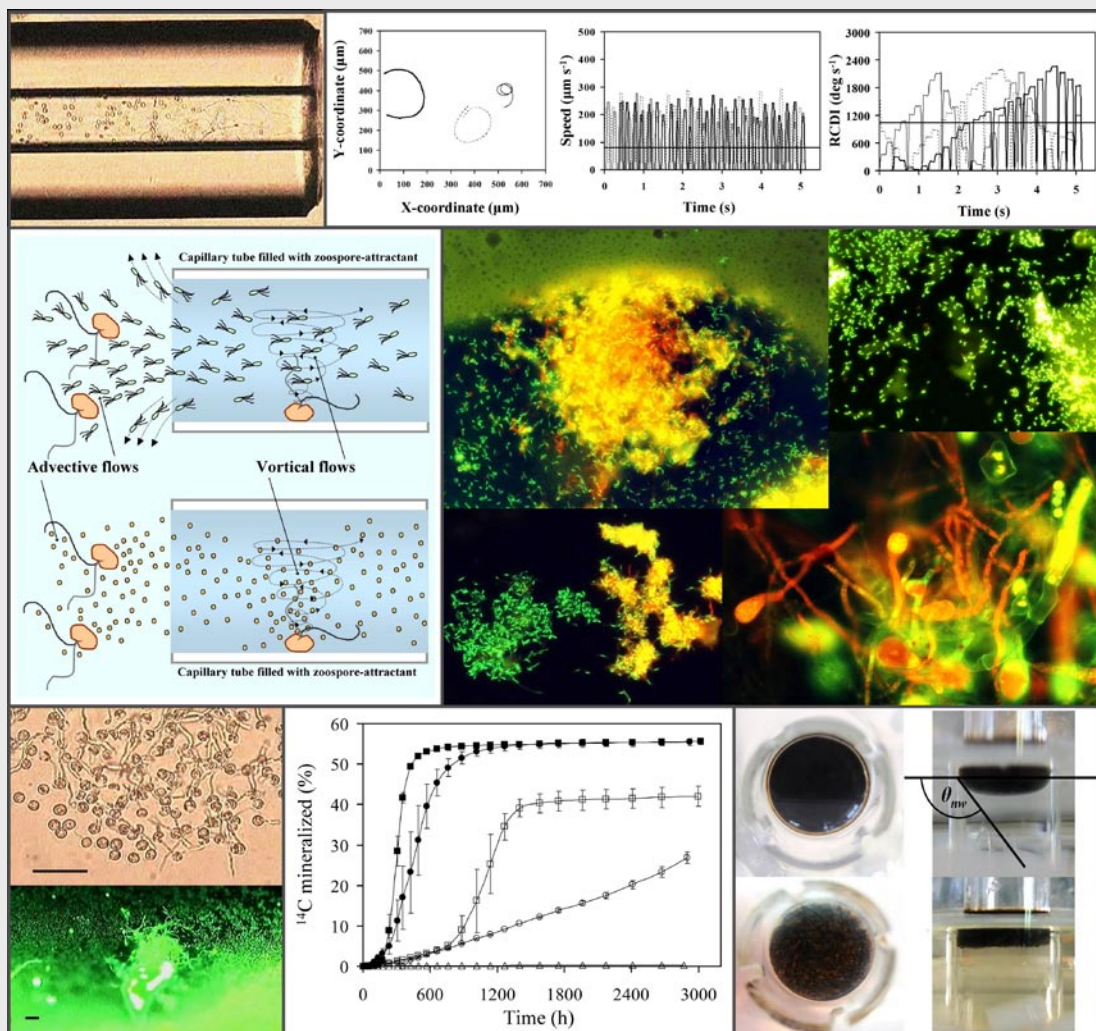


IMPACTS OF OOMYCETE MYCELIA AND ZOOSPORES IN BIOREMEDIATION OF POLYCYCLIC AROMATIC HYDROCARBONS



Rungroch Sungthong

SEVILLE, 2014



IMPACTS OF OOMYCETE MYCELIA AND ZOOSPORES IN BIOREMEDIATION OF POLYCYCLIC AROMATIC HYDROCARBONS

Memoria que presenta

Rungroch Sungthong

para optar al título de **Doctor por la Universidad de Sevilla**

Sevilla, Junio de 2014

(a)	(b)	
(c)		(d)
(e)	(f)	(g)

Cover photos:

(a) Chemotactic response of eukaryotic zoospores towards sunflower root exudates containing naphthalene in the presence *Pseudomonas putida* G7.

(b) Circular swimming pattern of eukaryotic zoospores analyzed with CellTrak motion analysis Program. The results are reported with trajectory (left), speed (middle) and rate of change of direction (RCDI) (right).

(c) Possible mechanisms (advective and vortical flows) by which zoospore chemotaxis enhance bacterial mobilization.

(d) Microbial life at nonaqueous phase liquid (NAPL)-water interface.

(e) Zoospore settlement on hexadecane (HD)-water interface, observed in the absence of bacteria (upper) and in the presence of *Mycobacterium gilvum* VM552 (down).

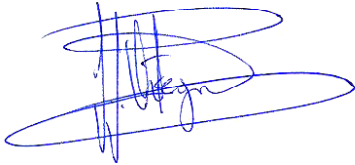
(f) Mineralization of [¹⁴C] labelled phenanthrene associated with NAPL in the presence of *Pythium oligandrum* mycelia under aeration condition (see section 4.3 for more information)

(g) Surface topography of NAPL in contact with the aqueous phase, determined with NAPL-water contact angle (θ_{nw}) (on the right) and the surface change caused by biofilm formation (on the left) (see section 4.3 for more information).

IMPACTS OF OOMYCETE MYCELIA AND ZOOSPORES IN BIOREMEDIATION OF POLYCYCLIC AROMATIC HYDROCARBONS

Visado en Sevilla, a 20 de Junio de 2014

EL DIRECTOR



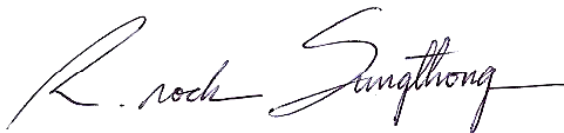
.....
Dr. D. José Julio Ortega-Calvo
Investigador Científico de OPI del
Instituto de Recursos Naturales y
Agrobiología de Sevilla (IRNAS-CSIC)

EL TUTOR



.....
Dr. D. Manuel Tejada Moral
Profesor Titular de
la Universidad de Sevilla

Memoria que presenta



.....
D. Rungroch Sungthong
para optar al título de Doctor por la Universidad de Sevilla
Sevilla, Junio de 2014

Dr. D. José Manuel Pardo DIRECTOR DEL INSTITUTO DE RECURSOS NATURALES Y AGROBIOLOGÍA DE SEVILLA DEL CONSEJO SUPERIOR DE INVESTIGACIONES CIENTÍFICAS

Certifica: Que la presente Memoria de Investigación titulada **“Impacts of oomycete mycelia and zoospores in bioremediation of polycyclic aromatic hydrocarbons”**, presentada por **D. Rungroch Sungthong** para optar al grado de **Doctor por la Universidad de Sevilla**, ha sido realizada en el Departamento de Agroquímica y Conservación de Suelos, bajo la dirección del **Dr. D. José Julio Ortega-Calvo**, reuniendo todas las condiciones exigidas a los trabajos de Tesis Doctorales.

En Sevilla, a 20 de Junio de 2014



.....
Fdo: Dr. D. José Manuel Pardo

El presente trabajo se ha realizado en el marco del proyecto CGL2010-22068-C02-01 del Plan Nacional de I+D (CYCIT) y dentro del Programa JAE-CSIC (PreDoc).

Acknowledgements

The success of this dissertation would have not been occurred without the support of persons and institutions to whom I would like to express my sincere and profound gratitude:

Dr. Jose Julio Ortega-Calvo, Chair of Department of Agrochemistry and Soil Conservation, Institute for Natural Resources and Agrobiology of Seville (IRNAS-CSIC), my thesis director. I thank for his excellent and kindness advices throughout my Ph.D. study, the grateful thanks are also given to all of his wonderful assistances, supports and hospitality.

Prof. Dr. Pieter van West, Aberdeen Oomycete Laboratory, University of Aberdeen, UK, I thank for his kindness to provide the zoospore producer and for his professional guidance on zoospore development throughout my Ph.D. study.

Prof. Dr. Dan Funck Jensen, Uppsala BioCenter, Department of Forest Mycology and Plant Pathology, Swedish University of Agricultural Sciences, Sweden, I thank for his kindness to accept me as a guest researcher for short-term training in zoospore production and chemotaxis, and for his valuable guidance on these topics.

Dr. Manuel Cantos, IRNAS-CSIC, I thank for his kindness to provide the potent root exudates and his kind support for some lab facilities.

Absolutely thanks to my wonderful colleagues at IRNAS-CSIC; Dr. Celia Jimenez-Sanchez, Dr. Eleonora Congiu, Dr. Maria del Carmen Tejada-Agredano, Alfonso Pérez Martín, Celia Rodríguez Domínguez, Dr. Virginia Hernández Santana and also some friends at IRNAS-CSIC who are not named here. Thank you for your kind assistance and hospitality with international mind. You made my 4 years in Seville full of comfort and happiness. Every moment we spent together is truly impressive and cannot be forgotten.

The thanks are also given to the Spanish National Research Council (CSIC) and the European Social Fund (ESF), for funding support of my Ph.D. study, and their beneficial intention to expand international collaboration by providing extra-supports for short-term research development aboard are also acknowledged.

I would like to express my gratitude also to the scientific evaluators who kindly review and evaluate this dissertation with all useful comments.

Lastly, I thank my family for their love and endless supports.

“Life is learning”

*“Thinking good, saying good, and doing good are highest glory and blessing,
neither god nor human blessing can be compared as good as you do”*

Nyanasamvara Suvaddhana

Contents

List of author's contributions	1
Abbreviations	2
Abstract	3
Resumen (Abstract in Spanish)	6
CHAPTER I: INTRODUCTION	9
1.1 Polycyclic aromatic hydrocarbons (PAHs)	9
1.1.1 <i>Routes of pollution by PAHs</i>	11
1.1.2 <i>Ecotoxicological effects of PAHs</i>	11
1.1.3 <i>Properties and environmental fate of PAHs</i>	13
1.2 Bioremediation of PAHs and its limitations	14
1.2.1 <i>Biodegradation of PAHs</i>	14
1.2.2 <i>Bioavailability of PAHs</i>	19
1.2.3 <i>Microbial accessibility towards PAHs</i>	22
1.3 Exploiting microbial influences on bioremediation of PAHs	23
1.3.1 <i>Production of surface-active compounds</i>	23
1.3.2 <i>Enhancing microbial mobilization</i>	24
1.3.3 <i>Promoting microbial life at pollutant interfaces</i>	26
1.4 What are oomycetes?	27
1.4.1 <i>Taxonomic position of oomycetes</i>	27
1.4.2 <i>Life cycle of oomycetes</i>	28
1.4.3 <i>Ecology of oomycetes</i>	29
1.5 Oomycetes in bioremediation of PAHs	30
1.5.1 <i>Mycelial networks</i>	30
1.5.2 <i>Eukaryotic zoospores?</i>	31
CHAPTER II: OBJECTIVES	34
CHAPTER III: MATERIALS AND METHODS	36
3.1 List of chemicals and solutions	36
3.1.1 <i>Chemicals</i>	36

3.1.2	<i>Organic carbon-containing solutions from natural sources</i>	36
3.1.3	<i>In vitro production of root exudates</i>	36
3.2	Microorganisms	39
3.2.1	<i>Microbial stocks and growing conditions</i>	39
3.2.2	<i>Preparation of oomycete biomass</i>	39
3.2.3	<i>Production of oomycete zoospores</i>	40
3.2.4	<i>Preparation of bacterial biomass</i>	40
3.3	Antagonism tests of oomycetes and PAH-degrading bacteria	41
3.3.1	<i>Dual culture test on solid agar</i>	41
3.3.2	<i>Dual culture test in aqueous solution</i>	42
3.4	Design of PAH-polluted scenarios	42
3.4.1	<i>Preparation of PAH-containing solutions</i>	42
3.4.2	<i>Estimation of exposure concentrations of PAHs</i>	42
3.5	Observation of zoospore development in PAH-polluted scenarios	45
3.5.1	<i>Evaluation of zoospore formation</i>	45
3.5.2	<i>Observation of zoospore chemotaxis</i>	45
3.5.3	<i>Observation of zoospore settlement</i>	46
3.6	Mineralization of PAHs under bioavailability restriction	47
3.6.1	<i>Preparation of NAPL</i>	47
3.6.2	<i>Preparation of microbial biomass</i>	47
3.6.3	<i>Set-up for radiorespiratory assays</i>	48
3.7	Metabolic evaluation of PAHs in mineralization experiments	49
3.7.1	<i>Calculation of mineralization rate</i>	49
3.7.2	<i>Measurement of end-point mass balance of [¹⁴C]</i>	49
3.7.3	<i>Analysis of residual NAPL</i>	49
3.8	Characterization of microbial colonization at NAPL-water interface	50
3.8.1	<i>Observation of NAPL-surface topography</i>	50
3.8.2	<i>Observation of biofilm formation</i>	50
3.9	Analysis of abiotic influences in mineralization experiment	51
3.9.1	<i>Measurement of dissolved oxygen (DO)</i>	51
3.9.2	<i>Measurement of TOC</i>	52
3.10	Determinations of motility and cell size of PAH-degrading bacteria	52
3.10.1	<i>Determination of bacterial motility</i>	52

3.10.2	<i>Cell size determination</i>	53
3.11	Evaluation of bacterial mobilization by zoospores	53
3.11.1	<i>Evaluation of zoospore chemotaxis</i>	53
3.11.2	<i>Biomobilization assay</i>	54
3.11.3	<i>Determination of biomass flow</i>	55
3.12	Observation of zoospore swimming behaviour	56
3.12.1	<i>Observation of intrinsic swimming behaviour</i>	56
3.12.2	<i>Evaluation of interactive motility between zoospores and bacteria</i>	57
3.13	Analysis of cellular interaction between zoospores and bacteria	57
3.13.1	<i>Evaluation of bacterial adhesion on surface of zoospores</i>	57
3.13.2	<i>Observation of bacterial chemotaxis towards encysted zoospores</i>	57
3.14	Statistical analysis	58
CHAPTER IV: RESULTS		59
4.1	Ecological interaction between eukaryotic zoospores and PAH-degrading bacteria in PAH-polluted scenarios	59
4.1.1	<i>Optimal condition for zoospore formation</i>	59
4.1.2	<i>Antagonistic effects among oomycetes and PAH-degrading bacteria</i>	60
4.1.3	<i>Zoospore formation</i>	61
4.1.4	<i>Zoospore chemotaxis</i>	63
4.1.5	<i>Zoospore settlement</i>	65
4.2	Promoting microbial life at the interface of NAPL and water: a strategy to enhance biodegradation of sparingly bioavailable PAHs	68
4.2.1	<i>Mineralization of NAPL-associated phenanthrene</i>	69
4.2.2	<i>Kinetics and end-point mass balance of mineralization of phenanthrene</i>	72
4.2.3	<i>Evolution of NAPL-water contact angle</i>	79
4.2.4	<i>Biofilm formation at NAPL-water interface</i>	79
4.2.5	<i>Influences of DO and DOC variations on mineralization kinetics</i>	83
4.3	Biomobilization of pollutant-degrading bacteria by chemotaxis of eukaryotic zoospores	86
4.3.1	<i>Chemotaxis of zoospores and bacterial mobilization</i>	86
4.3.2	<i>Possible mechanisms of bacterial mobilization by zoospore chemotaxis</i>	90
4.3.3	<i>Swimming behaviour and interactive motility of zoospores and bacteria</i>	93

CHAPTER V: DISCUSSION	100
5.1 Ecological interaction between eukaryotic zoospores and PAH-degrading bacteria	100
5.2 Roles of oomycetes/bacteria interaction in biodegradation of PAHs	103
5.3 Biomobilization of pollutant-degrading bacteria by chemotaxis of eukaryotic zoospores	106
CHAPTER VI: CONCLUSIONS	110
CHAPTER VII: CONCLUSIONES (Conclusions in Spanish)	112
CHAPTER VIII: REFERENCES	114

List of author's contributions

- I Ortega-Calvo JJ, Tejeda-Agredano MC, Jimenez-Sanchez C, Congiu E, **Sunghong R**, Niqui-Arroyo JL, Cantos M (2013) Is it possible to increase bioavailability but not risk for improved bioremediation of PAHs? **J Hazard Mater** 261:733-745
- II Krell T, Lacal J, Reyes-Darías JA, Jimenez-Sanchez C, **Sunghong R**, Ortega-Calvo JJ (2013) Bioavailability of pollutants and chemotaxis. **Curr Opin Biotechnol** 24:451-456
- III **Sunghong R**, van West P, Cantos M, Ortega-Calvo JJ (2014) Ecological interaction between eukaryotic zoospores and polycyclic aromatic hydrocarbon (PAH)-degrading bacteria in PAH-polluted scenarios. (Submitted to **Microbial Ecology**)
- IV **Sunghong R**, Tauler M, Grifoll M, Ortega-Calvo JJ (2014) Promoting microbial life at the interface of nonaqueous phase liquid (NAPL) and water: a strategy to enhance biodegradation of sparingly bioavailable polycyclic aromatic hydrocarbons (PAHs). (In preparation for **Environmental Science and Technology**)
- V **Sunghong R**, van West P, Heyman F, Jensen DF, Ortega-Calvo JJ (2014) Biomobilization of pollutant-degrading bacteria by chemotaxis of eukaryotic zoospores. (Submitted to **Environmental Microbiology**)

Abbreviations

ANOVA	One-way analysis of variance
C_{exp}	Exposure concentration of organic pollutant
CFU	Colony forming unit
Ci	Curie (1 Ci = 3.7×10^{10} decays per second)
DO	Dissolved oxygen
DOC	Dissolved organic carbon
dpm	Disintegrations per minute
DV8	Diluted V8 vegetable juice
F	Fisher-Snedecor distribution (or F -distribution)
f_w	Fraction of organic pollutant freely dissolved in aqueous solution
HCl	Hydrochloric acid
HD	<i>n</i> -Hexadecane
HMN	2,2,4,4,6,8,8-Heptamethylnonane
K_{oc}	Organic carbon-normalized sorption coefficient
K_{ow}	Octanol-water partitioning coefficient
NaOH	Sodium hydroxide
NAPL(s)	Non-aqueous phase liquid(s)
$\text{OD}_{600 \text{ nm}}$	Optical density at 600 nm of wavelength
PAH(s)	Polycyclic aromatic hydrocarbon(s)
R^2	Coefficient of determination
RCDI	Rate of change of direction
rpm	Round per minute
SD	Standard deviation
SE	Standard error
S_w	Aqueous solubility
TOC	Total organic carbon
TSA	Tryptic soy agar
US-EPA	The United States Environmental Protection Agency

Abstract

With the aim to evaluate possible roles of oomycetes in bioremediation of polycyclic aromatic hydrocarbons (PAHs), we explored in this thesis the functional interactions between these microorganisms and PAH-degrading bacteria. The interactions were studied at two different modes of oomycete development: mycelia and zoospores. The first part of this thesis focused on the ecological interaction between an oomycete *Pythium aphanidermatum* and two representative PAH-degrading bacteria (*Mycobacterium gilvum* VM552 and *Pseudomonas putida* G7). We chose a set of chemicals to imitate PAH-polluted scenarios, which included aqueous solutions with dissolved organic carbon (DOC) of diverse origins (plant root exudates and humic acid) and organic solvents. The oomycete mycelia and both bacteria were not antagonist during growth on solid media. The bacteria diminished zoospore formation only at the highest bacterial cell density (10^8 - 10^{10} cells mL⁻¹), while *M. gilvum* VM552 exhibited the greatest antagonism. A negative influence of PAHs on zoospore formation and chemotaxis was observed when the chemicals were exposed from DOC solutions and polar solvents, but this influence was diminished by PAH-degrading bacteria. When PAHs were exposed from substrata made by non-polar solvents, hexadecane (HD) and heptamethylnonane (HMN), that formed a nonaqueous phase liquid (NAPL) separated from the water phase, they did not prevent zoospore settlement on these substrata. The zoospore settlement occurred at HD-water interface but not at HMN-water interface, and it was not influenced by PAH-degrading bacteria. We also observed that zoospores encysted at the HD-water interface and created a mycelial network expanding the interfacial area between the NAPL and the water phase. Such network initiated biofilm formation by microbial consortia composed by the oomycete and PAH-degrading bacteria. On the basis of these results, we suggest that both mycelia and zoospores of the oomycete were able to develop in PAH-polluted scenarios, and were influenced both by pollutant bioavailability and by interactions with PAH-degrading bacteria.

For further investigation of oomycete/bacteria interactions in bioremediation of PAH, we explored in the second part of this thesis the influence of two oomycetes (*Py. aphanidermatum* and *Pythium oligandrum*) on biodegradation of PAHs by *M. gilvum* VM552. The experiments were designed to create bioavailability restrictions through the association of PAHs with a NAPL, which was composed by a mixture of heavy fuel and

HMN. Two experimental sets were used, one under aerated conditions (by shaking reciprocally at 80 rpm), and the other under static conditions. Mineralization activity of *M. gilvum* VM552 was estimated continuously through $^{14}\text{CO}_2$ production from ^{14}C -labelled phenanthrene dissolved in the NAPL. End-point concentrations of PAHs and alkanes present in the NAPL were determined by GC/MS. It was found that, under aerated conditions, both oomycetes enhanced bacterial mineralization of phenanthrene with the rates of 5.86-8.27 $\text{ng mL}^{-1} \text{h}^{-1}$. A similar trend of results was also observed under static conditions, although the lag phases of mineralization extended longer than aerated conditions. The high rate of mineralization corresponded with the formation of dense microbial biofilms that formed at the interface between NAPL and water. In the absence of oomycetes, mineralization rates of phenanthrene were slow. An excess of DOC in the aqueous phase, provided either by adding diluted V8 (DV8) agar medium or oomycete growing on this medium, also enhanced biodegradation of PAHs, which suggests that oomycete growth provided nutrients passively dissolved from the solid medium to the aqueous phase for supplying the metabolic activity of the bacterium. We also propose that differences in biomass content and zoospores formation by different oomycetes might also be a key factor influencing either biofilm formation or biodegradation of PAHs at the NAPL-water interface. Interestingly, static conditions enhanced the mineralization activity of *M. gilvum* VM552 in the absence of any supplements, suggesting that the physical interference caused by aeration did not only stabilize the biodegrading capacity of the bacterium, but also affected the bacterial growth and biofilm formation at the NAPL-water interface.

To discriminate the effects caused by oomycete zoospores from those directly caused by the mycelia, the third part of this thesis examined the possible role of the swimming behaviour of zoospores in the mobilization of PAH-degrading bacteria. During the coexistence of zoospores and bacteria in the presence of a zoospore attractant (5% (v/v) ethanol), we observed the bacterial mobilization by the chemotactic behaviour of zoospores. It was found that *M. gilvum* VM552 cells (non-flagellated) and slightly motile cells of *P. putida* G7 (collected at stationary phase of growth) were mobilized by zoospores at the rates of 22-24 $\text{cells } \mu\text{L}^{-1} \text{s}^{-1}$. These rates resulted in enhanced biomass flow velocities of 25.85-68.38 $\mu\text{m s}^{-1}$ that were higher than the spontaneous flow velocity (19.51 $\mu\text{m s}^{-1}$). The mobilization was caused by the change of hydraulic activity (advection and vortical flows) driven by the chemotactic behaviour of zoospores. In addition, we observed an influence of the interactive motility among zoospores and bacteria, together with specific effects of bacterial physiology

and motility, on mobilization of bacterial cells. In the absence of zoospore attractant, zoospores showed four typical patterns of swimming (linear, circular, sine wave and freestyle). Zoospore encystment was often preceded by the circular mode of movement. In the presence of *M. gilvum* VM552 cells, the rate of change of direction (RCDI) in zoospore trajectories decreased significantly and the circular movement was increased. The swimming speed and RCDI of zoospores were diminished significantly by highly motile cells of *P. putida* G7 (collected at exponential phase of growth). Zoospores did increase the swimming speed of slightly motile cells of *P. putida* G7 and increase the RCDI of its highly motile cells. In addition, we observed no adhesion between zoospores and bacteria and no bacterial chemotaxis towards encysted zoospores. We conclude that chemotaxis of zoospores did enhance the bacterial mobilization through the modified hydraulic activity of aqueous microenvironments and their interactive motility with bacterial cells. This finding may further expand the accessibility towards pollutants of bacterial degraders in bioremediation.

We conclude that oomycetes provide new insights in biotechnological strategies for improvement of bioremediation. The oomycetes showed a strong subsistence in PAH-polluted scenarios, and their zoospores and mycelia could enhance bioavailability of PAHs through different mechanisms. The mechanisms of this enhancement were driven by the ecological lifestyle of oomycetes. Zoospores played as bio-vectors to facilitate microbial mobilization, which consequently provided the effective expansion of mycelial network to promote biofilm formation and on-site biodegradation at the interface between the pollutant and the aqueous environment.

Resumen (Abstract in Spanish)

Con el objetivo de evaluar el papel de los oomicetos en la biorremediación de hidrocarburos aromáticos policíclicos (HAPs), exploramos en esta tesis las interacciones funcionales entre estos microorganismos y las bacterias degradadoras de HAPs. Estas interacciones se estudiaron en dos diferentes modos del desarrollo de los oomicetos: micelios y zoosporas. La primera parte de esta tesis se centró en la interacción ecológica entre el oomiceto *Pythium aphanidermatum* y dos bacterias representativas degradadoras de HAPs (*Mycobacterium gilvum* VM552 y *Pseudomonas putida* G7). Elegimos una serie de compuestos químicos para imitar escenarios de contaminación por HAPs, que incluían disoluciones acuosas con carbono orgánico de origen diverso (exudados radicales de plantas y ácidos húmicos) y disolventes orgánicos. El micelio del oomiceto y ambas bacterias no actuaron de forma antagonista durante el crecimiento en medio sólido. Sólo a la densidad más alta de células bacterianas (10^8 - 10^{10} células mL⁻¹) ambas bacterias disminuyeron la formación de zoosporas. *M. gilvum* VM552 mostró el mayor antagonismo. Se observó una influencia negativa de los HAPs sobre la formación y la quimiotaxis de zoosporas cuando se expuso los productos químicos desde soluciones de carbono orgánico disuelto (COD) y disolventes polares, pero esta influencia fué disminuida por las bacterias. Cuando los PAHs fueron expuestos a partir de disolventes no polares, que formaban una fase diferenciada con el agua (o líquido en fase no acuosa – NAPL), no impidieron el asentamiento de las zoosporas sobre estos sustratos. El asentamiento se produjo en la interfase con hexadecano (HD) como NAPL, pero no con heptametilnonano, y no fue influido por las bacterias degradadoras de HAPs. También se observó que las zoosporas se enquistaron sobre la interfase agua-HD, creando una red de micelio que colonizaba la interfase, expandiendo el área interfásica entre el NAPL y la fase acuosa. Dicha red inició la formación de un biofilm por los consorcios microbianos compuestos por el oomiceto y las bacterias degradadoras de HAPs. En base a estos resultados, sugerimos que los micelios y las zoosporas del oomiceto fueron capaces de desarrollarse en escenarios de contaminación por HAPs, y que fueron influidos por la biodisponibilidad de los contaminantes y por las interacciones con las bacterias degradadoras de HAPs.

Para continuar nuestra investigación sobre las interacciones oomiceto/bacterias en el contexto de la biorremediación de HAPs, exploramos, en la segunda parte de esta tesis, la

influencia de micelios de dos oomicetos (*Py. aphanidermatum* y *Pythium oligandrum*) sobre la biodegradación de HAPs por *M. gilvum* VM552. Los experimentos se diseñaron para crear restricciones de biodisponibilidad a través de la asociación de los HAPs con un NAPL, que estaba constituido por una mezcla de fuel pesado y HMN. Se utilizaron dos sistemas experimentales, uno bajo condiciones de aireación (mediante agitación orbital continua a 80 rpm), y el otro bajo condiciones estáticas. La biodegradación se estimó de forma continua a través de la producción de $^{14}\text{CO}_2$ a partir de fenantreno marcado con ^{14}C , y mediante la determinación de las concentraciones finales de HAPs y alcanos presentes en el NAPL con CG/EM. Observamos que, en condiciones de agitación, ambos oomicetos aumentaron la tasa de mineralización de fenantreno ($5.86\text{-}8.27 \text{ ng mL}^{-1} \text{ h}^{-1}$) por la bacteria. Se observó una tendencia similar en la mineralización bajo condiciones estáticas, aunque las fases de aclimatación fueron más largas que bajo agitación continua. Las tasa alta de mineralización se correspondió con la formación de densos biofilms microbianos sobre la interfase agua/NAPL. En ausencia de oomicetos, la mineralización de fenantreno fue lenta y lineal. El exceso de COD en la fase acuosa, producido mediante la adición de agar DV8 o de biomasa de oomiceto cultivado con agar DV8, también estimuló la biodegradación de HAPs, lo que sugiere que el crecimiento del oomiceto proporcionó nutrientes que se disolvieron pasivamente desde el medio sólido hacia la fase acuosa, lo cual estimuló la actividad metabólica de la bacteria. También proponemos que las diferencias en el contenido en biomasa y en la formación de zoosporas producidas por los diferentes oomicetos pueden también ser un mecanismo clave en la formación de biofilm o en la biodegradación de HAPs en la interfase NAPL/agua. Interesantemente, las condiciones estáticas aumentaron la tasa de mineralización de fenantreno en ausencia de suplementos, lo que indicó que la interferencia física causada por la aireación no sólo estabilizó la capacidad de biodegradación por la bacteria, sino que también afectó el crecimiento bacteriano y la formación de biofilm en la interfase NAPL/agua.

Para discriminar los efectos causados por las zoosporas de los causados directamente por los micelios, la tercera parte de esta tesis examinó el posible papel del comportamiento de natación de las zoosporas en la movilización de bacterias degradadoras de HAPs. Durante la coexistencia de zoosporas y bacterias en presencia de un atrayente de zoosporas (5 % (v/v) de etanol) se observó la movilización bacteriana por el comportamiento quimiotáctico de las zoosporas. Observamos que las células (no flageladas) de *M. gilvum* VM552 y células en fase estacionaria de *P. putida* G7, que exhibían un bajo nivel de movilidad, fueron

movilizadas por las zoosporas a tasas de 22 a 24 células $\mu\text{L}^{-1} \text{s}^{-1}$. Estas tasas resultaron en unas velocidades de flujo de biomasa de 25,85 a 68,38 $\mu\text{m s}^{-1}$, que fueron superiores a la velocidad de flujo espontáneo (19,51 $\mu\text{m s}^{-1}$). En ausencia del atrayente, las zoosporas mostraron cuatro patrones típicos de natación (lineal, circular, de onda sinusoidal y estilo libre). El enquistamiento de las zoosporas fue a menudo precedido por el modo de movimiento circular. En presencia de células de *M. gilvum* VM552, la tasa de cambio de dirección (RCDI) en las trayectorias de las zoosporas descendió de forma significativa, y se aumentó el movimiento circular. Las células de *P. putida* G7 en fase exponencial (altamente móviles) y en fase estacionaria no causaron ningún cambio en el comportamiento de natación de las zoosporas, aunque éstas sí causaron un aumento de RCDI en el patrón de natación de la bacteria. Además, no se observó la adhesión entre zoosporas y bacterias ni la quimiotaxis bacteriana hacia zoosporas enquistadas. Proponemos dos posibles mecanismos clave para la biomovilización, incluyendo la advección directa causada por la quimiotaxis de las zoosporas y los flujos de torbellino a través del movimiento circular de zoosporas. El tamaño y la motilidad bacteriana afectaron estos mecanismos, ya que las células en fase estacionaria (más pequeñas y menos móviles que las células en fase exponencial) se movilizaron de manera más eficaz. Con estos resultados, se concluye que el comportamiento quimiotáctico de las zoosporas puede mejorar la movilización de bacterias mediante la modificación de la actividad hidráulica del microambiente acuoso.

Concluimos que los oomicetos proporcionan nuevas perspectivas en las estrategias biotecnológicas para la mejora de la biorremediación. Los oomicetos mostraron una fuerte subsistencia en situaciones de contaminación por HAPs, y sus zoosporas y micelios pueden aumentar, a través de mecanismos diferentes, la biodisponibilidad de los HAP. Los mecanismos de esta mejora fueron posibles por el estilo de vida ecológico de los oomicetos. Las zoosporas actuaron como bio-vectores para facilitar la movilización microbiana, lo cual puede proporcionar una expansión de red micelial y así promover la formación de biopelículas y la biodegradación en interfases de microambientes contaminados por HAPs.

CHAPTER I: INTRODUCTION

1.1 Polycyclic aromatic hydrocarbons (PAHs)

Polycyclic aromatic hydrocarbons (PAHs), known also as polynuclear aromatic hydrocarbons are organic chemicals constituted of at least 2 benzene rings (**Table 1**). These rings may be fused in linear, angular or clustered arrangements. Carbon and hydrogen elements present in PAHs, whichever may be substituted by alkyl groups or other elements such as sulphur, oxygen or nitrogen to form heterocyclic aromatic compounds (**Fig. 1**).

Table 1 Some environmental properties of the 16 US-EPA PAHs ordered according to the water solubility

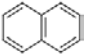
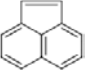
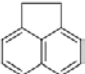
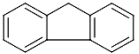
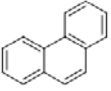
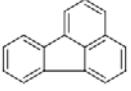
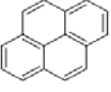
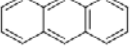
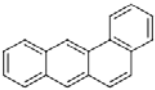
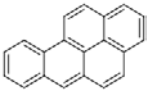
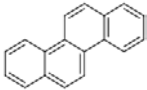
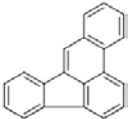
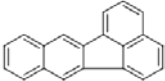
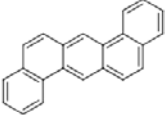
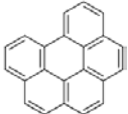
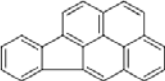
PAHs	Structure	Molecular weight ^a	S_w (mg L ⁻¹) ^a	$\log K_{ow}$ ^a	$\log K_{oc}$ ^b
Naphthalene		128.17	31	3.37	2.98
Acenaphthylene		150.19	16	4.00	3.60
Acenaphthene		154.21	3.8	3.92	3.52
Fluorene		166.22	1.9	4.18	3.78
Phenanthrene		178.23	1.1	4.57	4.16
Fluoranthene		202.25	0.26	5.22	4.80
Pyrene		202.25	0.13	5.18	4.76
Anthracene		178.23	0.045	4.54	4.13

Table 1 (Continued)

PAHs	Structures	Molecular weight ^a	S_w (mg L ⁻¹) ^a	log K_{ow} ^a	log K_{oc} ^b
Benz[<i>a</i>]anthracene		228.29	0.011	5.91	5.47
Benzo[<i>a</i>]pyrene		252.31	0.0038	6.04	5.60
Chrysene		228.29	0.0020	5.60	5.17
Benzo[<i>b</i>]fluoranthene		252.31	0.0015	5.80	5.36
Benzo[<i>k</i>]fluoranthene		252.31	0.00080	6.00	5.56
Dibenz[<i>a,h</i>]anthracene		278.35	0.00060	6.75	6.30
Benzo[<i>g,h,i</i>]perylene		276.33	0.00026	6.50	6.05
Indeno[1,2,3- <i>c,d</i>]pyrene		276.33	0.00019	6.72	6.27

^aData were taken from Mackay *et al.* (2006). ^bData were calculated with equation (i) described by Schwarzenbach *et al.* (2003). The chemical structures were drawn with MarvinSketch (<http://www.chemaxon.com/marvin/sketch/index.php>, Available on 5 Feb., 2014).

PAHs are known as ubiquitous pollutants, and their ecotoxicological effects are recognized worldwide. Polluted routes of PAHs in nature together with their toxicity, properties and environmental fate were briefly summarized in this section.

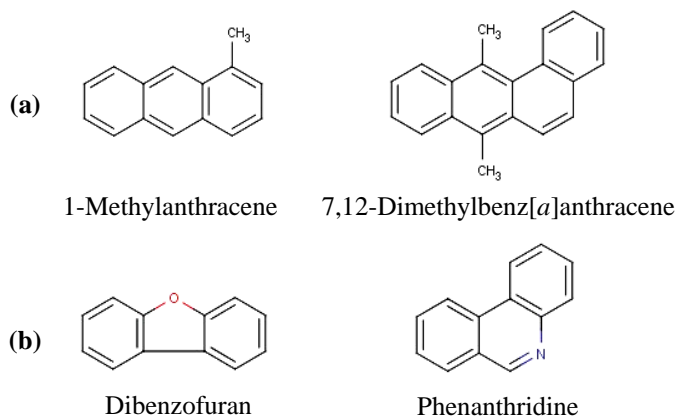


Figure 1 Some alkyl-PAHs (a) and heterocyclic aromatic compounds derived from PAHs (b). The chemical structures were drawn with MarvinSketch (<http://www.chemaxon.com/marvin/sketch/index.php>, Available on 5 Feb., 2014).

1.1.1 Routes of pollution by PAHs

PAHs exist in nature as a result of natural events and anthropogenic activities. Volcanic eruptions and forest fires are the main natural sources of PAHs. These PAHs generally occur in vast scale, which may disperse to diverse ecosystems by environmental carriers like wind and/or rain (Martínez-Lladó *et al.*, 2007; Vergnoux *et al.*, 2011). However, the main emissions of PAHs occur through anthropogenic activities, including incomplete combustion of organic materials, transport accidents, fossil fuel refineries, and productions of coal-tar, asphalt and wood preservatives. The persistence of these PAHs is often caused by binding to either organic matter in soils and sediments or nonaqueous phase liquids (NAPLs) such as light or crude oil, creosote, coal tar, and soot-like materials (Ortega-Calvo *et al.*, 2013; Tejada-Agredano *et al.*, 2011; 2014). Scenarios typically polluted by PAHs are shown in **Fig. 2**.

1.1.2 Ecotoxicological effects of PAHs

According to the United States Environmental Protection Agency (US-EPA), 16 PAHs have been proposed as priority pollutants (Keith and Telliard, 1979). They are listed in **Table 1**. Both PAHs and their derivatives exhibit ecotoxicity to diverse targets. The effects may range from the sub-cellular genomics (genotoxicity) to the physiology and behaviour of single or complex cells (cytotoxicity), or complex living communities and ecological food webs

(ecotoxicity). Each PAH species can cause toxicity at different levels, depending on its structure, properties and environmental fate.

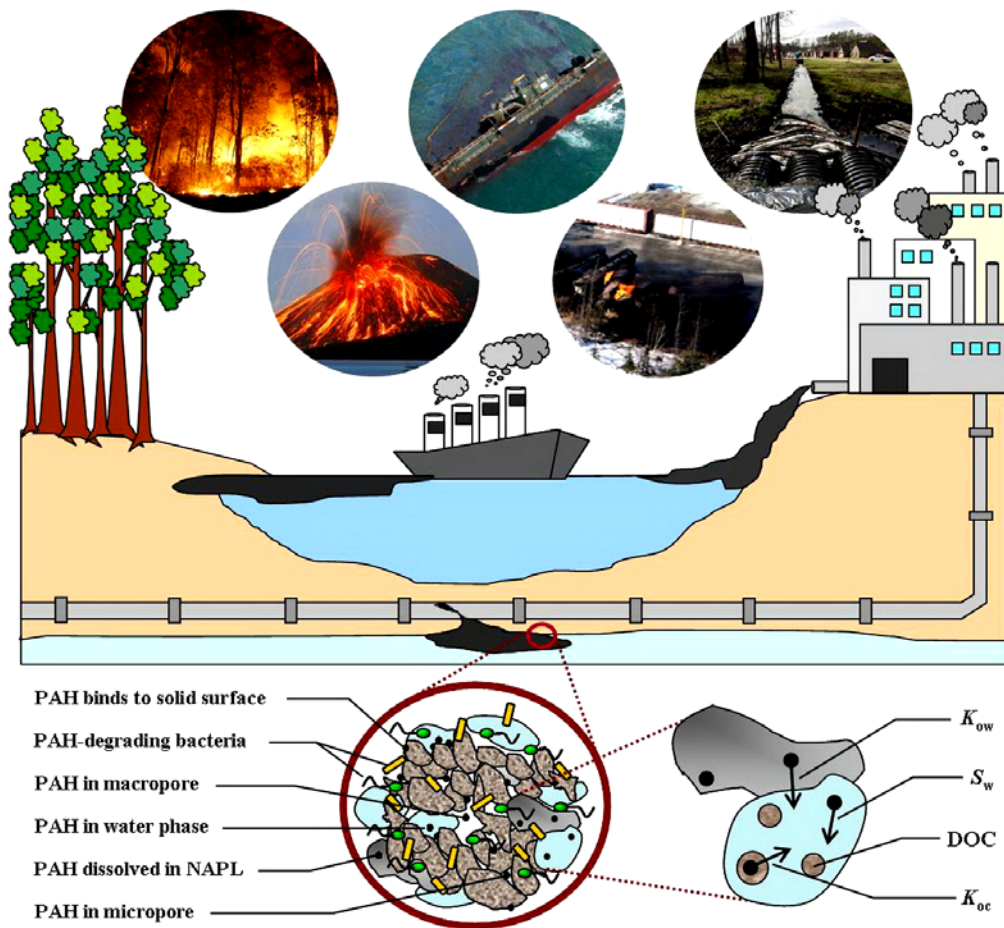


Figure 2 Macro- and micro-scale showing PAH-polluted scenarios and environmental fate of PAHs.

It was found that PAHs possessing bay or fjord regions in their molecular structures (**Fig. 3**) are the most potent carcinogens (Sundberg *et al.*, 1997). However, a number of studies evidenced that the environmental fate of PAHs is a critical factor influencing their ecotoxicity (Bellas *et al.*, 2008; Martínez-Lladó *et al.*, 2007; Su and Yang, 2009; Verrhiest *et al.*, 2001). Among these studies, bioavailability of PAHs is a factor that exerts a strong influence on their toxicity. For example, sediments polluted with PAHs are more toxic to

benthic biomarkers than the overlying water column (Bellas *et al.*, 2008; Verrhiest *et al.*, 2001).

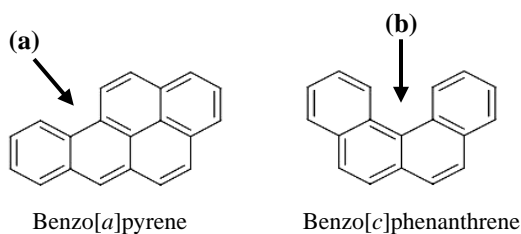


Figure 3 Molecular structures of PAHs. The arrows show bay (a) and fjord (b) regions. The chemical structures were drawn with MarvinSketch (<http://www.chemaxon.com/marvin/sketch/index.php>, Available on 5 Feb., 2014).

1.1.3 Properties and environmental fate of PAHs

PAHs are lipophilic compounds with a strong hydrophobicity. The number of benzene rings in PAHs is in accordance to their molecular weight, which reflects the hydrophobicity and can divide PAHs into 2 groups: low molecular weight (LMW)-PAHs (comprised of less than 4 benzene rings) and high molecular weight (HMW)-PAHs (comprised of at least 4 benzene rings). The molecular weight influences water solubility (S_w), volatility and hydrophobicity of PAHs, where LMW-PAHs show higher S_w and volatility but lower hydrophobicity than HMW-PAHs. The difference of hydrophobicity is also described by the octanol-water partitioning coefficient (K_{ow}) and the organic carbon-normalized sorption coefficient (K_{oc}). These two coefficients are important to describe the environmental fate of PAHs. The sorption capacity of PAHs to the organic matter shows a linear regression relationship with the partitioning capacity of PAHs. This linear regression is described by equation (i) with a coefficient of determination (R^2) = 0.98 (Schwarzenbach *et al.*, 2003). The slope on the intercept in this equation increases in accordance to the molecular weight of PAHs. Some environmental properties of the 16 US-EPA PAHs are shown in **Table 1** and described in **Fig. 2**.

$$\log K_{oc} = 0.98 \cdot \log K_{ow} - 0.32 \quad (\text{i})$$

1.2 Bioremediation of PAHs and its limitations

Bioremediation is a treatment technology for restoration of polluted environments, and it is recognized as an environmentally benign strategy. Bioremediation may be driven either by microbial functions only or by interconnection between microbes and the plant rhizosphere (Fester *et al.*, 2014). Biological and non-biological remediation processes optimized for PAH pollution has been reviewed recently (Gan *et al.*, 2009). Bioremediation may provide more advantages over other technologies, because the rehabilitated soil or sediment can retain many of its key functions, allowing its reuse after treatment. A set of bioremediation technologies for rehabilitation of PAH-polluted environments such as land farming (Wang *et al.*, 1990), composting (Šašek *et al.*, 2003), prepared-bed bioreactor (Ellis *et al.*, 1991) and slurry-phase bioreactor (Mueller *et al.*, 1991), is valid and available in the remediation market. The price of bioremediation is comparable to other non-biological techniques, such as chemical extraction, incineration and thermal desorption, which ranges from 20 to 70 €m⁻³ (Elskens and Harmsen, 2007; Hyman and Dupont, 2001). Bioremediation at an average cost of 45 €m⁻³, is a realistic alternative to excavation and disposal, priced usually at 200 €m⁻³. Although biodegradation is the driving force for bioremediation of PAHs, the environmental factors that influence its biodegradation such as bioavailability remain unpredictable. This poor predictability in bioremediation of PAHs is a large limitation when evaluating the viability of this technology for treating contaminated soils and sediments (Ortega-Calvo *et al.*, 2013). To this end, the integration of a bioavailability-efficient technology into current bioremediation practices at no additional cost will ensure that the target values for risk reduction and the cost-effectiveness of the treatment can be achieved.

1.2.1 Biodegradation of PAHs

Biodegradation driven by many bacteria and fungi is one of the most direct pathways for the dissipation of PAHs in nature. This microbial activity is dependent on the stability of the benzene rings in the PAH molecules and on other factors related to the hydrophobicity of PAHs (Niqui-Arroyo *et al.*, 2011). The half lives of LMW-PAHs in nature, such as phenanthrene, range from 16-126 days, while HMW-PAHs, such as benzo(*a*)pyrene, possess substantially longer half lives of up to 1400 days (Husain, 2008). The estimation of half-life takes into account the reduction in PAH concentrations caused mainly by biodegradation.

The metabolic pathways for utilizing LMW-PAHs by microorganisms were studied since the 1980s, and later (in the 1990s) for HMW-PAHs. Some metabolic pathways of such LMW-PAHs like naphthalene and phenanthrene have been proposed, which are shown in **Fig. 4** and **5**, respectively. In case of HMW-PAHs, their metabolic pathways found in diverse bacterial taxa were well summarized by Kanaly and Harayama (2000; 2010).

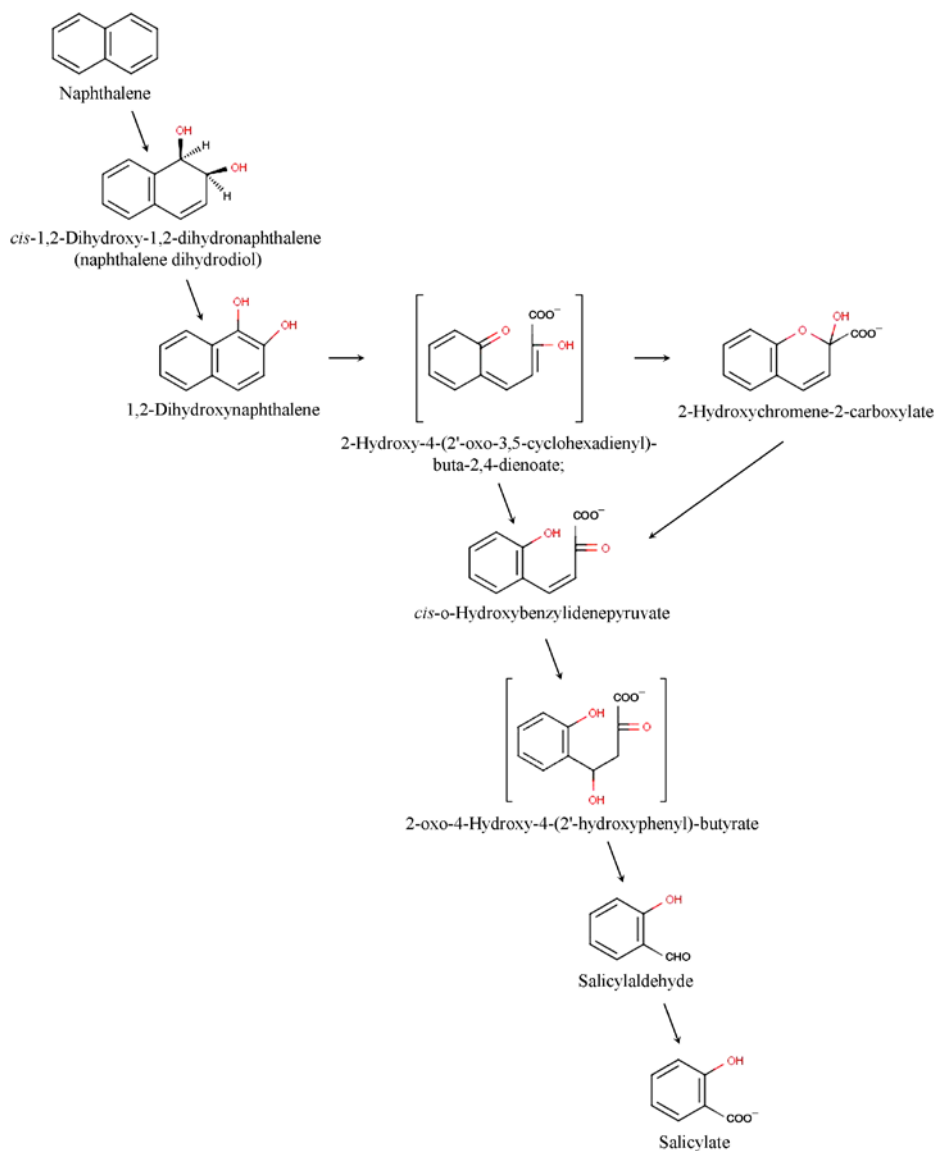


Figure 4 Bacterial metabolic pathways of naphthalene to salicylate. The pathways were modified according to a summary of Eaton and Chapman (1992), where the chemical structures were drawn with MarvinSketch (<http://www.chemaxon.com/marvin/sketch/index.php>, Available on 5 Feb., 2014).

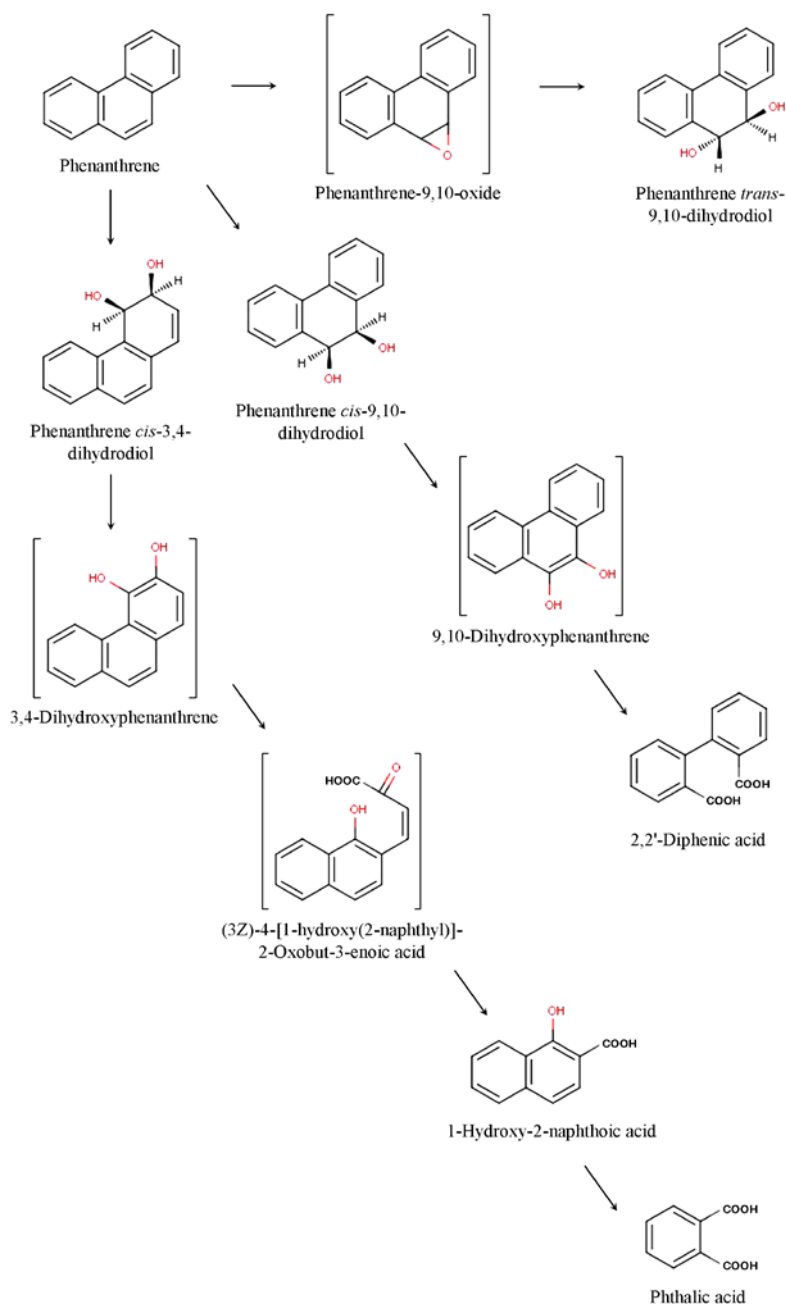


Figure 5 Bacterial metabolic pathways of phenanthrene. The figure was modified according to the proposed pathways elucidated by Moody *et al.* (2001), where the chemical structures were drawn with MarvinSketch (<http://www.chemaxon.com/marvin/sketch/index.php>, Available on 5 Feb., 2014).

The aerobic metabolism of PAHs has been well studied, and it occurs through three main catabolic activities (Cerniglia, 1992; Haritash and Kaushik, 2009; Husain, 2008; Kanaly and Harayama, 2000; Peng *et al.*, 2008; Semple *et al.*, 1999; Steffen *et al.*, 2000):

- 1) Oxidation of aromatic ring by dioxygenase (**Fig. 6**), exclusively for bacteria and usually through their metabolism to use PAHs as a carbon and energy source, which may lead to a co-metabolic process;

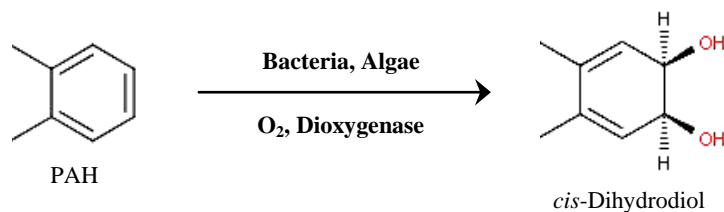


Figure 6 Biodegradation at the first step for breaking down the aromatic ring of PAHs by dioxygenase. The figure was summed up from the literatures cited. The chemical structures were drawn with MarvinSketch (<http://www.chemaxon.com/marvin/sketch/index.php>, Available on 5 Feb., 2014).

- 2) Oxidation by means of lignin and manganese peroxidases excreted from white-rot fungi (**Fig. 7**), considered as a co-metabolic process of PAHs in nature;

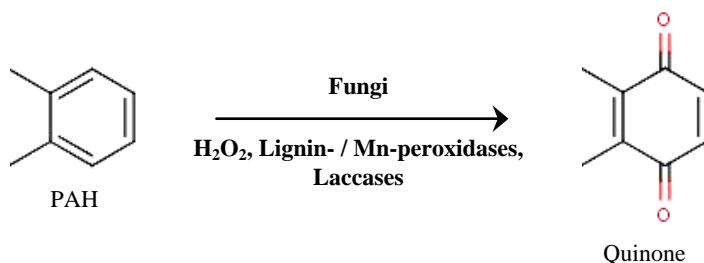


Figure 7 Biodegradation at the first step for breaking down the aromatic ring of PAHs by lignin and manganese peroxidases. The figure was summed up from the literatures cited. The chemical structures were drawn with MarvinSketch (<http://www.chemaxon.com/marvin/sketch/index.php>, Available on 5 Feb., 2014).

- 3) Oxidation with cytochrome P450 monooxygenase found in both prokaryotes and eukaryotes (**Fig. 8**), it is typically relevant to the detoxification and metabolite transform, but does not usually entail the mineralization of PAHs.

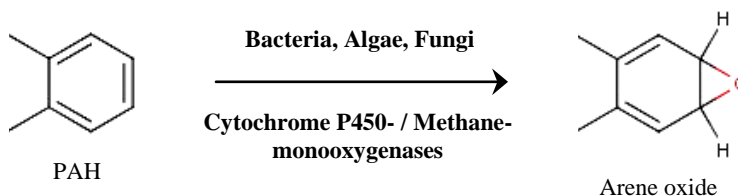


Figure 8 Biodegradation at the first step for breaking down the aromatic ring of PAHs by cytochrome P450 monooxygenase. The figure was summed up from the literatures cited. The chemical structures were drawn with MarvinSketch (<http://www.chemaxon.com/marvin/sketch/index.php>, Available on 5 Feb., 2014).

The current knowledge on the biodegradation of PAHs reveals that most PAHs listed in **Table 1** can be degraded through aerobic metabolism, except for some HMW-PAHs such as benzo[*a*]pyrene that require co-metabolic process (Kanaly and Harayama, 2000; 2010). The co-metabolism of PAHs does not provide any benefit to the microbial cells, as because it does not cause extensive modification of PAHs neither incorporation them into biomass nor direct conversion them into CO₂. Recent findings have demonstrated also that microorganisms can use other electron acceptors, such as nitrates and sulphates, for oxidation of PAHs (Quantin *et al.*, 2005; Rothermich *et al.*, 2002). Futhermore, it was evidenced that biodegradation of PAHs in anaerobic environments could occur only in the presence of a second carbon source like acetate or glucose (Ambrosoli *et al.*, 2005).

The biodegradation of PAHs sorbed to black carbon or NAPLs is typically a slow process that contributes to their long-term persistence in environments (Lopez *et al.*, 2008; Ortega-Calvo and Gschwend, 2010; Ortega-Calvo *et al.*, 1995). Dissolved organic carbon (DOC) also plays a key role in the biodegradation of PAHs. It was found that the addition of DOC in the form of humic fractions to PAH-polluted soils caused an enhancement of biodegradation, probably as a result of the enhanced desorption of PAHs from soils to the aqueous fraction (Bengtsson and Zerhouni, 2003; Bogan and Sullivan, 2003; Haderlein *et al.*, 2001). The other DOC-mediated enhancements of PAH biodegradation include the enlargement of PAH solubility (Liang *et al.*, 2007), a direct access to DOC-sorbed PAHs due to the physical association of bacteria and DOC (Ortega-Calvo and Saiz-Jimenez, 1998), and an increased diffusive flux toward bacterial cells caused by DOC (Haftka *et al.*, 2008).

Due to their charged nature and high specific surface, natural clay minerals also play an important role in the biodegradation of PAHs. Microbial cells often show a high affinity for clay surfaces, as evidenced by their spontaneous association in suspensions and percolation columns (Lahlou *et al.*, 2000; Ortega-Calvo *et al.*, 1999; Velasco-Casal *et al.*, 2008). This association can explain, for example, the population density of PAH-degrading mycobacteria in the PAH-enriched clay fraction of a long-term polluted soil (Uyttebroek *et al.*, 2006). Surface of clay can also scavenge organic chemoeffectors from the pore water by sorption, thereby eliminating their effect in promoting the transport of chemotactic bacteria through porous materials (Velasco-Casal *et al.*, 2008), and associate with organic matter, resulting in slow desorption of PAHs with limited bioavailability to microbial degradation (Lahlou and Ortega-Calvo, 1999). Clay-rich soil may also present a limited oxygen and nutrient supply to PAH-degrading populations, due to slow diffusion and low hydraulic conductivity (Niqui-Arroyo *et al.*, 2006).

The biodegradation in bioremediation of PAHs is often found to have a conceptual link with pollutant bioavailability and microbial accessibility toward these pollutants. This interconnection is proposed with a graphical model described in **Fig. 9**.

1.2.2 Bioavailability of PAHs

Due to their strong hydrophobicity and sorption behaviour, PAHs are recognized as poorly available pollutants in nature. However, aged PAHs can still be extracted by vigorous solvent extraction, but they possess a lower bioavailability and risks compared with the more recently introduced pollutants (Alexander *et al.*, 2000). Partitioning of PAHs from sorbents and NAPLs may occur through weak chemical activity gradients that promote their uptake and transformation by active microbial cells. The partitioning kinetics can be determined in a biphasic NAPL/water system that maintains the integrity of the organic phase, resulting in a constant interfacial area (Ortega-Calvo and Alexander, 1994). This method allows the accurate estimations of partitioning rates and equilibrium concentrations, avoiding potential interferences caused by the dispersions of NAPL due to shaking, microorganisms and biostimulants (Garcia-Junco *et al.*, 2003; Ortega-Calvo *et al.*, 1995; Tejada-Agredano *et al.*, 2011). It also allows for a direct comparison of biodegradation rates measured under the same conditions. Hence, biodegradation rates may reflect the dependencies of restricted phase exchanges, and the pollutants may persist for longer periods of time. This persistence may increase environmental risk of PAHs. Understandings of both environmental fate of

PAHs and microbial functions and responses in PAH-polluted scenarios together with taking environmental risk of PAHs into account are essential for improving the bioremediation technology. An interconnection between pollutant bioavailability, bioremediation and environmental risk of PAHs is represented in Fig. 10.

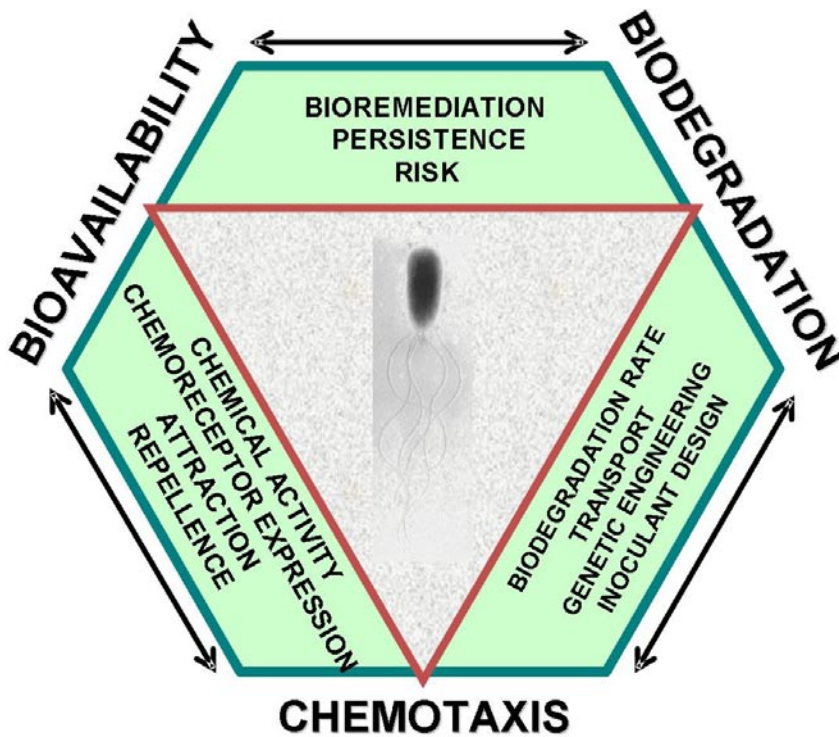


Figure 9 Impact of microbial chemotaxis on bioavailability and biodegradation of pollutants in PAH bioremediation (Krell *et al.*, 2013, see also the list of author's publications, page 1).

A useful indicator of bioavailability is the fraction of potentially biodegradable PAHs over time in the absence of limitations other than restricted phase exchanges. This is also known as the bioaccessible fraction (Semple *et al.*, 2007). Another bioavailability indicator is the chemical activity of PAHs, which is the fraction of the aqueous solubility of PAHs in liquid state that can be measured as freely dissolved chemical concentrations (C_{free}) in the aqueous phase of an environmental sample (Reichenberg and Mayer, 2006). Desorption of PAHs from polluted soils and sediments, is well represented by a biphasic pattern. A slow desorption rate of PAHs may be prominent if soils are enriched with semisolid components,

such as NAPL-like creosote materials that possess a strong sorption affinity for PAHs. These materials limit biodegradation rate of PAHs because they possess restricted surface areas and allow the PAHs to diffuse slowly from these sorbents. Bioavailability of native PAHs present in soils and sediments can also be assessed with an accelerated biodegradation assay, characterized by a) inoculation of a sample containing PAHs with a sufficient number of PAH-degraders, b) monitoring the biodegradation activity through ^{14}C -mineralization measurements, and c) a single-step chemical analysis of native PAHs in the residues (Ortega-Calvo *et al.*, 2013).



Figure 10 Overview of conceptual interconnection of pollutant bioavailability, bioremediation and environmental risk in PAH bioremediation (Ortega-Calvo *et al.*, 2013, see also the list of author’s publications, page 1).

Some recent strategies for bioremediation of PAHs, focusing on the enhancement of pollutant bioavailability under acceptable environmental risks have been well addressed (Ortega-Calvo *et al.*, 2013).

1.2.3 Microbial accessibility towards PAHs

Chemotaxis has been proposed as an effective tool of microorganisms to access the pollutants and further increase pollutant bioavailability and biodegradation. During the past decade, it has been conceived that bacterial chemotaxis increases bioavailability and biodegradation rate of PAHs either they exist freely or with binding to their sorbents at low bioavailable regimes (Grimm and Harwood, 1999; Krell *et al.*, 2013; Law and Aitken, 2003; Marx and Aitken, 2000; Ortega-Calvo *et al.*, 2003). The best studied example is the capacity of *P. putida* G7 to degrade naphthalene. Grimm and Harwood (1999) have proposed that NahY-mediated taxis towards naphthalene might facilitate its biodegradation. Proof of this hypothesis was brought by Aitken and co-workers. Using a heterogeneous aqueous system, they were able to demonstrate that chemotaxis enhances naphthalene biodegradation (Marx and Aitken, 2000). Subsequent studies using chemotactic and non-chemotactic strains of *P. putida* G7 clearly evidenced that chemotaxis increased naphthalene degradation when the compound is present in a NAPL (Law and Aitken, 2003). There are some studies that compare the pollutant-degrading capacity of microorganisms with their chemotactic capacity. Interestingly, in some cases chemotaxis was only observed towards compounds which were degraded by the microorganism whereas structurally similar non-substrate compounds were not found to be chemoattractants (Pandey *et al.*, 2012; Samanta *et al.*, 2000), which confirms the link between chemotaxis and biodegradation.

Although the chemical gradients of partitioned PAHs from their sorbents may result in exclusively low exposure concentrations, they are still detectable by bacterial chemotaxis. Particularly, the existence of PAH-degrading bacteria at the interface of such low bioavailable PAHs and aqueous microenvironments is required for effective biodegradation. However, bacterial chemotaxis needs to be mediated with water saturated systems. Recently, it was evidenced that bioavailability of naphthalene can also be promoted by the chemotactic transport of *P. putida* G7 through liquid films of water along the oomycete mycelia, which act as pathways for mobilization (Furuno *et al.*, 2010). The impacts of microbial accessibility through chemotactic mechanism on bioavailability and biodegradation of pollutants in bioremediation are represented in **Figs. 9** and **10**.

In general, microbial accessibility towards pollutants in soils or sediments is limited by either microbial cell physiology or environmental factors. The pollutant-degrading bacteria are

usually limited in the accessibility towards pollutants in the soil structure (Fredslund *et al.*, 2008; Uyttebroek *et al.*, 2006). However, diverse strategies with the aim to improve microbial accessibility in bioremediation of PAHs have been proposed (Ortega-Calvo *et al.*, 2013). Notwithstanding, the transport of non-flagellated PAH-degrading bacteria through water-saturated porous media is somehow difficult even with such strategies, for example, electroosmotic mobilization (Wick *et al.*, 2004; 2007b) and mycelial networking (Kohlmeier *et al.*, 2005; Wick *et al.*, 2007a).

1.3 Exploiting microbial influences on bioremediation of PAHs

1.3.1 Production of surface-active compounds

The production of surface-active compounds (surfactants) by microorganisms is an important microbial process that affects the bioavailability of hydrophobic organic pollutants like PAHs. Many different surfactants are synthesized by a wide variety of microorganisms, such as *Pseudomonas*, *Bacillus*, *Acinetobacter* and *Mycobacterium* (Desai and Banat, 1997; Lang and Wullbrandt, 1999; Maier and Soberon-Chavez, 2000). Despite considerable amounts of effort expended in researching these compounds, the exact physiological role that microbial surfactants play has not yet been completely elucidated. Otherwise, it does not seem to be restricted exclusively to the solubilization of hydrophobic carbon sources, as surfactants can also be produced when the microorganisms are grown with water-soluble substrates, such as glucose. The surfactants produced biologically are known as biosurfactants that are important in diverse biotechnological aspects. These biosurfactants play a key function in numerous ecological processes and have been linked to microbial adhesion, antagonistic effects toward other microorganisms, heavy metal sequestration and cell-cell communication. Laboratory and field studies have also shown that biosurfactants can be used successfully for environmental applications, such as the restoration of pollution caused by heavy metals and hydrocarbons (Harvey *et al.*, 1990; Herman *et al.*, 1995; McCray *et al.*, 2001; Mulligan *et al.*, 1999). It is conceivable, therefore, that biosurfactants are able to improve PAH-bioremediation performance.

Indeed, biosurfactants exhibit the ability to dissolve pure, solid PAHs, such as phenanthrene, hence increasing their rate of biodegradation (Garcia-Junco *et al.*, 2001; 2003; Resina-Pelfort *et al.*, 2003). Although the synthesis of biosurfactants is not universal among all

microorganisms, their role in increasing the bioavailability of PAHs in natural environments is significant. This important function of biosurfactants should be considered for optimizing the bioremediation of PAHs under acceptable level of environmental risk. Besides biosurfactants, there is a wide variety of other natural organic compounds derived from either microbes or plants that can potentially increase the bioavailability of PAHs. For instance, cyclodextrins (Garon *et al.*, 2004) and unsaturated fatty acids (Yi and Crowley, 2007) that have been proposed to stimulate the biodegradation of PAHs in soil through surface-influencing mechanism.

1.3.2 Enhancing microbial mobilization

The bioavailability of PAHs can be increased not only by solubilizing the pollutants, but also by promoting the dispersal of microorganisms throughout the polluted matrix. However, the positive effect resulting from the mobilization of these microbes in bioremediation is dependent on the efficiency of bacterial movement in porous media. It is often restricted by high deposition rates and adhesion to soil surfaces of microbial cells. Bacterial active motility and taxis may help to overcome the limitation. Meanwhile, chemotaxis as the diverse tactic reactions to pollutants of bacteria has been considered through flagellar motility as a major tool for accessing the pollutants. Biodegradation studies based on carbon tetrachloride (Witt *et al.*, 1999), BTEX compounds (Parales *et al.*, 2000), pesticides (Hawkins and Harwood, 2002) and one of the most water soluble PAHs, naphthalene (Grimm and Harwood, 1997; Marx and Aitken, 2000), have demonstrated the capability of chemotaxis to enhance biodegradation in laboratory-scale microcosms. There have been reports on chemotactic responses towards moderately hydrophobic PAHs, such as phenanthrene, anthracene and pyrene (Ortega-Calvo *et al.*, 2003). Chemotactic influences may be particularly important for the degradation of the most hydrophobic PAHs, such as benzo(a)pyrene, which are strongly sorbed to the soil and experience a reduced mobility. However, utilization of chemotaxis for enhancing the biodegradation of these PAHs requires new experimental and analytical methods, as well as a consideration of new concepts that need to be developed.

The best example of chemotaxis-enhanced bioavailability and hence biodegradation of PAHs has been studied with naphthalene-degrading *P. putida* G7. Using a heterogeneous aqueous system under a slow-diffusion regime, the rate of biodegradation of naphthalene by *P. putida* G7 was found to exceed the predictions from a model based on diffusion-limited

biodegradation (Marx and Aitken, 2000). This indicated that bacterial movement through chemotaxis was faster than substrate mass transfer within the aqueous phase, thus enhancing the rate of substrate acquisition. A subsequent study that also used chemotactic and non-chemotactic strains of *P. putida* G7 clearly demonstrated that chemotaxis increased naphthalene degradation when the compound is present in a NAPL (Law and Aitken, 2003). In this case, chemotaxis promoted partitioning and biodegradation of naphthalene by creating a steeper gradient as the cells accumulated near the NAPL-water interface. Ecological service using mycelial network of fungi and oomycetes has recently been found to facilitate chemotactic transport of *P. putida* G7 towards PAHs, which later promote bioavailability and biodegradation of such PAHs (Furuno *et al.*, 2010; Harms *et al.*, 2011; Kohlmeier *et al.*, 2005). This study evidenced that bacterial chemotaxis requires a liquid phase for motility. Interestingly, the liquid films surrounding fungal mycelia provide appropriate environments for chemical gradients and chemotactic responses by motile bacteria. Another study showed that the exposure regime of the chemical also appears to influence the type of tactic response (Hanzel *et al.*, 2010). Naphthalene caused in the aqueous phase chemoattraction by *P. putida* G7, but when such chemical was exposed from a vapor phase, it acted as a repellent, even at lower doses than in the aqueous phase.

Bacterial chemotaxis has the potential to not only increase the degradation of chemoattractants, but it also has an important role in the establishment of biofilms (O'Toole and Kolter, 1998; Singh *et al.*, 2006) and mixed microbial communities (Perumbakkam *et al.*, 2006) that may facilitate bioremediation. The co-adhesion and synergistic interaction of various microbial species might be strategic to improving the biodegradation of recalcitrant compounds. A technological innovation based on this concept relies on the mobilization potential of chemotactic pollutant-degrading microbes taken from plant samples (Ortega-Calvo *et al.*, 2003). It was found that chemotaxis towards PAHs in bacteria isolated from rhizospheric soils that were contaminated with hydrocarbons, where these bacteria are able to move chemotactically at speeds of approximately 1 mm min^{-1} (Ortega-Calvo *et al.*, 2003). It has been shown also in later research that bacterial motility and transport can be controlled through an optimal set of chemical effectors (Jimenez-Sanchez *et al.*, 2012; Ortega-Calvo *et al.*, 2011; Velasco-Casal *et al.*, 2008). In well-controlled column systems, the authors found that different effectors could influence the deposition of a chemotactic, naphthalene-degrading *P. putida* G7, in selected porous environments (sand, forest soil, and clay aggregates). Cellular deposition, however, was concomitantly dependent on the cellular

motility (hyper-motility, attraction or repulsion), the sorption of chemical effectors to the column packing materials, and the resulting pore-water concentration. For example, an exposure of the bacterial cells to salicylate induced a smooth movement with few acceleration events and positive taxis, while cells exposed to silver nanoparticles (AgNPs) exhibited tortuous movement and repulsion (Jimenez-Sanchez *et al.*, 2012). Although glucose was metabolized by *P. putida* G7, it did not cause any attraction, but it could induce hyper-motile mode of the bacterial cells, characterized by a high frequency of acceleration events, a high swimming speed ($> 60 \mu\text{m s}^{-1}$) and a high tortuosity in the trajectories. The chemically-induced motility behaviours demonstrated a distinct affinity for sand particles in batch assays, resulting in the development of breakthrough curves in percolation column experiments (Jimenez-Sanchez *et al.*, 2012). The author also found that salicylate reduced significantly the deposition of *P. putida* G7 cells in the column experiments, while glucose and AgNPs enhanced the attachment and caused a blocking of the filter, which resulted in a progressive decrease in deposition of the bacterial cells. Therefore, modification of chemical effectors in environment could assist the improvement of bacterial mobilization in bioremediation of pollutants.

1.3.3 Promoting microbial life at pollutant interfaces

Microorganisms can also increase the bioavailability of PAHs when they are in a direct contact with the pollutants, thereby enabling biodegradation to proceed more rapidly (Garcia-Junco *et al.*, 2003; Ortega-Calvo and Alexander, 1994). The main goal of a recent study (Tejeda-Agredano *et al.*, 2011) was to target the potential nutritional limitations of microorganisms to enhance the biodegradation of PAHs at the interface between NAPL and water phase. The study found that biodegradation of PAHs present in fuel-containing NAPLs was slow and followed zero-order kinetics, indicating bioavailability restrictions (Tejeda-Agredano *et al.*, 2011). The authors found that addition of an oleophilic biostimulant enhanced the biodegradation, resulting as an S-shaped logistic kinetics curve, and yielded a ten-fold increase in the mineralization rates of PAHs. A chemical analysis of residual fuel oil also showed that there was an enhanced biodegradation of the alkyl-PAHs and *n*-alkanes. This enhancement in biodegradation was not the result of an increase in the rate of the partitioning of PAHs into the aqueous phase, nor was it generated to compensate for any nutritional deficiency in the medium. These results indicate that the biodegradation of PAHs by bacterial cells attached to NAPLs can be limited by nutrient availability as a result of the

simultaneous consumption of PAHs within the NAPLs, but this limitation can be overcome by interface fertilization.

As the general concepts for promoting bioavailability and biodegradation are an attempt to increase face-to-face interaction between pollutant-degrading microorganisms and their carbon and energy source (pollutants). Flagellated pollutant-degrading microorganisms can get greater access towards pollutants and hence reside at the pollutant interfaces. However, non-flagellated pollutant-degrading microorganisms require much longer time to access such pollutant interfaces. As mentioned previously, even under the aeration system that could enhance chemical partitioning of PAHs from NAPL and/or ideally increase the dissolution of atmospheric oxygen to the aqueous phase has been established, the mineralization rate of PAHs was not accelerated (Tejeda-Agredano *et al.*, 2011). Hence, the aeration system with physical movement within aqueous microenvironment may be an influencing factor interrupting the bacterial dwelling at the pollutant interface. It would be a challenging issue to evaluate this physical influence on microbial biofilm formation, especially in the biodegradation of pollutants at low bioavailable regimes.

1.4 What are oomycetes?

1.4.1 Taxonomic position of oomycetes

Oomycetes (Öomycetes Winter, 1897; classified into the class Peronosporomycetes Dick, 2001) are fungus-like eukaryotic microorganisms (also known as pseudofungi, lower fungi or water moulds, on the basis of earlier classifications). They belong to a major lineage of “heterokonts or stramenopiles” (correct Latin spelling, straminopiles (Adl *et al.*, 2005)). Heterokonts belong to the phylum Heterokontophyta and comprise mainly algae and pseudofungi, which has been classified recently under the super-group of Chromalveolata (Adl *et al.*, 2005) (called here as the kingdom Chromalveolata). The word “heterokonts” refers to biflagellated motile cells with anterior and posterior flagella (Adl *et al.*, 2005). The recent taxonomic position of oomycetes and some of their notable members are shown in **Fig. 11**. The typical life cycle and unique ecological impacts of oomycetes are addressed below.

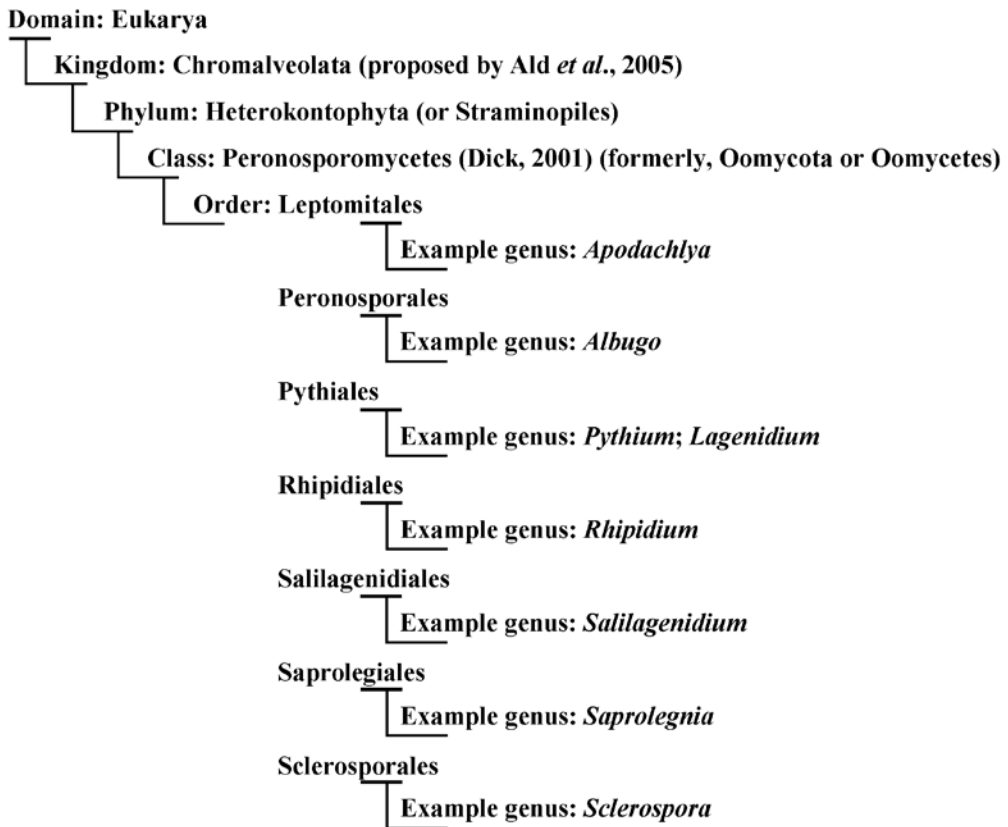


Figure 11 Taxonomic position of oomycetes and their notable members.

1.4.2 Life cycle of oomycetes

As oomycetes are fungus-like eukaryotic microorganisms, they are able to grow in the filamentous mode. The filamentous formation is a vegetative stage of the oomycete growth. This filament is mostly not partitioned by septa, called as aseptate (or coenocytic) hypha. This kind of hypha is similar to a pipeline, where the cytoplasm and genetic material are homogeneously flowing inside. The hyphal growth typically forms a structure of hyphal mat, known as mycelium. In the reproductive stage, oomycetes are able to reproduce through sexual and asexual systems. The sexual reproduction of oomycetes originates a reproductive propagule called as oospore, which is produced from a cytoplasm merged between the parent mycelia (female one called oogonium and male one called antheridium). Oospores are characterized by their spherical shape, thick walls and absence of motility. They are known

to be produced in adverse environmental conditions, where the thick cell wall guarantees their survival. Under favourable conditions, these sexual spores germinate and produce germ tubes. These germ tubes may develop further to be mycelial networks or sporangia that are able to form asexual spores called as zoospores. These zoospores are motile with two flagella (posterior and anterior). These zoospores are produced with the aim to interact with their target locations, sensing the environment selectively and directionally through chemotaxis, electro taxis, autotaxis, or autoaggregation. Once they find their target locations, zoospores perform encystment and form germ tubes. Zoospore development in oomycetes is well documented (Walker and van West, 2007). The typical life cycle of oomycetes is shown in **Fig. 12**.

1.4.3 Ecology of oomycetes

Most oomycetes are saprophytes and parasites. They are often found in terrestrial and aquatic rhizospheres (i.e. water-saturated soils or sediments of wetlands, mangrove forests, streams, lakes and etc.), and few of them have been described in marine habitats (Dick, 2001; Hulvey *et al.*, 2010). They live at the interface of biphasic habitats (solid-liquid, solid-air or liquid-air). They are known for on their parasitic lifestyles interacting with diverse hosts. Among them, some are known as pathogens of several economic crops (i.e. *Phytophthora* and *Pythium*) and fishes (i.e. *Saprolegnia*) (Walker and van West, 2007), and some are known as biocontrol agents like *Pythium oligandrum* (a mycoparasite of other plant pathogenic oomycetes and fungi) (Benhamou *et al.*, 2012) and *Lagenidium giganteum* (a parasite of mosquito larvae) (Kerwin, 2007). Based on the unique lifestyle of oomycetes to form zoospores as a dispersal tool to localize remote places, most studies focus on how these zoospores interact with other organisms in nature. Numerous studies have revealed interactions between oomycete zoospores and their host plants or antagonistic microorganisms (Blanco and Judelson, 2005; Heungens and Parke, 2000; Timmusk *et al.*, 2009; van West *et al.*, 2003). Although they are recognized as invasive parasites, they also cause beneficial impacts in ecosystem against pathogens of plants and animals (Benhamou *et al.*, 2012; Kerwin, 2007). Moreover, some studies evidence that leaf litter-decomposing oomycetes are one of the key interacting microbes, enhancing the consumption behaviour of this leaf litter by benthic invertebrates, what results in effective biogeochemical turnover and nutrient cycling in freshwater ecosystem (Aßmann *et al.*, 2010; 2011).

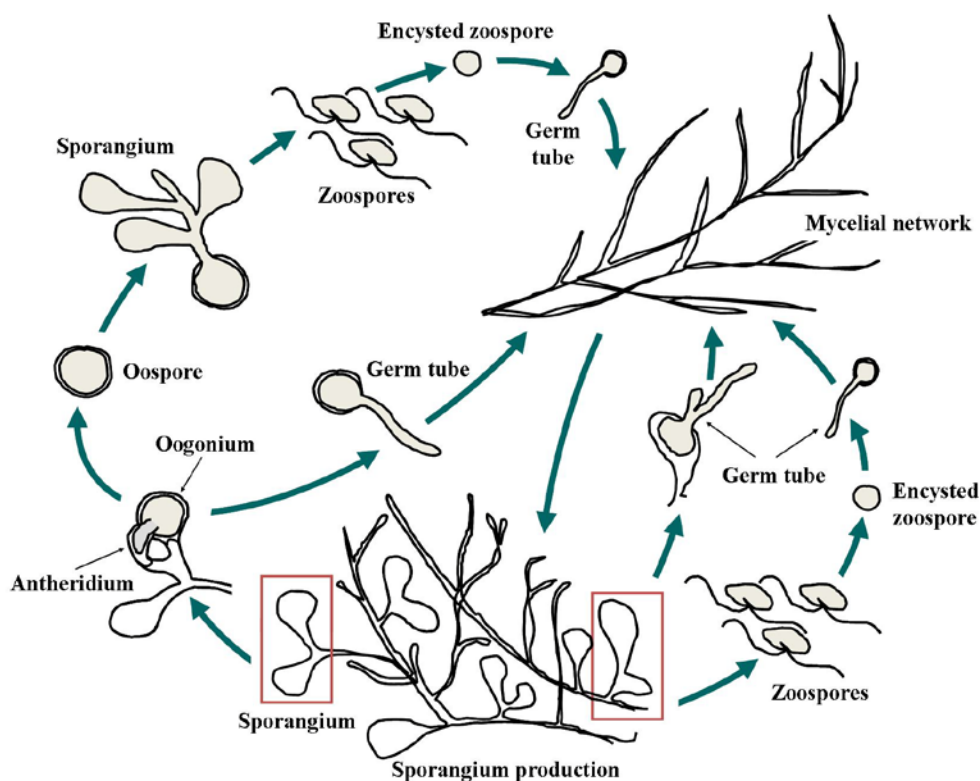


Figure 12 Life cycle of oomycetes. The figure was drawn based on own microscopic observations of *Pythium aphanidermatum* and information taken from the literature.

1.5 Oomycetes in bioremediation of PAHs

1.5.1 Mycelial networks

Application of oomycetes in bioremediation is likely unknown. However, the potential of mycelial networks in bioremediation of PAHs was firstly revealed by Kohlmeier *et al.* (2005). The authors found that mycelial networks of higher fungi could facilitate the mobilization of flagellated PAH-degrading bacteria. They also hypothesized that the bacteria may swim along the liquid film surrounding the fungal hyphae, while a limitation of this fungal facility had yet been found with non-flagellated PAH-degrading bacteria. The author also proposed the concept of “fungal highway”, which well describes this ecological service of mycelial networks of filamentous fungi. Later on, the role of mycelial networks formed by a rhizosphere oomycete, *Pythium ultimum* was investigated (Wick *et al.*, 2007a). This work

showed that the oomycete could promote the accessibility of a pollutant-degrading bacterium; *Pseudomonas putida* PpG7 (NAH7) to its carbon source by providing a continuous network of water-paths within the soil matrix. Moreover, the liquid film created along the mycelial network was found to be a cross bridge simulated with a chemical gradient of pollutant that was further attracted by motile pollutant-degrading bacteria through chemotaxis (Furano *et al.*, 2010). This fungal model system could potentially apply to the bioavailability and biodegradation of pollutants in soil. In addition to the interesting unique feature of oomycete hyphae without partition septa (i.e. all the cytoplasm flows through along the hyphae), it was found that the pollutants accumulated in the form of vacuole and they were transported within this “biological pipeline” (Furano *et al.*, 2012). These effective ecological services (**Fig. 13**) of oomycetes reveal a great impact of biotechnological development in bioremediation technology. Further than the mycelial network, when we look at the life cycle of oomycetes, other compartment of their cycle such as zoospores would be a challenging component for understanding the whole concept of their ecological services in bioremediation of pollutants. While, the impacts of these eukaryotic zoospores and their development within polluted scenarios are still unknown. The possible applications of these zoospores for bioremediation of pollutants are addressed below.

1.5.2 Eukaryotic zoospores?

Eukaryotic zoospores can be formed not only by fungi and oomycetes but also by algae and protists (Fan *et al.*, 2002; Gleason and Lilje, 2009; James *et al.*, 2006; Rasconi *et al.*, 2012; Walker and van West, 2007). These zoospore-producing organisms play diverse ecological roles as phototrophs, saprophytes, parasites or symbionts. They live in a wide scale of habitats, ranging from the unique mutual lifestyle within the cattle rumen to freshwater lakes, mangrove forests and oceans. Numerous studies have revealed interactions between phytopathogenic zoospores and their host plants or microbial antagonists (Blanco and Judelson, 2005; Heungens and Perke, 2000; Timmusk *et al.*, 2009; van West *et al.*, 2003). The physiology of zoospores is different dependent on each taxonomic species but reveals similarity with a possession of at least a flagellum for their translocation. Generally, an aqueous phase is required for the induction and formation of zoospores, in which they can swim along for a distance prior to settlement and encystment.

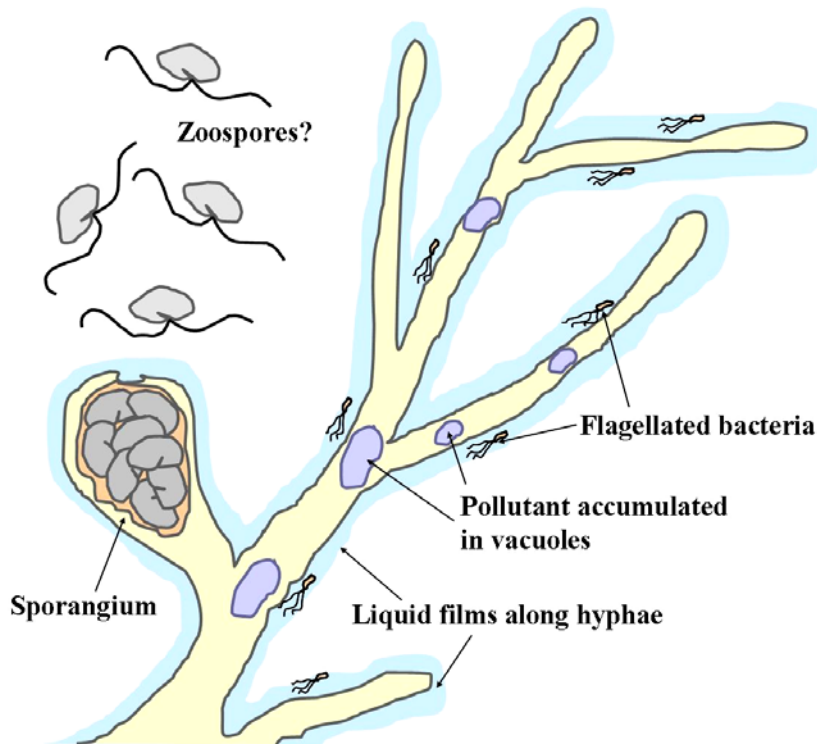


Figure 13 Ecological services of oomycete mycelia for an enhanced mobilization of pollutants and flagellated pollutant-degrading bacteria. The figure was drawn based on the literature cited, and points at the question how zoospores survive in polluted scenarios and how they can be applied for enhanced bioremediation of pollutants.

The orientation of zoospores to their appropriate target is directed by their swimming behaviour and motility responses mainly through chemotaxis (Appiah *et al.*, 2005; Blanco and Judelson, 2005; Latijnhouwers *et al.*, 2004). A long swimming period up to 2 days in axenic aqueous solution can be observed with some fungal zoospores (Gleason and Lilje, 2009). Moreover, some eukaryotic zoospores of marine algae showed a chemotactic response toward signalling molecules produced by bacterial populations, which leads to complex biofilm formation of this eukaryote-prokaryote consortium (Joint *et al.*, 2002; Patel *et al.*, 2003; Twigg *et al.*, 2014). The ecological impacts of zoospores have been studied mainly in their natural habitats, but their development within polluted environments has remained relatively unexplored. Moreover, the mechanisms of how eukaryotic zoospores interact with prokaryotic population during their swimming and their interference in hydraulic activity within aqueous microenvironments are still unknown. These ecological impacts of zoospores

may enhance bioaccessibility of pollutant-degrading bacteria, which may further increase bioavailability of pollutants in bioremediation.

CHAPTER II: OBJECTIVES

This work aims to evaluate the impacts of oomycete mycelia and zoospores in bioremediation of PAHs. Within this framework, we have examined the idea on how to utilize the ecological services provided by the unique lifestyles of oomycetes either their filamentous growth or in the formation of zoospores that create subsequently the mycelial network at their remote places. These ecological applications of oomycetes are proposed here as a possible tool for enhancing microbial accessibility and pollutant bioavailability. The overall knowledge for such applications in promoting bacterial degradation of PAHs was also investigated. The research studied the roles of oomycetes/bacteria interactions in ecological aspects, in the biodegradation of PAHs and in the bacterial mobilization. The objectives of each study are indicated below.

Ecological aspects:

- Evaluation of microbial antagonisms among oomycetes and PAH-degrading bacteria.
- Investigation of PAH-polluted scenarios affecting filamentous growth and zoospore development in oomycetes.
- Exploration of ecological interaction between oomycetes and PAH-degrading bacteria within PAH-polluted scenarios.

Biodegradation of PAHs:

- Investigation of functional interaction between oomycetes and PAH-degrading bacteria in promoting bacterial degradation of sparingly available pollutants, using non-flagellated phenanthrene-degrading *Mycobacterium gilvum* VM552 in a NAPL-polluted system.
- Evaluation of biological and physicochemical factors influencing such interaction between oomycetes and PAH-degrading bacteria in biodegradation of pollutants.

Bacterial mobilization:

- Investigation of swimming, chemotaxis and encystment behaviours of oomycete zoospores on hydraulic activity within aqueous microenvironments.

- Evaluation of possible roles of oomycete zoospores in mobilization of PAH-degrading bacteria.

CHAPTER III: MATERIALS AND METHODS

3.1 List of chemicals and solutions

3.1.1 Chemicals

Non-polar solvents (*n*-hexadecane (HD) and 2,2,4,4,6,8,8-heptamethylnonane (HMN)), all PAHs (naphthalene, fluorene, phenanthrene, fluoranthene, pyrene and anthracene), acridine orange, *o*-terphenyl and 17 α (H),21 β (H)-hopane were purchased from Sigma-Aldrich, Germany. Polar solvents (pure grade acetone and absolute ethanol) and NaOH were purchased from Panreac, Barcelona, Spain. Heavy fuel oil RMG 35 (ISO 8217) was obtained from the Technical Office of Accidental Marine Spills, University of Vigo, Spain. This fuel has a high viscosity and other characteristics similar to the Prestige heavy oil, which is highly resistant for degradation (Tejeda-Agredano *et al.*, 2011). ¹⁴C-labelled phenanthrene (13.1 mCi mmol⁻¹, radiochemical purity >98%) was purchased from Sigma-Aldrich, Germany.

3.1.2 Organic carbon-containing solutions from natural sources

Natural lake water was collected in the summer of 2012, at Embalse Torre del Águila, Seville, Spain and kept frozen (-80 °C) until use. It was sterilized with autoclave at 121 °C, 15 psi for 15 min before uses. Humic acid was collected from a soil located in the National Park of Doñana, Huelva, Spain. It was prepared by dissolving in 1 M NaOH with a final concentration of 0.1% (w/v), and the pH 6 was adjusted with HCl (Tejeda-Agredano *et al.*, 2014). Relevant physicochemical properties of these solutions can be found in **Table 2** and **Fig. 14**.

3.1.3 In vitro production of root exudates

Root exudates of three representative plants commonly used in bioremediation of PAHs (*Festuca arundinacea*, *Lolium perenne* and *Helianthus annuus* (sunflower)) were prepared with the following protocols. Briefly, seeds of *F. arundinacea* and *L. perenne* were surface-sterilized with absolute ethanol for 1 min, followed by sodium hypochlorite (1% active chlorine) for 30 min. The surface-sterilized seeds were rinsed 3 times with sterilized distilled water for 5 min each time. Two surface-sterilized seeds of either *L. perenne* or *F.*

arundinacea were placed on a perlite layer (0.25 g) in a sterilized test tube (150×25 mm) containing an inorganic salt solution (MM, pH 5.7) (Tejeda-Agredano *et al.*, 2011). The test tube was closed with transparent polypropylene caps (BELLCO, K25) and incubated in darkness at 25 ± 1 °C to allow the germination of the seeds. Then, the test tube was transferred to an incubation room under the same temperature with an irradiation of light at $30 \mu\text{E m}^{-2} \text{s}^{-1}$ for 18-hour photoperiod and maintained there for 45 days.

Table 2 Relevant physicochemical properties of organic carbon-containing solutions used in this thesis

Solution	TOC ^a (mg L ⁻¹)	pH	Conductivity (S m ⁻¹)
Humic acid	470 ^b	6.10 ± 0.03	1.12 ± 0.00
<i>Helianthus</i> root exudates	56.77 ± 1.97	4.85 ± 0.05	0.07 ± 0.00
<i>Festuca</i> root exudates	17.87 ± 0.35	5.74 ± 0.01	0.12 ± 0.00
<i>Lolium</i> root exudates	10.07 ± 4.05	6.05 ± 0.05	0.12 ± 0.00
Sterilized lake water	9.00 ± 0.12	7.80 ± 0.14	0.42 ± 0.01

All the measurements were done at least in duplicate. The results are reported with mean ± standard deviation (SD). ^aTotal organic carbon (TOC) was measured using Shimadzu TOC-VCSH with ASI-V auto sampler after filtration through Whatman[®] No. 1 (pore size, $\varnothing = 11 \mu\text{m}$). ^bTOC concentration in 1 g L^{-1} humic acid solution was in accordance to the elemental analysis reported by Lahlou *et al.* (2000).

In the case of *H. annuus*, the seeds were surface-sterilized with absolute ethanol for 3 min, followed by 57% sodium hypochlorite (14% active chlorine) for 25 min. The surface-sterilized seeds were rinsed 3 times with sterilized distilled water for 5 min each time. These seeds (50 seeds) were placed on a square piece of stainless steel wire cloth installed within a glass jar (1-L capacity, 28×11.5 cm) that contained 500 ml of MM. The jar was closed firmly with a pressure system that used a glass lid and sealed with Parafilm. The jar was transferred to an incubation room at 25 ± 1 °C with an irradiation of light at $65.24 \mu\text{E m}^{-2} \text{s}^{-1}$ and for 18-hour photoperiod and maintained there for 30 days. The experiments were carried out under aseptic condition, and were done in triplicate for each plant species. More details of the procedure can be found elsewhere (Tejeda-Agredano *et al.*, 2013). To harvest root exudates derived from each plant, the whole volume of MM-containing the plant exudates was collected and centrifuged at $31000 \times g$ for 3 h to remove unwanted residuals, following the method described by Haftka *et al.* (2008). The root exudates were stored at -20 °C until further use. Note that the plant seeds shall be situated at the surface of either perlite or

stainless steel wire cloth, and must not be submerged for avoiding the anoxic condition in the plantlet and allowing the development of plant roots lead to production of the root exudates. Some of their physicochemical properties of the different root exudates can be found in **Table 2** and **Fig. 14**.

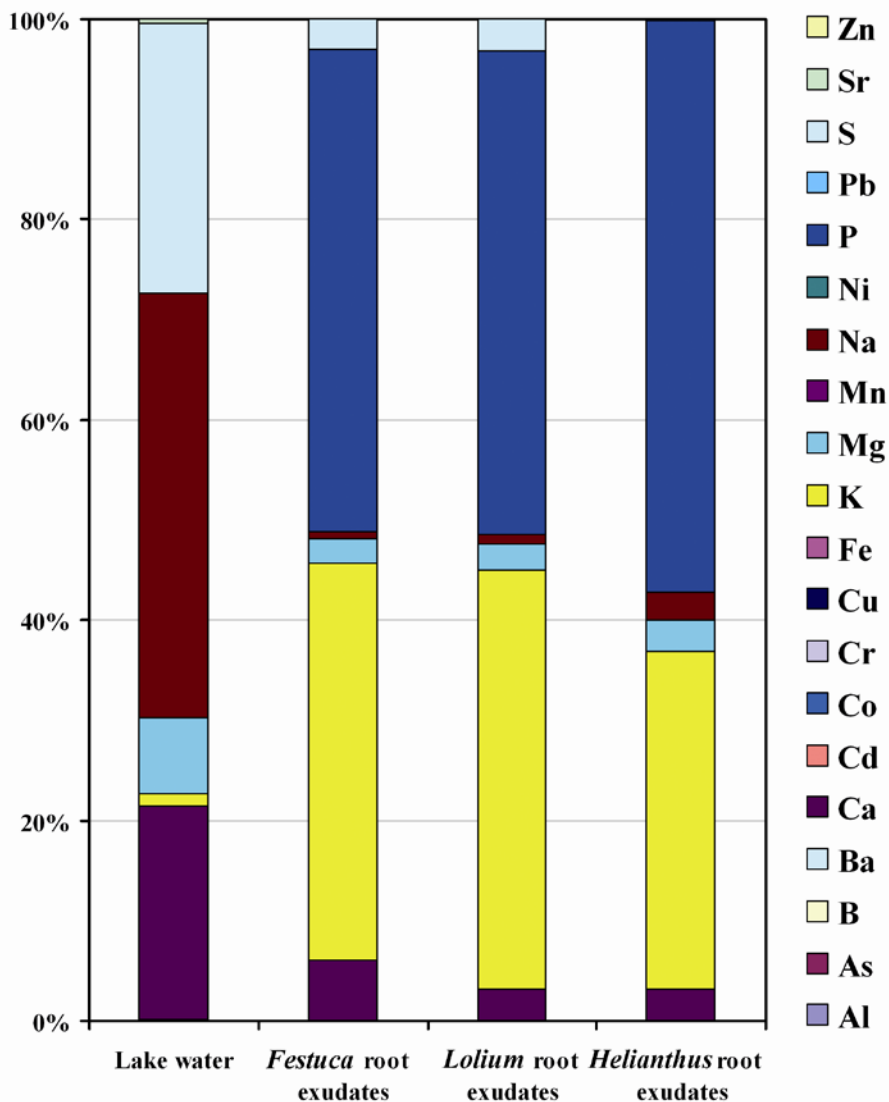


Figure 14 Elemental compositions of lake water and root exudates. The compositions were determined with ICP-OES (Varian ICP 720-ES simultaneous ICP-OES with axially viewed plasma) after filtration through nylon filters (pore size, $\varnothing = 0.45 \mu\text{m}$) and acidification with 2% HNO_3 (30%).

3.2 Microorganisms

3.2.1 Microbial stocks and growing conditions

A primary stock of an oomycete, *Pythium aphanidermatum* (a massive zoospore-producing oomycete) originated from the culture collection at Aberdeen Oomycete Laboratory, University of Aberdeen, UK. Together with another oomycete, *Pythium oligandrum* CBS 530.74 (mycoparasitic oomycete used for biological control of diverse fungal and other oomycete infections) that was purchased from Centraalbureau voor Schimmelcultures (CBS), Fungal Biodiversity Centre, Institute of the Royal Netherlands Academy of Arts and Sciences (KNAW), Utrecht, The Netherlands. Both oomycetes were grown routinely at 25 °C on diluted V8 (DV8) agar [4% (v/v) filtered Campbell's V8 juice; 20 g agar powder (Panreac, Barcelona, Spain); 1 L distilled water].

PAH-degrading bacteria used in this thesis were a non-flagellated *Mycobacterium gilvum* VM552 (isolated from a PAH-polluted soil and able to use phenanthrene, naphthalene, fluoranthene, pyrene and anthracene as a sole source of carbon and energy) and a motile naphthalene-degrading bacterium, *P. putida* G7. These bacteria were grown previously in mineral salt medium supplemented with phenanthrene for *M. gilvum* VM552 (described by Tejada-Agredano *et al.* (2011)) or salicylate for *P. putida* G7 (described by Jimenez-Sanchez *et al.* (2012)) as their sole sources of carbon and energy, aiming to preserve their metabolic capacity. Bacterial cells were then collected at their exponential phases (~12 h for *P. putida* G7 and ~96 h for *M. gilvum* VM552) and maintained by mixing with 20% (v/v) glycerol, which were further kept at -80 °C as a primary stock.

3.2.2 Preparation of oomycete biomass

The biomass (sole mycelia) of both oomycetes was prepared by growing them for 4 days at 25 °C on V8 agar [200 mL Campbell's V8 juice; 20 g agar powder (Panreac, Barcelona, Spain); 3 g CaCO₃; 1 L distilled water]. The hyphal mats growing on the agar were cut into a piece of 1 cm², and the aerial hyphae were scraped out by sterilized spatula. This hyphal mat was used in mineralization experiments (see also 3.6) aiming to evaluate the influence of oomycetes on bacterial mineralization of PAHs initially present in a NAPL. The differences of biomass dry weight and capacity of the hyphal mats to be a source of zoospore formation according to the different oomycetes were evaluated by considering the same growing area (cm²) of the hyphal mats tested.

3.2.3 Production of oomycete zoospores

The 4-day-old hyphal mats of *Py. aphanidermatum* growing on DV8 agar (described in 3.2.1) were used for production of zoospores. Briefly, ten pieces (1 cm²) of the hyphal mats growing on the agar were cut, and were then soaked with 10 mL of test solutions. The test solutions including distilled water, lake water (see also 3.1.2) and pond water (collected from Maria Luisa Park, Seville, Spain) were sterilized with autoclave at 121 °C, 15 psi for 15 min and tested for zoospore formation. Zoospores were released by the oomycete after incubation at 25 °C for 5-6 h. The approximate number of zoospores formed was quantified with BLAUBRAND® counting chambers (Germany). The lake water solution, which gave the highest number of zoospores, was selected and used for zoospore production throughout this thesis. Under the same production protocol, no zoospore formed by *Py. oligandrum* was observed.

3.2.4 Preparation of bacterial biomass

Bacterial biomass was prepared in accordance to the purposes of experiments. For all tests except for mineralization experiments, both PAH-degrading bacteria were transferred from primary stocks (see also 3.2.1) and re-grown in tryptic soy broth (TSB) (Sigma-Aldrich, Germany) at 30 °C with shaking at 150 rpm for two different periods of incubation (overnight (~12 h) or 4 days (~96 h)). These periods refer to the exponential and stationary phases of *P. putida* G7 growth at 12 h and 96 h, respectively, while only exponential phase cells (96 h) of *M. gilvum* VM552 were prepared. The bacterial cells were collected by centrifugation at 4303 ×g for 5 min, then washed twice and re-suspended with the sterilized lake water for further uses. The initial cell density of bacteria was adjusted by an optical density at 600 nm (OD_{600 nm}) of 1.5. This OD value corresponded to 10¹⁰ and 10⁸ colony forming units (CFU) mL⁻¹ for *P. putida* G7 and *M. gilvum* VM552, respectively.

M. gilvum VM552 was used as PAH-degrader in mineralization experiments (see also 3.6). The bacterium was transferred from primary stocks (see also 3.2.1) and re-grown on tryptic soy agar (TSA) (Sigma-Aldrich, Germany) for a few days. Then, this culture was transferred to grow in its mineral salt medium supplemented with phenanthrene (Tejeda-Agredano *et al.*, 2011) as a sole source of carbon and energy. Bacterial cells were collected at its exponential phase (96 h) of growth. The culture broth was collected by filtrating through a glass filter (pore size, Ø = 40 µm) to remove excess phenanthrene. This culture filtrate was then

incubated overnight to allow the complete degradation of remaining phenanthrene. The biomass was collected by centrifugation at $4303 \times g$, then washed twice and re-suspended in sterilized lake water. The cell density of bacterial suspension was adjusted at an $OD_{600 \text{ nm}}$ of 1, which corresponded to 10^6 CFU mL^{-1} .

Bacterial cells with different growth phases and conditions, used in different experiments were summarized below.

- 1) 4-day old cultures of both *P. putida* G7 and *M. gilvum* VM552 grown in TSB at 30 °C were used in section **4.1 Ecological interaction between eukaryotic zoospores and PAH-degrading bacteria in PAH-polluted scenarios.**
- 2) 4-day old culture of *M. gilvum* VM552 grown in mineral salt medium supplemented with phenanthrene at 30 °C were used in section **4.2 Promoting microbial life at the interface of NAPL and water: a strategy to enhance biodegradation of sparingly bioavailable PAHs.**
- 3) 4-day old cultures of both *P. putida* G7 and *M. gilvum* VM552, together with overnight culture of *P. putida* G7 grown in TSB at 30 °C were used in section **4.3 Biomobilization of pollutant-degrading bacteria by chemotaxis of eukaryotic zoospores.**

3.3 Antagonism tests of oomycetes and PAH-degrading bacteria

3.3.1 Dual culture test on solid agar

The antagonism tests among oomycetes (*Py. aphanidermatum* and *Py. oligandrum*) and PAH-degrading bacteria (*M. gilvum* VM552 and *P. putida* G7) were carried out using dual culture streak plate technique. Two different media (DV8 agar and TSA) were used. These two media were differentiated by their constituents and by the concentration of total carbon available for growth, as indicated by the manufacturers. The concentration of total carbon was 2% (w/v) in TSA and 0.2 % (w/v) in DV8 agar. The bacteria were streaked firstly on the agar at ~2 cm from the edge of agar plates, which were then incubated at 30 °C until the opaque colonies of the bacteria appeared. An agar plug ($\varnothing = 0.5$ cm) of the 4-day old culture of each oomycete grown on DV8 agar was placed on the opposite of the bacterial colony in

the test agar plates. All the plates were incubated at 25 °C and observed everyday. Appearance of inhibition zone (no growth of oomycete hyphae) around the bacterial colony indicates the positive antagonistic activity, while mycelial growth of oomycetes at this zone and/or covering the bacterial colony indicates the absence of antagonistic activity. The experiments were done in triplicate.

3.3.2 Dual culture test in aqueous solution

This test aims to evaluate the influence of PAH-degrading bacteria (*M. gilvum* VM552 and *P. putida* G7) on zoospores formation, which was performed in sterilized lake water at different bacterial cell densities. It was done only with the massive zoospore-producing oomycete, *Py. aphanidermatum*. The bacteria were grown for 4 days under the condition described previously (see also 3.2.4). Then, the initial cell density was adjusted at OD_{600 nm} of 1.5. The bacterial suspension was diluted 10-fold serially with sterilized lake water before being used in the production of zoospores (see also 3.2.3). The number of zoospores formed in each bacterial cell suspension was counted and compared to the control without bacterial cells. The count was done twice after 4 and 6 h of incubation. The experiments were done at least in triplicate.

3.4 Design of PAH-polluted scenarios

3.4.1 Preparation of PAH-containing solutions

PAHs (naphthalene, fluorene, phenanthrene, fluoranthene, pyrene and anthracene) listed in **Table 3** were previously sterilized by dissolving them in pure dichloromethane, and recrystallizing after the complete volatilization of the solvent at ambient temperature for 12 h. PAH-containing solutions were prepared by adding 100 mg L⁻¹ of each sterilized PAH to non-polar or polar solvents and organic solutions (shown in **Table 4**), and maintaining for 15 days to allow its dissolution and/or saturation. Some properties of each PAH can be found in **Table 1**.

3.4.2 Estimation of exposure concentrations of PAHs

The different exposure regimes of PAHs existing in aqueous microenvironments were designed for evaluating their influences on the zoospore development and the interaction between zoospores and PAH-degrading bacteria. At high exposure regimes of PAHs, either

dissolved in polar solvents or in solutions containing DOC, the exposure concentration (C_{exp}) of PAHs was estimated from the solubility of PAHs and the properties of solutions used. PAHs present in polar solvents dissolved completely, and were considered to cause a maximum value of C_{exp} , because these solutions mixed well with the aqueous phase of the microbial suspensions. The C_{exp} of PAHs dissolved in equilibrated (15 days of saturation) DOC-containing solutions resulted from the simultaneous dissolution of solid PAHs and sorption to DOC (Schwarzenbach *et al.*, 2003), which was estimated by equations (ii) and (iii), and the results are shown in **Table 3**.

$$f_w = \frac{1}{1 + [\text{DOC}] \cdot K_{\text{oc}}} \quad (\text{ii})$$

In equation (ii), f_w is the fraction of PAH remaining freely dissolved (i.e. not associated to DOC) in water at equilibrium, [DOC] is the concentration of DOC (in kg L^{-1} of total organic carbon (TOC) of the solution shown in **Table 2**), and K_{oc} (in L kg^{-1}) is the organic carbon-normalized sorption coefficient of the considered PAH (**Table 1**). Once equilibrium is achieved after 15 days of saturation, f_w corresponds to the aqueous solubility (S_w) of each PAH. Therefore, C_{exp} in each DOC-containing solution was estimated by equation (iii):

$$C_{\text{exp}} = \frac{S_w}{f_w} \quad (\text{iii})$$

Table 3 Exposure concentrations of PAHs dissolved in lake water

PAHs	$C_{\text{exp}} (\text{mg L}^{-1})^{\text{a}}$
Naphthalene	31.3
Fluorene	2.0
Phenanthrene	1.3
Fluoranthene	0.41
Pyrene	0.20
Anthracene	0.050

^a C_{exp} of each PAH dissolved in lake water, which contained 9 mg L^{-1} of dissolved organic carbon (**Table 2**), was calculated with equations (ii) and (iii).

At low exposure regimes with non-polar solvents, PAHs also dissolved completely but the solvents exhibited a differentiated phase with the aqueous suspensions that contained the microbial cells. Therefore, the C_{exp} of PAHs exposed from non-polar solvents was estimated from the octanol-water partitioning coefficient (K_{ow}) shown in **Table 1** by equation (iv), where [PAH] is the concentration of each PAH added in the solvents. The results are shown in **Table 4**.

$$C_{\text{exp}} = \frac{[\text{PAH}]}{K_{\text{ow}}} \quad (\text{iv})$$

Table 4 Exposure concentrations of naphthalene and phenanthrene in diverse solutions used for chemotaxis and settlement assays with zoospores

Solutions	TOC ^a (mg L ⁻¹)	C_{exp} (mg L ⁻¹)	
		Naphthalene	Phenanthrene
Non-polar solvents ^b :			
HD and HMN	NA	0.043	0.003
Polar solvents ^c :			
Acetone and ethanol	NA	100	100
Organic solutions ^d :			
Humic acid	470 ^e		8.5
<i>Helianthus</i> root exudates	56.77 ± 1.97		2.0
<i>Festuca</i> root exudates	17.87 ± 0.35		1.3
<i>Lolium</i> root exudates	10.07 ± 4.05		1.3
Lake water	9.00 ± 0.12		1.3

All the measurements of TOC were done at least in duplicate; the results are reported as means ± SDs. ^aTOC was measured using a Shimadzu TOC-VCSH equipment with ASI-V auto sampler after filtration through Whatman[®] No. 1 (pore size, Ø = 11 µm). ^b C_{exp} of PAHs partitioning from these solvents was calculated by equation (iv). ^cBoth PAHs were completely dissolved. ^d C_{exp} of PAHs dissolved in these solutions containing DOC was calculated by equations (ii) and (iii). ^eTOC concentration in 1 g L⁻¹ humic acid solution was in accordance to elemental analysis reported by Lahlou *et al.* (2000).

3.5 Observation of zoospore development in PAH-polluted scenarios

Zoospore development was observed at three stages: formation, chemotaxis and settlement. All developmental stages of zoospores were visualized by either normal light or fluorescence mode of a phase contrast Axioskop 2 Carl Zeiss microscope (Jena, Germany) connected with a Sony ExwaveHAD color video camera (Tokyo, Japan). The fluorescence was observed after staining with 0.02% (w/v) acridine orange.

3.5.1 Evaluation of zoospore formation

The influence of PAHs on formation of zoospores was assessed using all 6 PAHs listed in **Table 3**, where the C_{exp} of each PAH was indicated. The assessment was done by quantifying the number of zoospores formed in organic solutions (sterilized lake water) either containing each PAH or not. For the assessment in the presence of PAH-degrading bacteria, a 10-fold dilution of bacterial cells ($OD_{600 \text{ nm}} = 1.5$) in each solution used above was prepared and used for zoospore formation. The number of zoospores was quantified with the counting chamber after incubation at 25 °C for 10-12 h (see also **3.2.3**). Only two PAHs that showed the highest effect on zoospore formation were selected and used for further tests of their influence on zoospore chemotaxis and settlement.

3.5.2 Observation of zoospore chemotaxis

Chemotaxis of zoospores was observed either in presence or absence of PAH-degrading bacteria. For tests in the presence of bacteria, a 10-fold diluted suspension of bacterial cells ($OD_{600 \text{ nm}} = 1.5$) was mixed with the zoospore suspension. A set of polar solvents (acetone and ethanol) and DOC solutions (humic acid, root exudates and lake water) either containing PAH or not, was used for chemotactic assay of zoospores. The chemotactic assay was carried out by modified chemical-in-capillary method (Ortega-Calvo *et al.*, 2003). A 1- μL capillary tube (inside diameter = 0.20 mm and outside diameter = 0.66 mm) (Microcaps[®], Drummond, Broomall, PA, USA) was filled with the test solvents or solutions by capillary force. The filled capillary tube was subsequently inserted into a chamber that was filled either with zoospore or zoospore-bacterium suspension (**Fig. 15a**). Chemotactic responses of zoospores towards those prepared solvents or solutions were observed after incubating such preparations at 25 °C for 0.5-1 h and quantified by counting the number of zoospores encysted inside the capillary tubes. The assay was done at least in four replications.

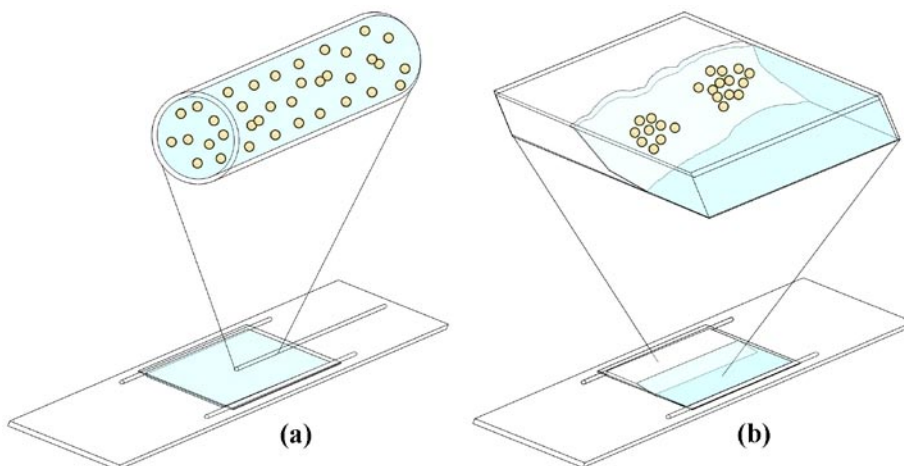


Figure 15 Schematic diagram of chemotaxis and settlement assays. The chemical-in-capillary method (a) was applied in chemotaxis assays. The chemotactic response of zoospores was quantified by counting directly the number of encysted zoospores inside the capillary tube filled with different test solutions. A chamber filled with different non-polar solvents (b) was prepared for observation of selective settlement by zoospores. The circles (yellow in online version) represent the encysted zoospores.

3.5.3 Observation of zoospore settlement

For the observation of zoospore settlement, non-polar solvents (HD and HMN) either containing PAH or not, were added into a chamber filled with the microbial suspensions (**Fig. 15b**). Both solvents formed a differentiated phase with water, and the interface constituted a substratum for zoospore settlement (**Fig. 15b**). Settlement of zoospores was observed either in presence or absence of PAH-degrading bacteria. For tests in the presence of bacteria, a 10-fold diluted suspension of bacterial cells ($OD_{600\text{ nm}} = 1.5$) was introduced in the zoospore suspension. The settlement behaviours within the chambers were also visualized with a phase contrast microscope connected with a colour video camera, using either normal light or fluorescence mode for tracking the position of microbial cells. The motion videos in the fluorescence mode were recorded after direct staining the chambers with 0.02% (w/v) acridine orange. Both light and fluorescence micrographs were taken from the video records processing by snapshot tool in Windows Movie Maker, Microsoft Windows XP. The side view of encysted zoospores germinated on different non-polar solvents was also observed using the chemical-in-capillary method, where the capillary tubes were filled with HD or

HMN. The micrographs derived from the last experiment were also taken and processed by the same protocol described before.

3.6 Mineralization of PAHs under bioavailability restrictions

3.6.1 Preparation of NAPL

The NAPL was constituted by heavy fuel oil (see also **3.1.1**) mixed with HMN at a ratio 1:1 (w/v), to reduce its viscosity. The ^{14}C -labelled phenanthrene (see also **3.1.1**) was dissolved in the NAPL at an approximate final concentration of 50,000 dpm mL⁻¹. The mixture was shaken at 120 rpm for a few hours to allow the homogenization of ^{14}C -labelled phenanthrene in the NAPL.

3.6.2 Preparation of microbial biomass

M. gilvum VM552 was used in the experiments as PAH-degrader. It was prepared as described previously (see also **3.2.4**). The initial cell density of this bacterium was adjusted at OD_{600 nm} = 1, and 1 mL of this bacterial suspension was introduced into a biometer flask containing 70 mL of sterilized lake water, giving the final cell density of 10⁶ cell mL⁻¹ in this system.

The impact of oomycetes on bacterial mineralization of PAHs initially present in a NAPL was evaluated using two oomycete species (*Py. aphanidermatum* and *Py. oligandrum*). Either sole oomycete mycelia (see also **3.2.2**) or mycelia grown on DV8 agar (see also **3.2.3**) were introduced in the biometric system prepared above (**Fig. 16**). Both types of oomycete biomass were prepared by considering the same growing area (20 cm²) of the oomycetes either grown on DV8 (for mycelia grown on DV8 agar) or V8 (for sole mycelia) agars. This growing area was cut into separated pieces with an area of 1 cm² each, and the whole 20 pieces of oomycete biomass were introduced into the biometer flask. The differences of biomass dry weight and capability to form zoospores of each oomycete species present in the biometric systems were evaluated.

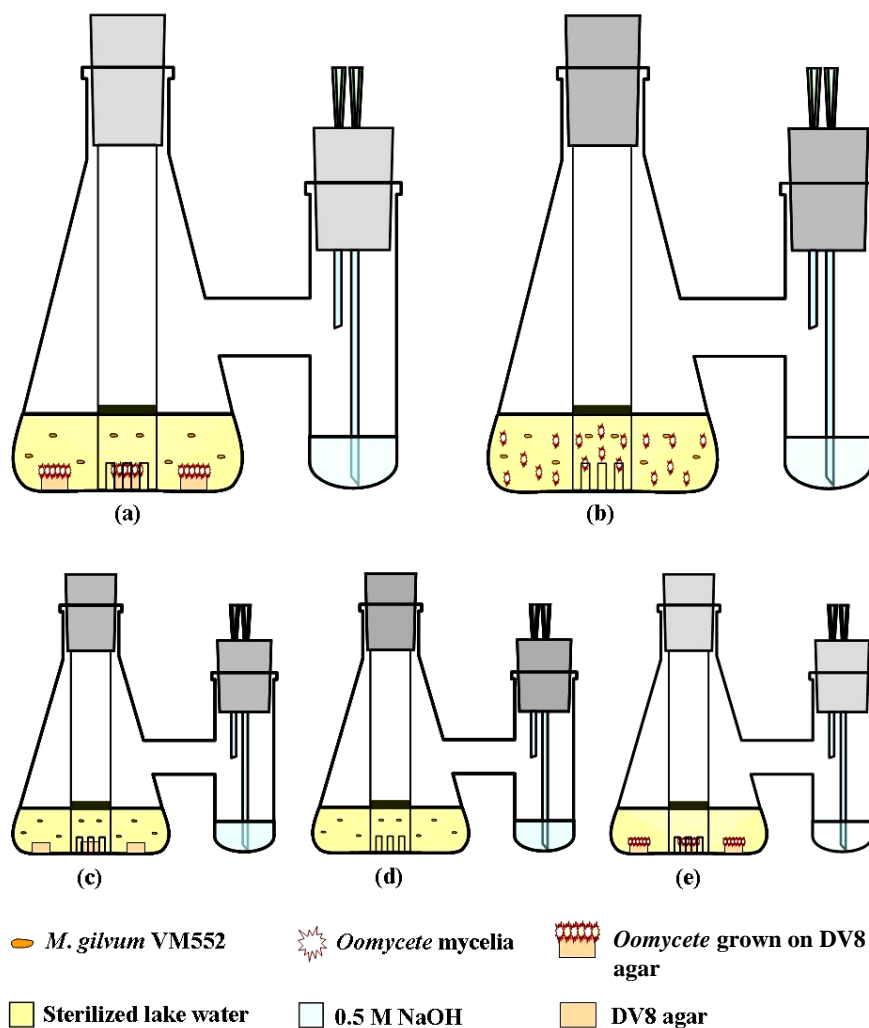


Figure 16 Set-up diagram of mineralization experiments. Five different sets of the experiments including the presence of bacteria and oomycete grown on DV8 agar (a), bacteria and oomycete mycelia (b), bacteria and DV8 agar (c), bacteria without any supplements (d) and a control of oomycete grown on DV8 agar (e), were prepared (see also 3.6 for the detailed procedures).

3.6.3 Set-up for radiorespiratory assays

The radiorespiratory assay was performed in biometer flasks following the protocol described by Tejada-Agredano *et al.* (2011). Briefly, a biphasic system of NAPL-water was installed by introducing the NAPL (see also 3.6.1) inside an open-ended glass tube ($\text{\O} = 2$ cm, 10 cm length, four slots in the base) upon the aqueous solution of 70-mL sterilized lake water **Fig. 16**. Respiration was determined by trapping $^{14}\text{CO}_2$ with 1 mL of 0.5 M NaOH. No significant loss of $^{14}\text{CO}_2$ was expected during the mineralization experiments, as all biometer

flasks were sealed with Teflon-lined closures. The trapped radioactivity was measured by the LS 6500 Scintillation Counter (BECKMAN COULTER, USA). The experiments were performed under aerated (shaking reciprocally at 80 rpm) and static conditions and incubated at 25 °C. The experiments were done at least in duplicate.

3.7 Metabolic evaluation of PAHs in mineralization experiments

3.7.1 Calculation of mineralization rate

The maximum mineralization rate was calculated as the slope of the linear regression line for at least five successive points of the mineralization curve for the approximate time period of 300-400 h. The total concentration of phenanthrene dissolved in the NAPL (1 g of fuel oil:HMN (1:1 w/v)) was 210 $\mu\text{g mL}^{-1}$, and therefore 1 dpm of ^{14}C -labelled phenanthrene corresponded to approximately 4.2 ng of the total phenanthrene.

3.7.2 Measurement of end-point mass balance of [^{14}C]

At the end of mineralization experiments, the NAPL was removed from each biometer flask, where the whole solid phase in the biometric system was separated from the whole liquid phase by centrifugation at 4303 $\times g$ for 10 min. The solid phase was broken down roughly by sterilized spatula, and was suspended with a known volume of sterilized distilled water. The suspension was then sonicated for 1 h in a sonicator bath (Branson 3510) and homogenized with a vortex for a few min. Radioactivity was determined in both solid and liquid phases with the scintillation counter. The percentages of ^{14}C accumulated in the solid phase and ^{14}C dissolved in liquid phase were calculated using the radioactivity data. These percentages were compared with the percentages of ^{14}C mineralized ($^{14}\text{CO}_2$ recovered in the trapping system), and ^{14}C remained in the NAPL phase that was calculated by the difference.

3.7.3 Analysis of residual NAPL

The residual NAPL collected from each biometer flask (**Fig. 16**) was analyzed for its composition of hydrocarbons. The NAPL sample was dissolved in dichloromethane, which was later dried over Na_2SO_4 and concentrated to 5 mL. A 0.5-mL aliquot of this suspension was used for gravimetric analysis. The fractions of either saturated or aromatic hydrocarbons in the aliquot were then processed with column chromatography following the US-EPA

method 3611b, using gas chromatography-mass spectrometry (GC-MS) as described by Vila and Grifoll (2009). Briefly, *o*-terphenyl was used as internal standard. Degradation percentages of alkanes were determined by comparing the hopane-normalized data from reconstructed extracted-ion chromatograms (ion m/z 85), obtained from the saturated fractions. The $17\alpha(H),21\beta(H)$ -hopane was used as a conserved internal marker, detected by the extracted-ion chromatograms (ion m/z 191). The 16 US-EPA PAHs (**Table 1**) and some of their alkyl derivatives were analyzed from reconstructed ion chromatograms of the aromatic fractions obtained by using correspondent molecular ions, and were quantified by the standard calibration curves derived from non-substituted PAHs (Kostecki and Calabrese, 1992). The analyses were performed using the samples obtained from triplicate biometric flasks.

3.8 Characterization of microbial colonization at NAPL-water interface

3.8.1 Observation of NAPL-surface topography

The shape of NAPL drops in contact with the water phase was considered in relevant for the microbial activity at the NAPL-water interface. The shapes of NAPLs (side view) in biometer flasks established for mineralization experiment were photographed (**Fig. 17**), and the NAPL-water contact angle (θ_{nw}) was measured (**Fig. 18**) with a protractor. Conceptual observation of the contact angle was performed following the theory described by Grate *et al.* (2012). The variation of this contact angle according to the time scale of the experiment was proposed here as a factor influenced by the surface tension and wettability of NAPL in contact with water phase, which has further relevance in the kinetics of chemical exchange between NAPL and water phase. The interconnections between the contact angle and either biofilm formation or microbial mineralization of PAHs were also addressed and discussed.

3.8.2 Observation of biofilm formation

The microbial consortium developed at the NAPL-water interface installed in the biometer flask of the mineralization experiments was observed directly and photographed, aiming to compare the change of surface roughness caused by microbial colonization across different treatments (**Fig. 16**) and conditions (see also **3.6.3**) achieved during mineralization experiments. This microbial consortium was considered as a biofilm at the NAPL-water interface, which was photographed from the bottom of the biometer flask (**Fig. 17**). At the

end of the mineralization experiments, the biofilms were sampled directly from the NAPL-water interfaces with a transfer loop and stained with 0.02% (w/v) acridine orange. The stained biofilm was then observed with a phase contrast microscope under fluorescence mode, connected with a photo camera (Photometrics CoolSNAP™). Micrographs were photographed and processed with RS Image Version 1.9.2 (Roper Scientific, Inc.).

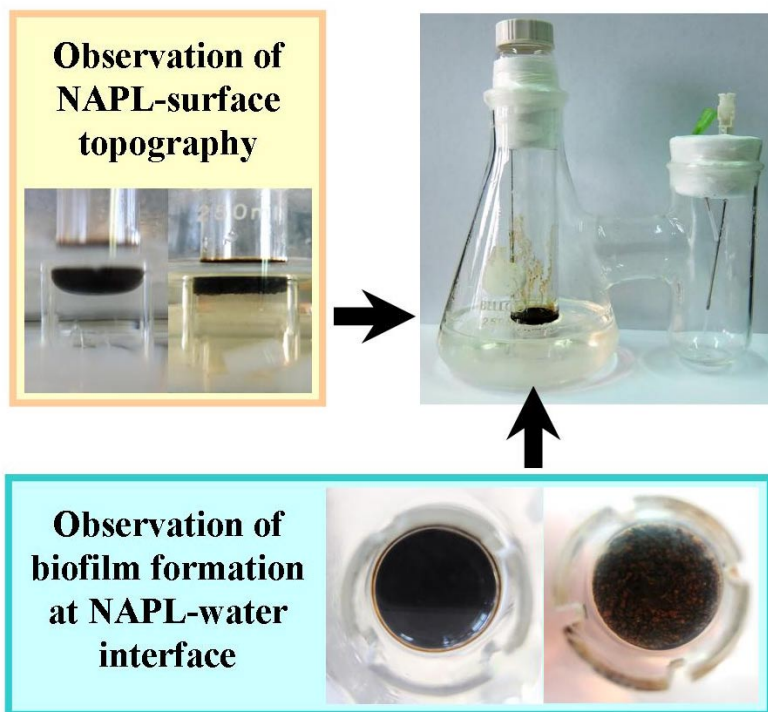


Figure 17 Observations of NAPL-surface topography and biofilm formation at NAPL-water interface. The arrows show the viewing directions of such observations.

3.9 Analysis of abiotic influences in mineralization experiment

3.9.1 Measurement of dissolved oxygen (DO)

A set of experiments that imitate the conditions achieved during mineralization experiments (**Fig. 16**) was established in the absence of NAPL. Variation of DO values in the water phase of the biometric systems influenced either by different oomycetes or by operating conditions

(aerated and static) was measured according to a time scale of incubation using an oxygen meter (OXI 45 DL, CRISON). The biometric systems prepared with adding the sterilized lake water alone were used as controls. The experiments were done at least in duplicate.

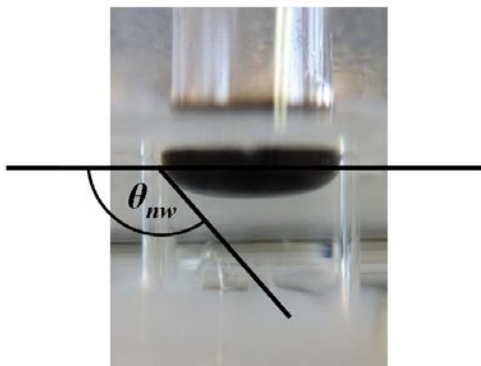


Figure 18 Determination of contact angle (θ_{nw}) of NAPL in contact with water phase.

3.9.2 Measurement of TOC

A set of experiments that imitated the conditions of the mineralization experiments (**Fig. 16**) was established either with or without the NAPL. The variation of TOC values, as influenced either by different oomycetes or by operating conditions (aerated and static), was measured with time. These TOC values were proposed as DOC within the biometric systems. TOC was measured using Shimadzu TOC-VCSH with ASI-V auto sampler after filtration through Whatman[®] No. 1 (pore size, $\varnothing = 11 \mu\text{m}$). The biometric systems prepared with sterilized lake water only were used as controls. All the measurements of TOC were done at least in duplicate.

3.10 Determinations of motility and cell size of PAH-degrading bacteria

3.10.1 Determination of bacterial motility

The motility levels of *P. putida* G7 cells, determined by their swimming speed, were affected by the growth phases (see also **3.2.4**). Briefly, swimming cells of *P. putida* G7 were collected by centrifugation at $1108 \times g$ after growing the bacterium in TSB at $30 \text{ }^\circ\text{C}$ for 12 h

(exponential phase) and 96 h (stationary phase). The bacterial cells were washed twice and re-suspended in sterilized lake water. Cell density of this bacterial suspension was adjusted to $OD_{600\text{ nm}} = 1.5$ and used for motion analysis accordingly. The motility of *P. putida* G7 cells was studied with a phase contrast microscope connected to a colour video camera. The video records were processed by the Windows Movie Maker. A time length of 5.54 s of the video records was cut and used for motion analysis. The longest swimming paths of bacterial cells were randomly selected, and their swimming speeds (in $\mu\text{m s}^{-1}$) were analysed with the CellTrak program (version 1.5, Motion Analysis Corporation, Santa Rosa, CA, USA). An average of all speeds computed was determined as global speed, and was indicated elsewhere with the population number (N) of bacterial cells analysed.

3.10.2 Cell size determination

Non-flagellated cells of *M. gilvum* VM552 and *P. putida* G7 cells from two different growth phases (as indicated in 3.10.1) were used for the cell size measurement. The cell size determined with means of length, breadth and length/breadth (L/B) ratio was used to characterize the bacterial physiology. The size was measured by image processing with snapshot tool in the Windows Movie Maker, using the video records taken from phase contrast microscope connected with a video camera as described in 3.10.1. Population number (N) of bacterial cells measured was indicated with the averages of length, breadth and L/B ratio in each bacterial population mentioned above.

3.11 Evaluation of bacterial mobilization by zoospores

3.11.1 Evaluation of zoospore chemotaxis

Modified chemical-in-capillary method was adapted from Ortega-Calvo *et al.* (2003) and used for testing the zoospore chemotaxis. The method was carried out for both qualification and quantification of zoospore chemotaxis towards different concentrations (5, 10, 20, 40, 60, 80 and 100% (v/v)) of a zoospore attractant (ethanol) diluted by the sterilized lake water. The modification of capillary assay was an enlargement of the chamber volume by using 50- μL capillary tubes (inside diameter = 0.80 mm and outside diameter = 1.09 mm) (Microcaps, Drummond, Broomall, PA, USA) as the arms of the chamber (**Fig. 19**). This chamber could have holding capacity up to 600 μL of zoospore suspension. The filled chamber was inserted by 1- μL capillary tubes either filled with zoospore attractant or sterilized lake water (control)

without heat end-sealing. The solutions were filled into the capillary tubes by capillary force, which were then inserted directly into the prepared chamber. The total length (32 mm) of these capillary tubes was divided into 4 parts where $\sim\frac{1}{4}$ of the capillary tube was inserted into the chamber filled with zoospore suspension. The zoospores entering inside the capillary tubes were determined as a positive chemotactic response as compared to the control. Encystment of zoospores after performing the chemotactic response was able to be observed during an hour after the insertion of the test capillary tubes. Therefore, the number of encysted zoospores inside the capillary tube was counted after incubating the assay at 25 °C for approximately 1 h. The count was done under a light microscope, where the length of capillary tubes containing encysted zoospores was estimated for determining the chemotactic reaction. The experiments were done at least in triplicate. The lowest concentration of zoospore attractant that showed chemotactic attraction by zoospores was chosen for use in any required experiments throughout this thesis.

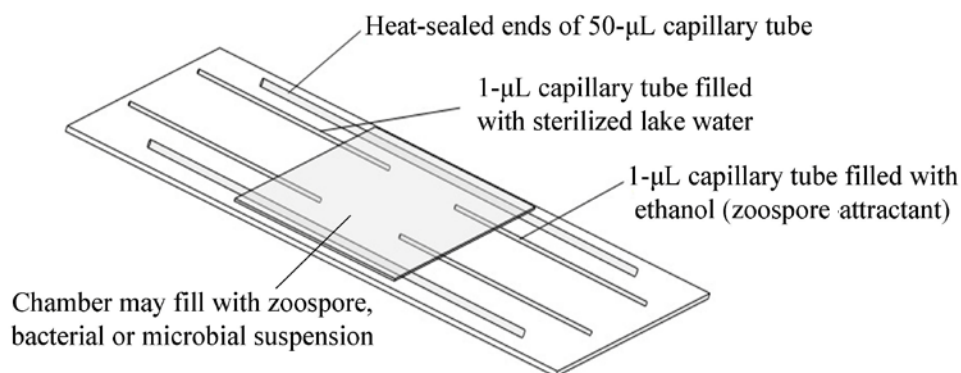


Figure 19 Modified chemical-in-capillary method for chemotaxis and biomobilization assays in this thesis.

3.11.2 *Biomobilization assay*

The chemotactic behaviour of zoospores was evaluated as a mechanism for mobilization of PAH-degrading bacteria. The modified chemical-in-capillary method as described previously was used for testing the mobilization of bacterial cells by zoospore chemotaxis. The bacterial suspension (control, without zoospores) or microbial mixture of zoospores and bacterial cells was filled into the enlarged chamber (**Fig. 19**). The microbial mixture was prepared by removing 1 mL from 10-mL zoospore suspension, and replacing with 1 mL of bacterial

suspension in the sterilized lake water prepared as described previously. The initial cell density of each bacterium used in this assay was adjusted at an $OD_{600\text{ nm}} = 1.5$, while the final cell density was approximately 10^9 CFU mL^{-1} and 10^7 CFU mL^{-1} for *P. putida* G7 and *M. gilvum* VM552, respectively. The prepared chambers were inserted with 1- μL capillary tubes filled with either the zoospore attractant or sterilized lake water as controls (**Fig. 19**). The experimental sets were incubated at 25 °C for approximately 1 h. The encysted zoospores in the capillary tubes (encysted zoospores μL^{-1}) were counted under a light microscope to ensure the chemotactic response of zoospores. The assayed capillary tubes were taken out of the chamber and cleaned their outer wall three times with sterilized distilled water. The whole liquid volume (1 μL) inside each capillary tube was transferred by pumping into a known volume of sterilized lake water, which was later diluted serially with the same solution. The number of bacterial cells entering into the capillary tube (CFU μL^{-1}) was quantified after spreading the appropriate dilution prepared previously on TSA supplemented with 0.3 g L^{-1} of cycloheximide (Sigma-Aldrich, Germany). The experiments were done at least in triplicate.

3.11.3 Determination of biomass flow

In order to discriminate the mobilizing efficiency of bacterial biomass caused by zoospores from the hydraulic influence of fluid flowing continuously through open-end capillary tubes, we determined here the spontaneous flow rate of fluid caused by either capillary force or aqueous evaporation. Flow velocity (u) of *M. gilvum* VM552 cells flowing through capillary tubes filled with zoospore attractant was tracked as a represent spontaneous flow velocity (u_0) of fluid body flowing through the capillary tubes. The experimental set-up was prepared as same as the biomobilization assay, which was incubated at 25 °C for approximately 10 min to allow the steady fluid flow. Motion videos of the flowing cells were recorded, which were then processed by the Windows Movie Maker as described previously (see also **3.10.1**). The u_0 was an average of flow velocities derived from ten bacterial cells randomly selected along the different periods of time record. The flow velocities were computed by the CellTrak program. This u_0 was used further to estimate the mobilizing efficiency and the biomass flow velocity, caused by zoospore chemotaxis. The u_0 was considered based on the theory of steady flow of fluid dynamics as described by equation (**v**), where u is the flow velocity and t is the time detected that u .

$$\frac{\partial u}{\partial t} = 0 \quad (\text{v})$$

The mobilizing efficiency refers to a mobilizing rate (R) of bacterial cell density mobilized in 1 s (cells $\mu\text{L}^{-1} \text{s}^{-1}$), considering that a CFU was developed from a bacterial cell. It was calculated by equation (vi), where CFU_{u_z} is the bacterial CFU μL^{-1} mobilized in the presence of zoospores and zoospore attractant, CFU_{u_o} is the bacterial CFU μL^{-1} mobilized at the u_o , N_z and N_o are the numbers of encysted zoospores counted in the presence and absence of zoospore attractant, respectively, and t is the incubation time of the biomobilization assay (~3600 s).

$$R = \frac{\text{CFU}_{u_z} - \text{CFU}_{u_o}}{(N_z - N_o) \cdot t} \quad (\text{vi})$$

The biomass flow velocity of bacterial cells due to the zoospore chemotaxis (u_z) was calculated by equation (vii), where the parameters were described elsewhere above.

$$u_z = u_o \cdot \left(\frac{\text{CFU}_{u_z}}{\text{CFU}_{u_o}} \right) \quad (\text{vii})$$

3.12 Observation of zoospore swimming behaviour

3.12.1 Observation of intrinsic swimming behaviour

The observation was done the same as described for motility analysis of *P. putida* G7 (see also 3.10.1). Preparation of zoospores was described in 3.2.3. The motion records with a length of 5.54 s were prepared for motion analysis with the CellTrak program, where the swimming trajectories, speed and rate of change of direction (RCDI) were computed. Ten representative zoospores were selected randomly for displaying their swimming trajectories. The global speed in $\mu\text{m s}^{-1}$ and the global RCDI in degree of turning even per second (deg s^{-1}) were reported with the population number (N) of zoospores analysed.

3.12.2 Evaluation of interactive motility between zoospores and bacteria

The observations were done under the microscope connected with video camera as described previously (see also 3.10.1 and 3.12.1). The motion records of swimming zoospores alone or with bacterial cells were processed as same as described in 3.12.1. The preparation of zoospores and bacteria was described elsewhere of this article. The motion records with a length of 5.54 s were prepared, where zoospores or *P. putida* G7 cells swimming at least for 5.00 s were randomly selected for motion analysis by the CellTrak program. Swimming trajectories of both zoospores and *P. putida* G7 cells were tracked, while their speed and RCDI were computed. The trajectory diagrams were created by randomly selecting the representative zoospores or *P. putida* G7 cells. The global speed and the global RCDI were reported with the population number (N) of zoospores and bacterial cells analysed.

3.13 Analysis of cellular interaction between zoospores and bacteria

3.13.1 Evaluation of bacterial adhesion on surface of zoospores

We hypothesized that the size of zoospores in the presence of bacterial cells might be influenced by bacterial adhesion. We assumed that if the bacterial cells adhered to the surface of zoospores, the apparent size of zoospores should increase. Therefore, the size of zoospores in the presence of bacterial cells was measured according to the protocol described in 3.10.2. A 10-fold dilution of bacterial cells ($OD_{600\text{ nm}} = 1.5$) suspended in sterilized lake water was prepared for zoospore production (see also 3.2.3).

3.13.2 Observation of bacterial chemotaxis towards encysted zoospores

Chemotaxis of *P. putida* G7 towards encysted zoospores was also evaluated as a possible mechanism that could influence bacterial mobilization. The modified chemical-in-capillary method (**Fig. 19**) was carried out in two steps for this evaluation. First, the chamber was filled with a zoospore suspension, and the capillary tube filled with the zoospore attractant was inserted into the chamber and incubated at 25 °C for 1 h. The zoospores were allowed to respond chemotactically to their attractant and then encysted inside the capillary tube. Number of encysted zoospores inside the capillary tube was counted to ensure the chemotactic response of zoospores towards their attractant. Second, the capillary tube from the first step was transferred and inserted into a second chamber filled with a bacterial

suspension (a 10-fold dilution of bacterial cells ($OD_{600\text{ nm}} = 1.5$), see also **3.2.4**). Only *P. putida* G7 cells collected at the exponential phase of growth (reported with actively motile by Jimenez-Sanchez *et al.* (2012)) were used in this experiment (see also **3.10.1**). The chamber was incubated at the same condition as the first step of the assay. The bacteria swimming into the capillary were quantified by CFU developed on TSA supplemented with 0.3 g L^{-1} cycloheximide. The experiments were done at least in triplicate. Difference in numbers of bacteria counted in the absence and presence of encysted zoospores was compared and considered the chemotactic reaction of bacterial cells.

3.14 Statistical analysis

Comparison of multiple means with standard deviations (SDs) were performed with the SPSS 16.0 computer program (SPSS, Chicago IL, USA), with one-way analysis of variance (ANOVA) and Tukey's *post hoc* tests at different significant levels indicating separately for each comparison. To avoid artifacts from data selection, the population number (N) of each dataset for the calculation of mean \pm SD or mean \pm standard error (SE) was not lower than 30 individuals. This N was determined elsewhere together with its respective mean and SD or SE together with its appropriate statistical value of *F*-distribution by ANOVA, while SE was calculated by equation (viii).

$$SE = \frac{SD}{\sqrt{N}} \quad (\text{viii})$$

CHAPTER IV: RESULTS

4.1 Ecological interaction between eukaryotic zoospores and PAH-degrading bacteria in PAH-polluted scenarios

4.1.1 Optimal condition for zoospore formation

We found that sterilized lake water was an optimal solution for zoospore formation of *Py. aphanidermatum*, as compared with the other solutions tested (Fig. 20). With this optimal solution, the oomycete gave the highest number of zoospores after incubation for 6 h. Therefore, sterilized lake water was selected and used for zoospore formation throughout this thesis.

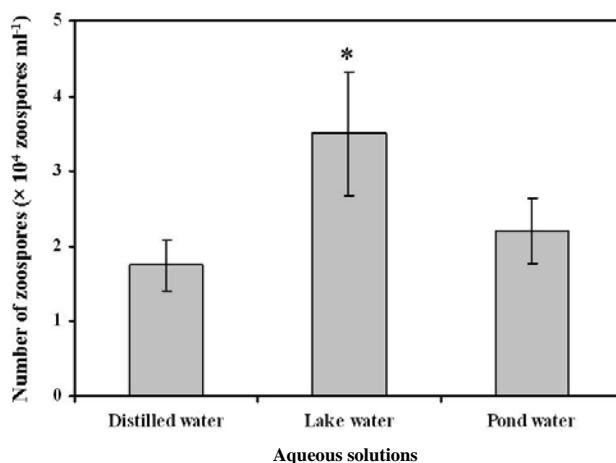


Figure 20 Zoospore formation of *Py. aphanidermatum* in different aqueous solutions. Ten pieces of 1 cm^2 hyphal mat of the oomycete growing on DV8 agar were used for this test. Number of zoospores counted after 6 h of incubation was significantly highest in sterilized lake water ($F_{(2,9)} = 10.078$, $P = 0.05$). The graph was plotted by means of zoospore numbers with error bars of SDs, derived from triplicate experiments. Asterisk refers to a statistical difference of means compared by ANOVA.

Furthermore, we investigated the influence of the size of hyphal mat on formation of zoospores by the oomycete, using the sterilized lake water. With this aim, zoospores were formed faster when using 1 cm^2 hyphal mat, compared to the one with smaller in size (0.8

cm²) (**Fig. 21**). However, the numbers of zoospores formed with both sizes of hyphal mats increased according to the incubation time.

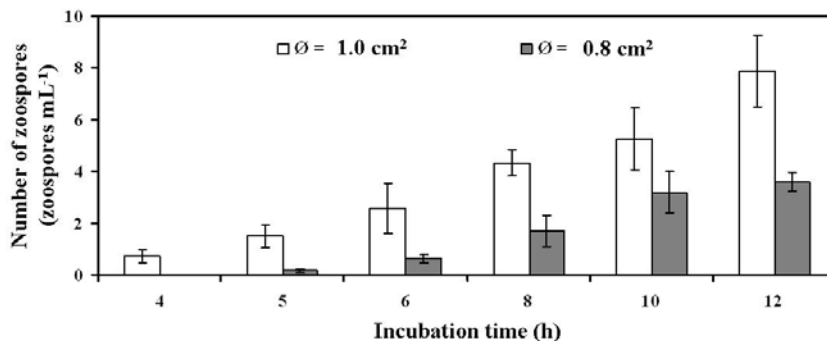


Figure 21 Zoospore formation of *Py. aphanidermatum* in lake water. Two different sizes of hyphal mat of *Py. aphanidermatum* growing on DV8 agar (1.0 cm² per each; with the total area of 10 cm² and 0.8 cm² per each; with the total area of 16 cm²) were tested for formation of zoospores. The graph was plotted by means of zoospore numbers with error bars of SDs, derived from triplicate experiments.

4.1.2 Antagonistic effects among oomycetes and PAH-degrading bacteria

The possible antagonistic effects of PAH-degrading bacteria (*M. gilvum* VM552 and *P. putida* G7) on filamentous growth and zoospore formation in oomycetes (*Py. aphanidermatum* and *Py. oligandrum*) were evaluated. Both effects were not observed when the tests among any bacteria and any oomycetes were performed (**Figs. 22** and **23**). The effects on filamentous growth of oomycetes were not different, even tested on different solid agars (TSA and DV8 agar). It was convinced that zoospores were not found in any tests with *Py. oligandrum*. Interestingly, *P. putida* G7 cells moved out from the colony and along the mycelia of the both oomycetes grown on TSA (**Figs. 22** and **23**). In addition, dense growth of *Py. aphanidermatum* mycelia were observed only over *M. gilvum* VM552 biomass that developed on DV8 agar (**Fig. 23b**). The number of zoospores produced by *Py. aphanidermatum* (**Fig. 23**) was decreased significantly in the presence of both bacterial cells only at the highest cell densities. Moreover, the decrease of zoospore number fromed in the presence of *M. gilvum* VM552 (10^8 cells mL⁻¹) (**Fig. 23c**) was observed after co-incubation with the oomycete for 6 h ($F_{(5, 18)} = 11.266$, $P = 0.01$). While such decrease in the presence of *P. putida* G7 (10^{10} cells mL⁻¹) (**Fig. 23f**) was observed after co-incubation with the oomycete for either 4 ($F_{(5, 18)} = 18.185$, $P = 0.01$) or 6 h ($F_{(5, 18)} = 14.985$, $P = 0.01$).

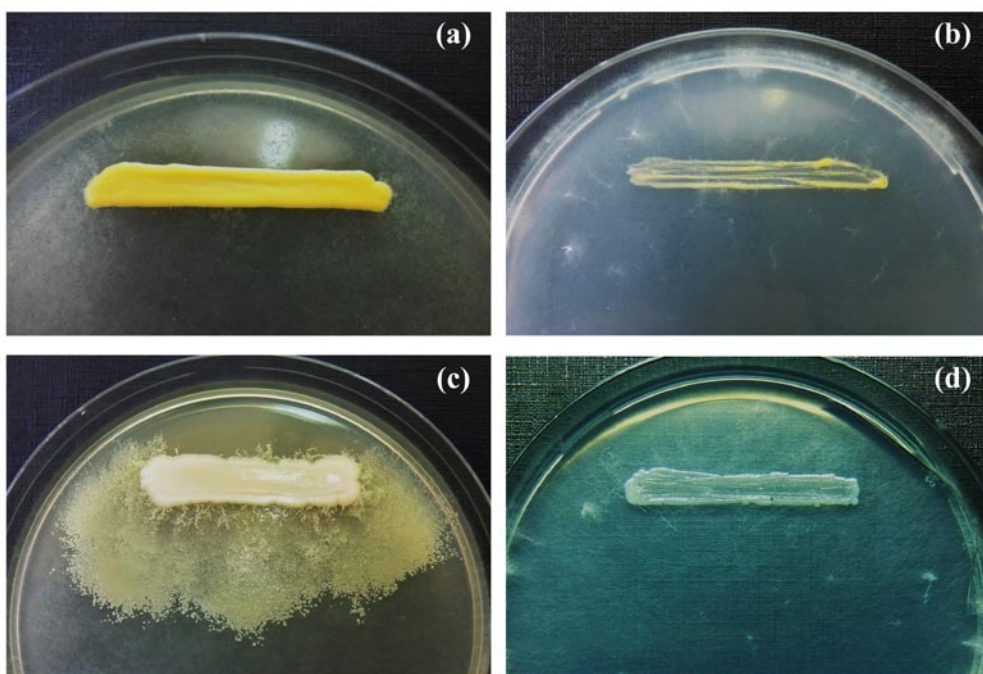


Figure 22 Antagonism tests among *Py. oligandrum* and PAH-degrading bacteria. The antagonistic activities of *M. gilvum* VM552 (a, b) and *P. putida* G7 (c, d) against mycelial growth of the oomycete on TSA (a, c) and DV8 agar (b, d) were tested by dual culture technique (see also **CHAPTER III**).

4.1.3 Zoospore formation

The number of zoospores formed by *Py. aphanidermatum* was used as an indicator of toxicity caused by individual PAH in the absence and presence of PAH-degrading bacteria (**Fig. 24**). The toxic influence was different according to each PAH. A negative correlation with the estimated C_{exp} of PAH was observed. Toxicity followed the order: naphthalene (91.67 ± 3.21 %) \geq phenanthrene (84.72 ± 2.78 %) = fluorene (73.61 ± 6.99 %) \geq fluoranthene (66.67 ± 4.54 %) $>$ pyrene (43.06 ± 18.36 %) = anthracene (20.83 ± 15.96 %), where % refers to the percentage of reduction in zoospore formation. The C_{exp} values of these PAHs are shown in **Table 3**. In the absence of PAH, neither *M. gilvum* VM552 nor *P. putida* G7 cells influenced the zoospore formation ($F_{(2, 10)} = 3.520$, $P = 0.05$). We also observed that both PAH-degrading bacteria diminished the toxic influence of all PAHs. However, this suppression was found at different levels, where *M. gilvum* VM552 was a greater detoxifier in phenanthrene solutions ($F_{(2, 9)} = 132.346$, $P = 0.05$), and *P. putida* G7 was more efficient in naphthalene solutions ($F_{(2, 9)} = 51.066$, $P = 0.05$).

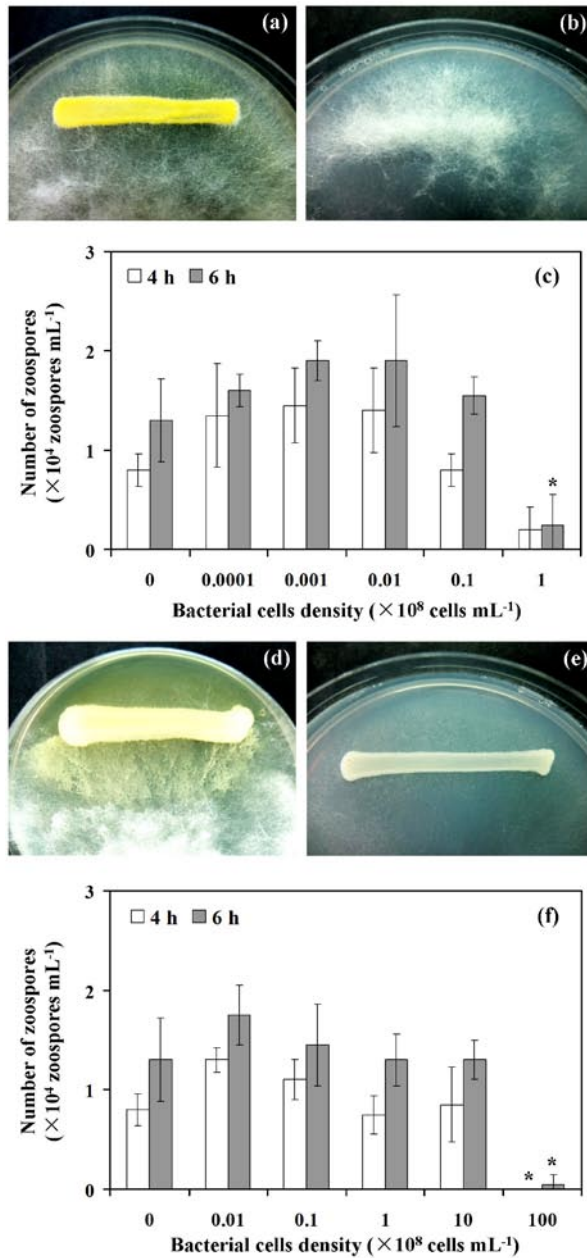


Figure 23 Antagonism tests among *Py. aphanidermatum* and PAH-degrading bacteria. The antagonistic activities of *M. gilvum* VM552 (a, b) and *P. putida* G7 (d, e) against mycelial growth of the oomycete on TSA (a, d) and DV8 agar (b, e) were tested by dual culture technique. The influence on the formation of zoospores by *M. gilvum* VM552 (c) and *P. putida* G7 (f) was evaluated with two different incubation periods (4 (empty bar) and 6 h (filled bar)) using the zoospore production protocol (see also **CHAPTER III**). The graphs were plotted by means of zoospore numbers with error bars of SDs, derived from triplicate experiments. Asterisks denote significant differences of means compared by ANOVA and Tukey's *post hoc* test at $P < 0.01$.

Both PAH-degrading bacteria showed equal level of toxic suppression with pyrene^{F1}, anthracene^{F2}, fluorene^{F3} and fluoranthene^{F4} ($F1-A_{(2,9)} = 11.466, 27.214, 19.840$ and $22.234, P = 0.05$). As naphthalene and phenanthrene showed the highest toxic influence on zoospore formation, they were selected for further studies of zoospore chemotaxis and settlement.

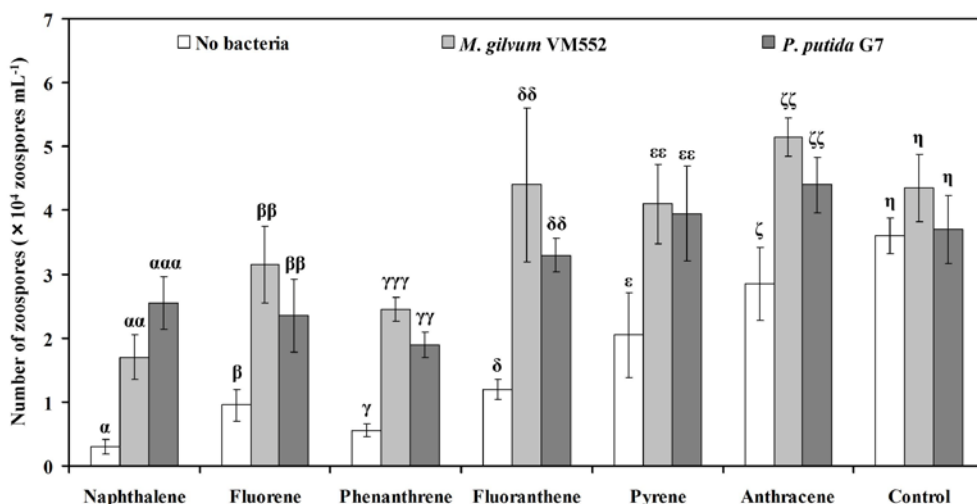


Figure 24 Influence of PAHs and PAH-degrading bacteria on zoospore formation of *Py. aphandermatum*. The number of zoospores formed after 10-12 h of incubation was used to determine toxicity of PAHs in the absence of PAH-degrading bacteria (empty bar) and presence of either *M. gilvum* VM552 (light grey bar) or *P. putida* G7 (dark grey bar) cells, compared to the control without PAHs. The graph was plotted by means of zoospore numbers with error bars of SDs derived from at least four-replicate experiments. Each Greek letter represents a statistical comparison of each PAH by ANOVA and Tukey's *post hoc* test, while a different number of letters refers to the significant differences of means \pm SDs.

4.1.4 Zoospore chemotaxis

Statistical comparison of zoospore chemotaxis resulted in four different levels of response (strong, medium, weak and less or no response) across all tests, which included measurements in the absence and presence of PAH-degrading bacteria, as well as different test solvents or solutions either containing naphthalene ($F_{(20, 107)} = 136.698, P = 0.01$) and phenanthrene ($F_{(20, 110)} = 100.652, P = 0.01$) or without PAH ($F_{(20, 116)} = 56.541, P = 0.01$) (**Fig. 25**). The estimated C_{exp} of each PAH in test solvents or solutions is given in **Table 2**.

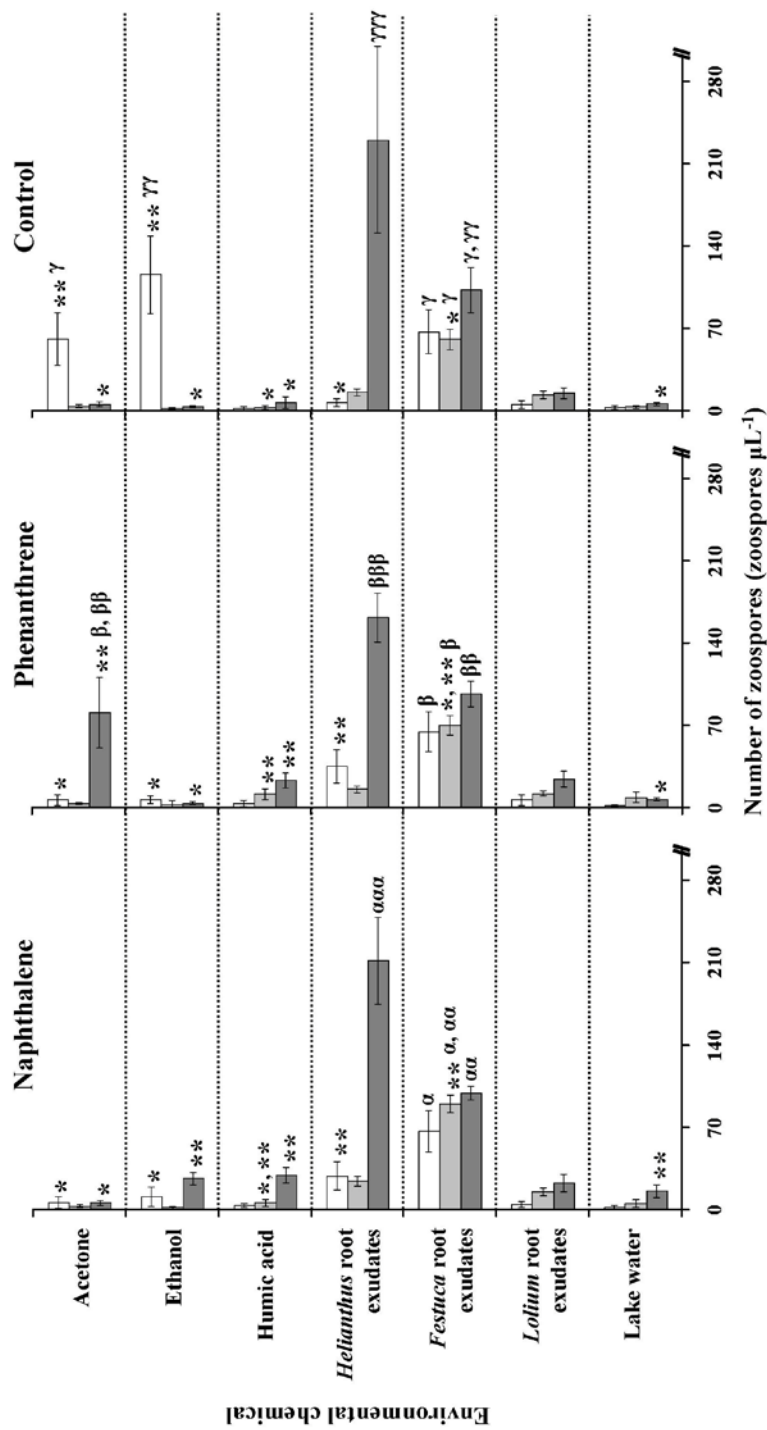


Figure 25 Chemotaxis of *Py. apphandermatum* zoospores toward different environmental chemicals including polar solvents (acetone and absolute ethanol), humic acid and root exudates of 3 plants representative in phytoremediation of PAHs: *Helianthus*, *Festuca*, and *Lolium*. The chemicals had either no PAH (control), or contained phenanthrene or naphthalene. Chemotactic responses were tested with zoospores only (empty bar) and in the presence of either *M. gilvum* VM552 (light grey bar) or *P. putida* G7 (dark grey bar) cells. All graphs were plotted by means with error bars of SDs derived from at least four-replicate experiments. Each Greek letter represents a statistical comparison by ANOVA and Tukey's *post hoc* test, vertically across all means \pm SDs present in each graph. Asterisks represent the statistical comparison of means derived from each test chemical horizontally among the graphs. Difference in number of either letters or asterisks refers to the significant difference of means \pm SDs compared, where the absence of both a letter and an asterisk indicates no chemotactic response.

In the absence of PAH (control) and PAH-degrading bacteria, zoospores exhibited a significant attraction toward polar solvents (acetone and ethanol) and *Festuca* root exudates. The attraction of zoospores toward the solvents was diminished in the presence of PAH-degrading bacteria, although the attraction for *Festuca* root exudates remained unchanged. Also, *P. putida* G7 slightly enhanced zoospore chemotaxis toward *Festuca* root exudates, while the greatest enhancement was found toward *Helianthus* root exudates. This strong attraction toward *Helianthus* root exudates mediated by the bacterium was also found with the root exudates containing naphthalene or phenanthrene (**Vid. 1(4.1)**), this video and the others that support section **4.1**, are available at <http://digital.csic.es/handle/10261/85538>). Similar observations of the chemotactic response toward the controls without PAH were also occurred in most tests that contained PAH but except for phenanthrene-containing acetone in the presence of *P. putida* G7 cells. Statistical comparisons performed horizontally across each environmental chemical confirmed that *P. putida* G7 cells enhanced significantly the positive chemotaxis of zoospores toward naphthalene-containing ethanol ($F_{(2, 10)} = 63.340$, $P = 0.01$) and lake water ($F_{(2, 9)} = 11.345$, $P = 0.01$), and also toward phenanthrene-containing acetone ($F_{(2, 9)} = 24.626$, $P = 0.01$) and humic acid ($F_{(2, 9)} = 15.514$, $P = 0.01$). Cells of *M. gilvum* VM552 enhanced the positive chemotaxis of zoospores only toward phenanthrene-containing humic acid ($F_{(2, 9)} = 8.601$, $P = 0.01$). Interestingly, in the absence of PAH-degrading bacteria, the attractive chemotaxis of zoospores toward acetone ($F_{(2, 20)} = 48.262$, $P = 0.01$) and ethanol ($F_{(2, 20)} = 95.614$, $P = 0.01$) was significantly diminished by the presence of PAHs. This was possibly due to the highest C_{exp} of PAH achieved in these solvents (**Table 4**). However, *Helianthus* root exudates that contained PAHs became significantly more attractive for zoospores than without PAHs ($F_{(2, 27)} = 29.654$, $P = 0.01$).

4.1.5 Zoospore settlement

We found that zoospores settled preferentially at the interface between water and hexadecane (HD) either containing PAH or not (**Fig. 26** and **Vid. 2(4.1)**). There was no difference among all replicate observations (experiments were performed at least in triplicate). This settlement could be clearly observed through the accumulative colonization of zoospores, followed by their encystment and germination after 1 h of incubation.

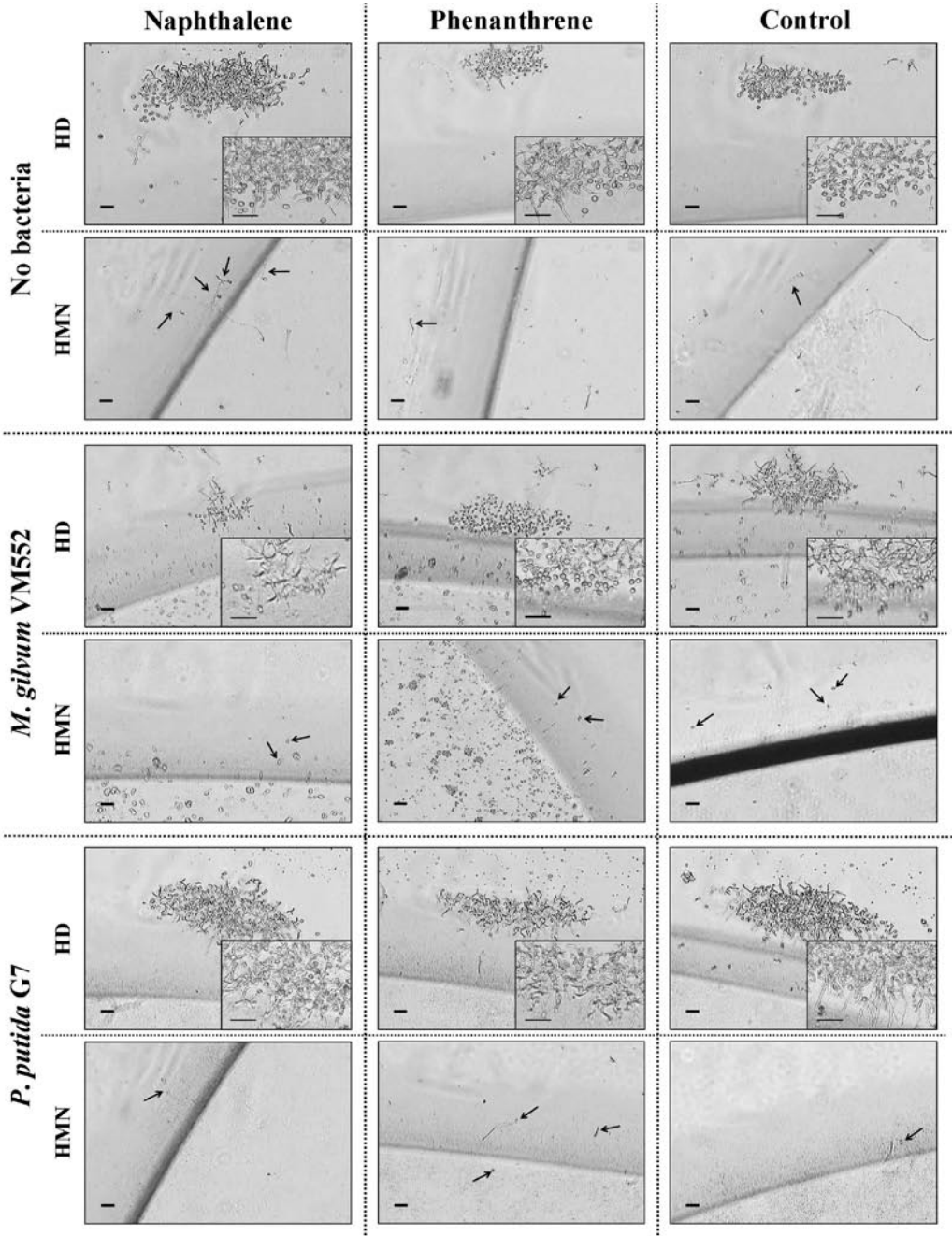


Figure 26 Settlement of *Py. aphanidermatum* zoospores in the absence and presence of PAH-degrading bacteria at the different pollutant-water interfaces. The substrata were prepared by HD or HMN either absence of PAHs (control) or containing with 0.1% (w/v) of naphthalene or phenanthrene. The arrows indicate the zoospores randomly touching or settling on the interfaces of water and either HMN alone or HMN containing with PAHs. Bars = 50 μ m.

In the presence of PAHs dissolved in the substrata (what lead to the lowest C_{exp} of PAH), PAH-degrading bacteria did not influence the zoospore settlement at the HD-water interface, while no zoospore settlement was observed between the interface of water and HMN (**Fig. 26**). The accumulation of PAH-degrading bacteria at the zoospore settlement areas was also observed (**Fig. 27a, b and Vid. 3(4.1)**). Interestingly, we observed that the germ tubes formed by encysted zoospores at the HD-water interface stabbed and extended directly into the hydrophobic layer of HD (**Fig. 27c, d, and Vid. 4(4.1)**). In addition, neither HD nor HMN was a carbon and/or energy source for growth of this oomycete (**Fig. 28**).

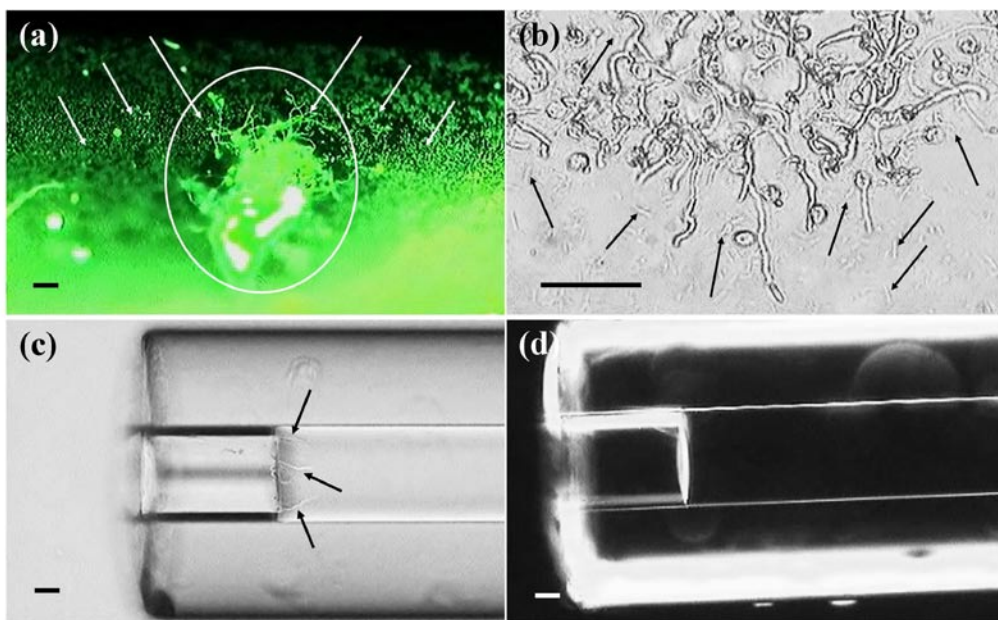


Figure 27 Co-settlement of *Py. apphanidermatum* zoospores with PAH-degrading bacteria at the HD-water interfaces. A fluorescence micrograph (a) showing *M. gilvum* VM552 cells (arrows, green particles) settled around and inside the germinated area (white circle) of encysted zoospores between the interface of water and HD-containing phenantrene. The micrograph was taken a few minutes later the direct staining with 0.02% (w/v) acridine orange. The enlarged scale of light micrograph (b) shows *P. putida* G7 cells (arrows) co-settled with germinated-encysted zoospores between the interface of water and HD-containing naphthalene. Side views of zoospores settlement at the HD-water (c) and HMN-water (d) interfaces were examined microscopically using the chemical-in-capillary method (see also **CHAPTER III**), where the zoospores encysted and germinated their germ tubes (arrows) only into the hexadecane layer (c). All observations were done at least in triplicate. Bars = 50 μm . All images were extracted from **Vids. 2-4(4.1)**.

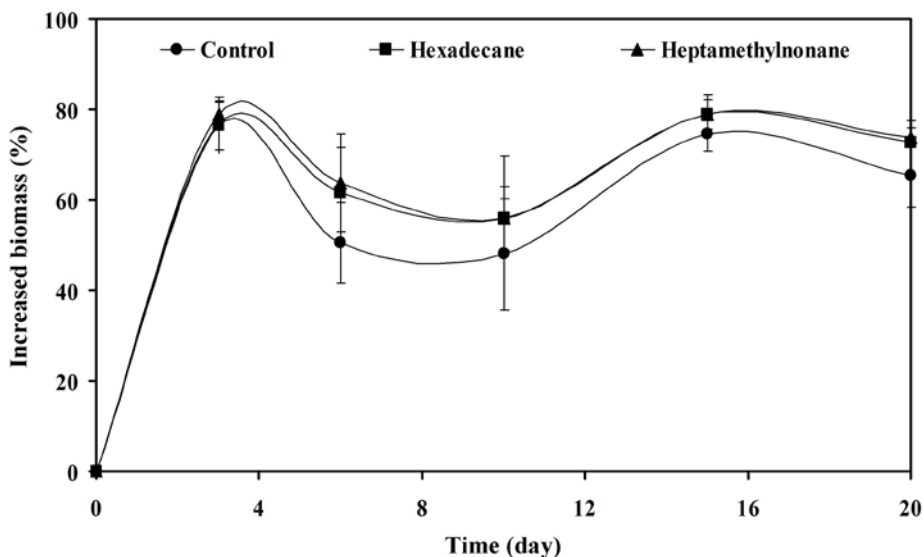


Figure 28 Growth of *Py. aphanidermatum* in the absence and presence of HD or HMN. Four plugs ($\varnothing = 0.8$ mm) of 4-day old hyphal mats of *Py. aphanidermatum* growing on DV8 agar (see also **CHAPTER III**) were inoculated in 20 mL of sterilized lake water supplemented with 1% (v/v) of HD or HMN. The oomycete growth was determined by measurement of the dry-weight biomass after drying in hot air oven at 55 °C for 3-4 days. The graphs were plotted by means of increased biomass (%) with error bars of SDs, derived from triplicate experiments. There were no significant differences of means compared by ANOVA and Tukey's *post hoc* test at $P > 0.001$. *F*-distribution values and significant levels derived from the statistical comparison of day 3, 6, 10, 15 and 20 were $F_{(2,6)} = 0.237$ ($P= 0.826$), 1.543 ($P= 0.305$), 0.486 ($P= 0.684$), 1.224 ($P= 0.414$) and 2.437 ($P= 0.168$), respectively.

4.2 Promoting microbial life at the interface of NAPL and water: a strategy to enhance biodegradation of sparingly bioavailable PAHs

To investigate further the role of oomycetes/bacteria interaction in the context of PAH bioremediation, we explored in the second part of this thesis the influence of two oomycetes (*Py. aphanidermatum* and *Py. oligandrum*) on biodegradation of PAHs initially present in a NAPL by *M. gilvum* VM552. The experiments were designed to create bioavailability restrictions through the association of the PAHs with a NAPL, which was composed by a mixture of heavy fuel and HMN. Mineralization activity of *M. gilvum* VM552 was estimated continuously through $^{14}\text{CO}_2$ production from ^{14}C -labelled phenanthrene dissolved in the NAPL, while its biodegrading capacity was measured with the end-point concentrations of PAHs in the NAPL by GC/MS.

4.2.1 Mineralization of NAPL-associated phenanthrene

The mineralization of ^{14}C -phenanthrene initially present in the NAPL under aerated conditions (through continuous shaking reciprocally at 80 rpm) is shown in **Fig. 29**. Different treatments, by adding oomycete mycelia and/or DV8 agar as a supplement, were tested for their effects on the mineralization activity of *M. gilvum* VM552. Mineralization curves in the presence of oomycete mycelia and/or DV8 agar were S-shaped, and the rates of mineralization were calculated from the slopes at exponential phase of the curves. The rates were highest in the presence of oomycetes grown on DV8 agar followed by the conditions where DV8 agar was solely the supplement (**Fig. 29** and **Table 5**).

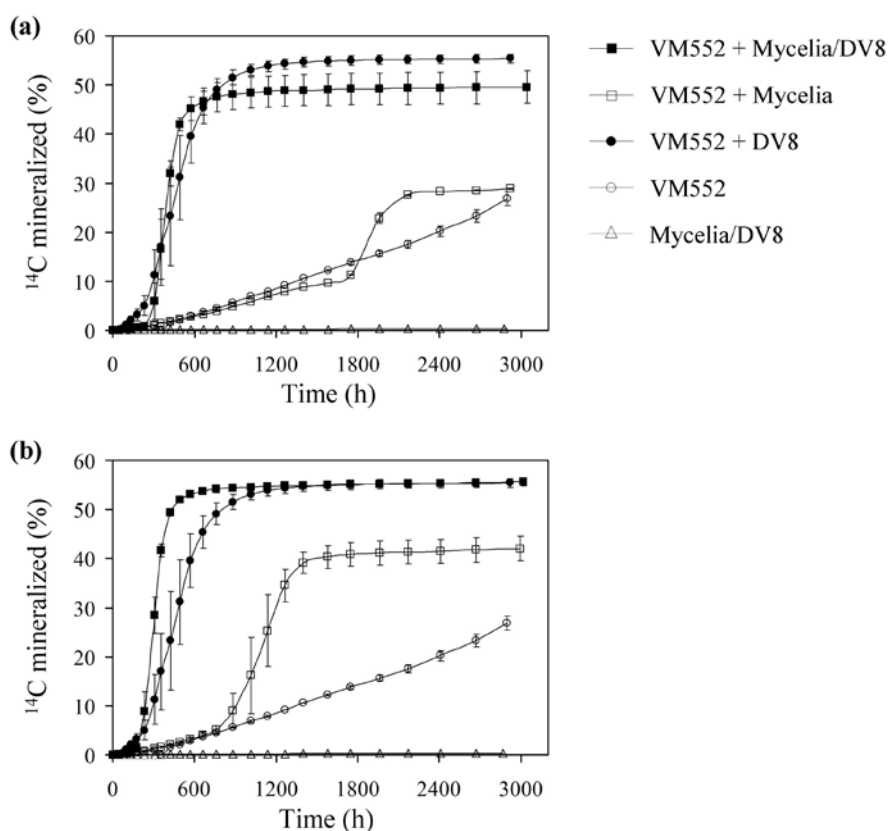


Figure 29 Role of oomycetes in mineralization of ^{14}C -phenanthrene associated to a NAPL by *M. gilvum* VM552 under aerated conditions. Two oomycetes were used, *Py. aphanidermatum* (a) and *Py. oligandrum* (b). The experiments were tested in the presence of the bacterial cells either without any supplements (VM552) or supplemented with DV8 agar (VM552 + DV8), oomycete mycelia (VM552 + Mycelia), or oomycete-growing DV8 agar (VM552 + Mycelia/DV8). A control without bacterial cells was constructed by adding solely oomycete-growing DV8 agar (Mycelia/DV8). The graphs were

plotted by means of ^{14}C mineralized (%) with error bars of SEs, derived from triplicate experiments. Mineralization by bacteria only (with and without DV8) is shown in both panels for better comparison.

Table 5 Role of oomycetes in bacterial mineralization of ^{14}C -phenanthrene associated to NAPL under aerated conditions

Oomycete	Treatment	Mineralization		
		Rate ($\text{ng mL}^{-1} \text{h}^{-1}$)*	Extent (%)*	Time (days)
None	VM552	$0.29 \pm 0.04\text{c}$	$26.84 \pm 2.03\text{c}$	121
	VM552 + DV8	$3.24 \pm 0.07\text{b}$	$55.45 \pm 1.53\text{a}$	122
<i>Py. aphanidermatum</i>	VM552 + Mycelia	$1.67 \pm 0.23\text{b,c}$	$28.91 \pm 0.19\text{c}$	122
	VM552 + Mycelia/DV8	$5.86 \pm 1.39\text{a}$	$49.59 \pm 5.74\text{a,b}$	127
<i>Py. oligandrum</i>	VM552 + Mycelia	$2.03 \pm 0.16\text{b,c}$	$42.01 \pm 4.33\text{b}$	125
	VM552 + Mycelia/DV8	$8.27 \pm 1.21\text{a}$	$55.59 \pm 1.28\text{a}$	126

Reported values are shown with mean \pm SD. *Different lower case letters in each column refer to a statistical difference of means compared, where F -distribution values and significant levels of mineralization rates and percentages of mineralization extent were computed with $F_{(5, 10)} = 33.713$ ($P = 0.05$) and $F_{(5, 10)} = 33.437$ ($P = 0.05$), respectively.

A similar trend of results was observed between different oomycetes (*Py. aphanidermatum* in **Fig. 29a** and *Py. oligandrum* in **Fig. 29b**). However, the highest rate of mineralization ($8.27 \text{ ng mL}^{-1} \text{ h}^{-1}$) was found in the presence of *Py. oligandrum* grown on DV8 agar. When the mycelia of the two oomycetes were the only supplement, the maximum rates of bacterial mineralization of ^{14}C -phenanthrene were not significantly different. However, the extent of mineralization was approximately two times higher, and the lag phase was shorter, in the presence of *Py. oligandrum* mycelia (**Fig. 29** and **Table 5**). Interestingly, in the absence of any supplement, mineralization by *M. gilvum* VM552 was linear ($R^2 = 0.99$) with a constant rate of $0.29 \text{ ng mL}^{-1} \text{ h}^{-1}$.

To check whether the enhancement of biodegradation by the oomycete also occurred under conditions that promoted biofilm development, a similar experiment as that explained above was carried out in static conditions. The results for mineralization of phenanthrene are shown in **Fig. 30**, and the corresponding rates are included in **Table 6**. We observed that, in all treatments, mineralization curves were S-shaped. Under these conditions, the mineralization activity of *M. gilvum* VM552 was enhanced. The maximum rates (2.72 - $2.90 \text{ ng mL}^{-1} \text{ h}^{-1}$,

Table 6) of bacterial mineralization were found in the presence of oomycete-growing DV8 agar, followed by the presence of DV8 agar as a sole supplement. This trend of results was similar between different oomycetes (*Py. aphanidermatum* in **Fig. 30a** and *Py. oligandrum* in **Fig. 30b**), and was similar also when compared with aerated conditions.

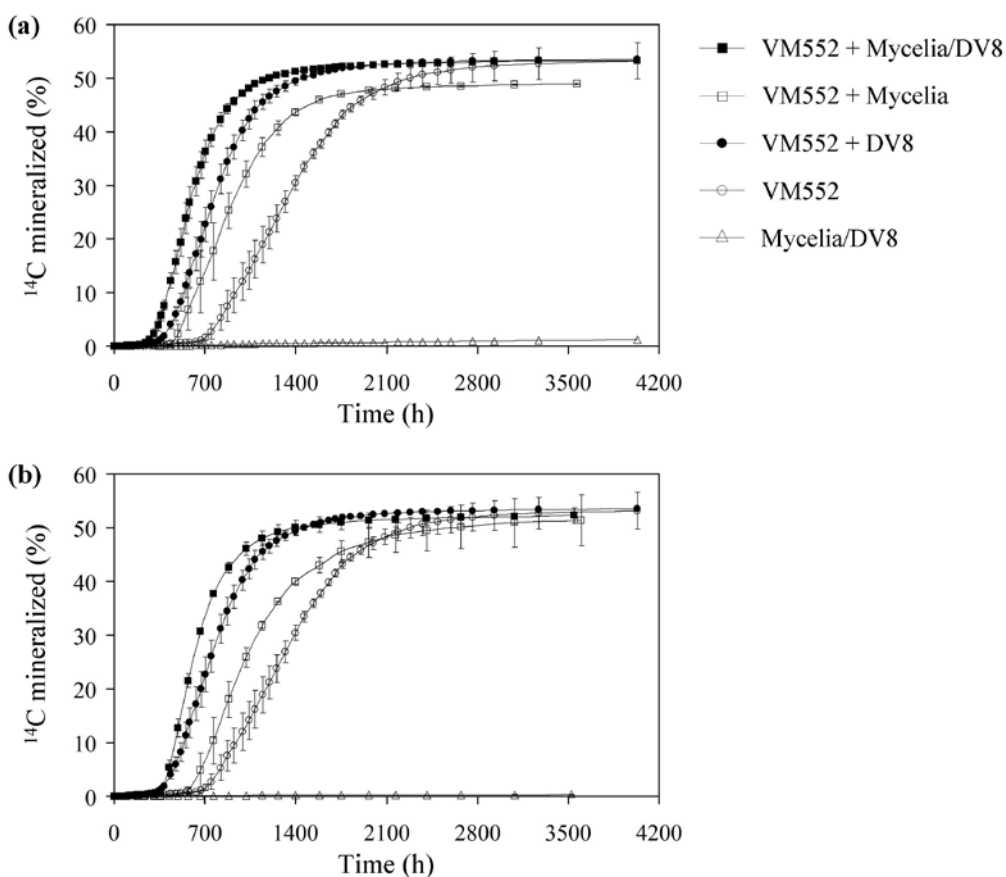


Figure 30 Role of oomycetes in mineralization of ^{14}C -phenanthrene associated to a NAPL by *M. gilvum* VM552 under static conditions. Two oomycetes were used, *Py. aphanidermatum* (a) and *Py. oligandrum* (b). The experiments were tested in the presence of the bacterial cells either without any supplements (VM552) or supplemented with DV8 agar (VM552 + DV8), oomycete mycelia (VM552 + Mycelia), or oomycete-growing DV8 agar (VM552 + Mycelia/DV8). A control without bacterial cells was constructed by adding solely oomycete-growing DV8 agar (Mycelia/DV8). The graphs were plotted by means of ^{14}C mineralized (%) with error bars of SEs, derived from triplicate experiments. Mineralization by bacteria only (with and without DV8) is shown in both panels for better comparison.

Interestingly, in the absence of any supplements, the bacterial mineralization exhibited an S-shaped curved under static conditions with a maximum rate of $1.31 \text{ ng mL}^{-1} \text{ h}^{-1}$. This rate was

approximately five times higher than the rate detected in aerated conditions ($0.29 \text{ ng mL}^{-1} \text{ h}^{-1}$), which suggested that the mineralization activity of *M. gilvum* VM552 was greater enhanced under static conditions. In addition, we observed that both oomycetes were not able to utilize phenanthrene as their carbon and energy source, as revealed by the negligible mineralization rates ($0.002\text{-}0.01 \text{ ng mL}^{-1} \text{ h}^{-1}$), either under aerated (**Fig. 29**) or static (**Fig. 30**) conditions.

Table 6 Role of oomycetes in bacterial mineralization of ^{14}C -phenanthrene associated to NAPL under static conditions

Oomycete	Treatment	Mineralization		
		Rate ($\text{ng mL}^{-1} \text{ h}^{-1}$)*	Extent (%)*	Time (days)
None	VM552	$1.31 \pm 0.09\text{d}$	$53.17 \pm 5.88\text{a}$	168
	VM552 + DV8	$2.10 \pm 0.10\text{b,c}$	$53.45 \pm 0.18\text{a}$	168
<i>Py. aphanidermatum</i>	VM552 + Mycelia	$1.75 \pm 0.14\text{c,d}$	$48.92 \pm 0.27\text{a}$	149
	VM552 + Mycelia/DV8	$2.72 \pm 0.35\text{a,b}$	$53.27 \pm 0.65\text{a}$	168
<i>Py. oligandrum</i>	VM552 + Mycelia	$1.72 \pm 0.22\text{c,d}$	$51.31 \pm 6.71\text{a}$	150
	VM552 + Mycelia/DV8	$2.90 \pm 0.28\text{a}$	$52.24 \pm 2.36\text{a}$	148

Reported values are shown with mean \pm SD. *Different lower case letters in each column refer to a statistical difference of means compared, where F -distribution values and significant levels of mineralization rates and percentages of mineralization extent were computed with $F_{(5, 11)} = 23.361$ ($P = 0.05$) and $F_{(5, 11)} = 0.777$ ($P = 0.05$), respectively.

4.2.2 Kinetics and end-point mass balance of mineralization of phenanthrene

Based on the S-shaped curves of bacterial mineralization, the kinetics of the mineralization activity could be divided into lag, exponential and stationary phases. Under aerated conditions, the lag phases were shorter than 300 h when the oomycete-growing DV8 agar or only DV8 agar was used as a supplement (**Fig. 29**). These lag phases were extended longer in static conditions (**Fig. 30**), up to 350 h. Moreover, these observations were similar between the two oomycetes used. In the supplement with oomycete mycelia alone, the lag phases in aerated conditions were extended longer (~ 1800 h) when the mycelia of *Py. aphanidermatum* (**Fig. 29a**) were applied, as compared to *Py. oligandrum* mycelia (~ 800 h) (**Fig. 29b**). This observation contrasted with the static conditions, where the lag phase was shorter (~ 400 h) in the presence of *Py. aphanidermatum* mycelia (**Fig. 30a**), but it was longer

(~600 h) in the presence of *Py. oligandrum* mycelia (**Fig. 30a**). This may relate to the different development of oomycetes in these experimental systems. It was found that, within the same area of growth, *Py. aphanidermatum* formed a double amount of biomass, as compared to *Py. oligandrum* (**Fig. 31**). Moreover, zoospore formation was observed only with *Py. aphanidermatum* (**Fig. 32**). When only mycelia of this oomycete were used, zoospores were formed slightly faster in aerated conditions than those formed in static conditions.

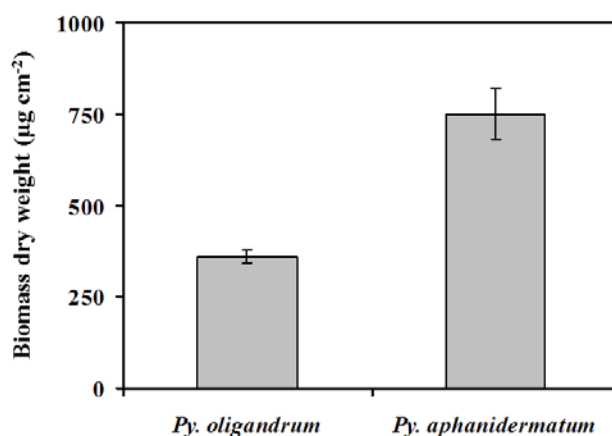


Figure 31 Biomass dry weights of oomycetes grown on V8 agar. The oomycetes were incubated at 25 °C for 4 days before cutting with a known area, and their aerial mycelia were scraped and dried in an oven at 55 °C for 5 days. The dried biomass was then weighed. The experiment was done in triplicate. The results are reported with means, where the error bars refer to SDs.

The exponential phases of the bacterial mineralization either compared among conditions or treatments tested were also different with variation of time scales. The shortest exponential phases (~300 h) were observed when oomycete-growing DV8 agar was supplemented under the aerated conditions (**Fig. 29**). The longer exponential phases (~300-400 h) were observed also under these conditions when the oomycete mycelia were supplemented solely, while exponential phases with an approximate 700 h were observed in the presence of DV8 agar as a sole supplement. Under the static conditions (**Fig. 30**), the exponential phases of all treatments were extended between 700-1800 h. There was also a similar observation between different oomycetes under these conditions. However, the extents of mineralization were dissimilar for each oomycete. Under aerated conditions, DV8 agar and *Py. oligandrum* grown on DV8 agar were the best supplements, causing a similar mineralization extent

(55.6%). These supplements were slightly better than *Py. aphanidermatum* grown on DV8 agar, with a mineralization extent at 49.6% (**Fig. 29** and **Table 5**). This could be observed clearly when oomycete mycelia were used solely as a supplement, with a mineralization extent that was significantly higher (42.0%) when *Py. oligandrum* mycelia were used instead of *Py. aphanidermatum* mycelia (28.9%). We observed no difference between different oomycetes under static conditions (**Fig. 30** and **Table 6**).

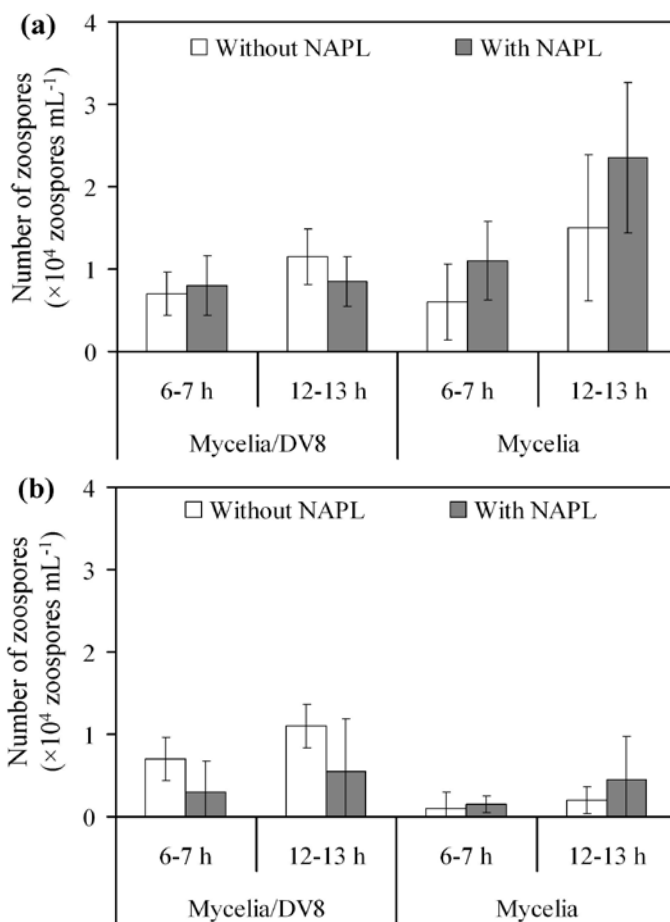


Figure 32 Zoospore formation of *Py. aphanidermatum* in mineralization experiments. The experimental conditions (aerated (a) and static (b)) imitated the mineralization experiments were established either in the absence (without) or presence (with) of NAPL. Either oomycete-growing DV8 agar (Mycelia/DV8) or solely oomycete mycelia (Mycelia) were prepared for quantification of zoospore formation. Number of zoospores was quantified at 6-7 h and 12-13 h after installing the experiments. The results are reported with means, where the error bars refer to SDs. There was no significant difference between means compared in (a) ($F_{(7, 24)} = 4.219$, $P = 0.001$) and in (b) ($F_{(7, 24)} = 3.471$, $P = 0.001$).

At the end of mineralization experiments, the mineralization and biodegradation activities of *M. gilvum* VM552 were confirmed by measurements of end-point mass balance of ^{14}C and end-point concentration of PAHs present in NAPL residuals, respectively. The end-point mass balance of ^{14}C was evaluated with a scintillation counter and resulted in four fractions: ^{14}C mineralized, ^{14}C dissolved in the aqueous phase, ^{14}C accumulated in the solid phase (biomass and/or agar residues) and ^{14}C that remained in the NAPL. These percentages were well related to the mineralization curves and revealed no losses of substrate carbon from the biometric systems. Under aerated conditions, the aqueous-dissolved fractions resulting from the treatments supplemented with the oomycetes and/or DV8 agar were not different (**Fig. 33**). This observation was similar to static conditions (**Fig. 34**), and no different results were observed between the two oomycetes. It was also observed that adding the sole mycelia of *Py. aphanidermatum* as a supplement did not affect the mineralization activity of *M. gilvum* VM552 (**Fig. 33a**), as indicated by no significant difference across the mass balance profile of ^{14}C . However, the sole mycelia of *Py. oligandrum* enhanced bacterial mineralization to a greater extent than *Py. aphanidermatum* mycelia (**Fig. 33b**). Moreover, the fractions of ^{14}C associated to the solid phase, either under aerated (**Fig. 33**) or static (**Fig. 34**) conditions, were often found to be inversely correlated to the fraction still present in the NAPL, what suggests that the biological uptake and transformation of ^{14}C -phenanthrene was involved in the partitioning of this chemical from the NAPL. Interestingly, the solid-associated fraction was often higher than the NAPL-associated fraction in the presence of oomycete mycelia and/or DV8 agar under static conditions (**Fig. 34**).

The biodegradation activities of *M. gilvum* VM552 (**Fig. 35**) also revealed the enhancement by oomycete mycelia and/or DV8 agar. Five PAHs (fluorene, phenanthrene, anthracene, fluoranthene and pyrene) present in NAPL residuals taken from all treatments were quantified by GC-MS, and compared to the untreated NAPL (**Fig. 35a**). It was found that the five PAHs could be degraded by the bacterium, while phenanthrene is the most degradable PAH followed by fluorene (**Fig. 35b**). Interestingly, and in accordance with mineralization results, oomycete mycelia and/or DV8 agar enhanced biodegradation of phenanthrene by the bacterium, what was supported by the nearly complete disappearance of phenanthrene that was degraded, as compared to the treatment without any supplements (where 50 % of phenanthrene was biodegraded) (**Fig. 35b**). However, the second abundant PAH found in the

untreated NAPL, pyrene, was slightly degraded by the bacterium, while the highest % of biodegradation occurred in the absence of any supplements.

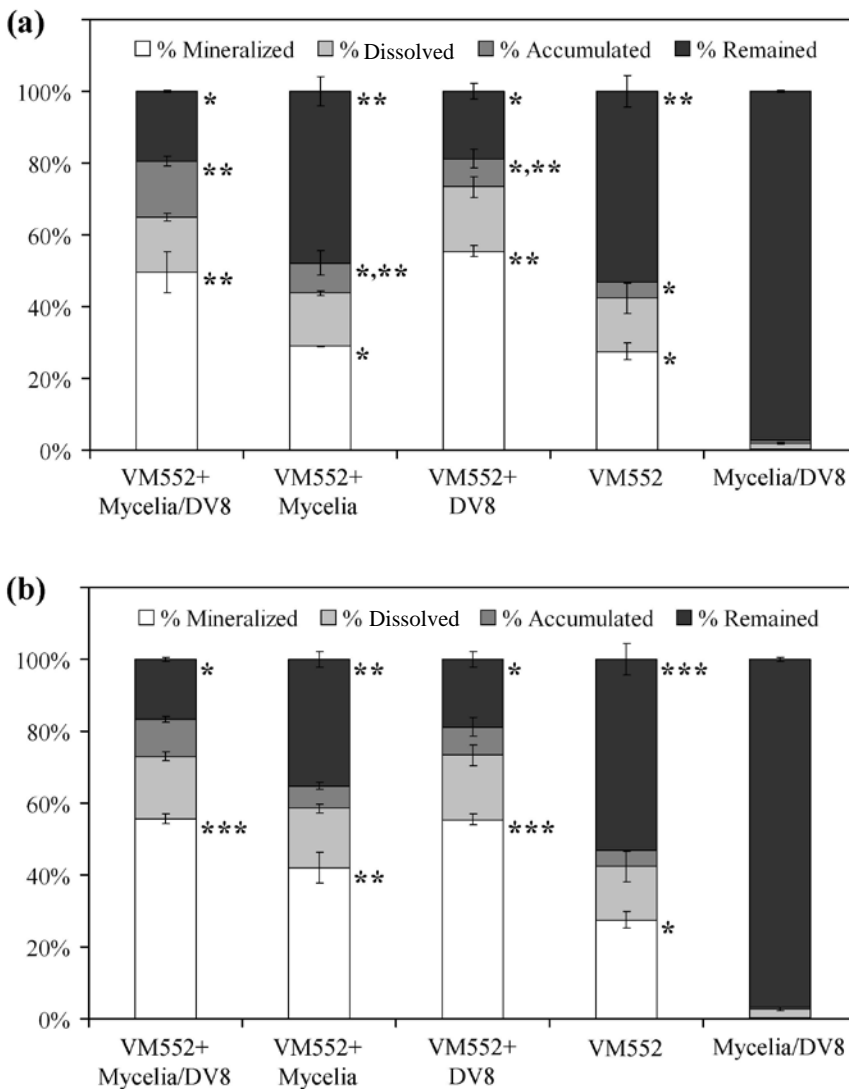


Figure 33 Mass balance of [^{14}C] present at the end of mineralization experiments under aerated conditions. The percentages of [^{14}C] mineralized by *M. gilvum* VM552 (% Mineralized)^{F1} were taken from the end-point of the mineralization curves (Fig. 29). The percentages of [^{14}C] dissolved in the liquid phase (% Dissolved)^{F2} and of [^{14}C] accumulated in the solid phase (% Accumulated)^{F3} were quantified by a scintillation counter (see also 3.6.3). The percentages of [^{14}C] remained in NAPL residuals (% Remained)^{F4} was calculated by the difference (see also 3.7.2). Asterisks refer to a statistical difference of means compared between each percentage in (a) ($F1-4_{(3, 6)} = 40.489, 0.927, 11.658, 104.297, P = 0.01$) and in (b) ($F1-4_{(3, 7)} = 62.287, 0.686, 6.176, 122.143, P = 0.01$), while the controls of sole oomycete mycelia-growing DV8 agar (Mycelia/DV8) was excluded from this comparison.

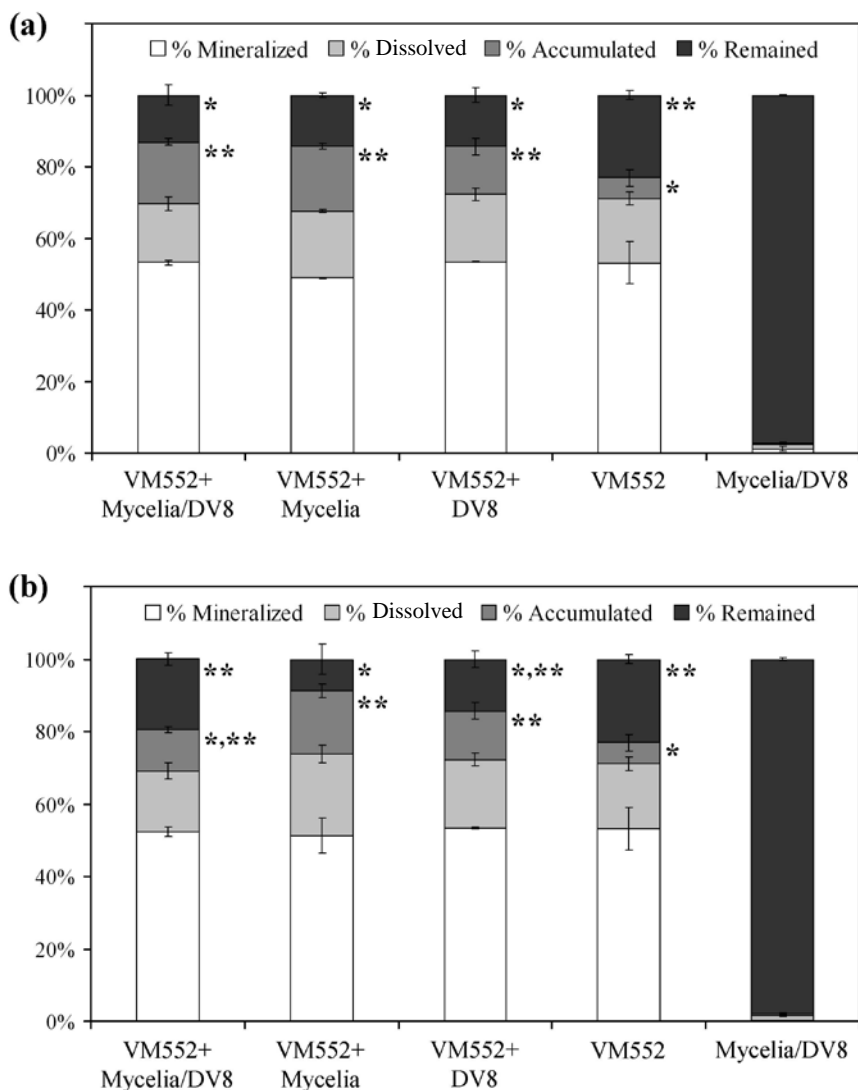


Figure 34 Mass balance of ^{14}C present at the end of mineralization experiments under static conditions. The percentages of ^{14}C mineralized by *M. gilvum* VM552 (% Mineralized)^{F1} were taken from the end-point of the mineralization curves (Fig. 30). The percentages of ^{14}C dissolved in the liquid phase (% Dissolved)^{F2} and of ^{14}C accumulated in the solid phase (% Accumulated)^{F3} were quantified by a scintillation counter (see also 3.6.3). The percentages of ^{14}C remained in NAPL residuals (% Remained)^{F4} was calculated by the difference (see also 3.7.2). Asterisks refer to a statistical difference of means compared between each percentage in (a) ($F1-4_{(3,8)} = 1.641, 1.493, 45.958, 17.001, P = 0.01$) and in (b) ($F1-4_{(3,7)} = 0.127, 3.348, 23.695, 18.304, P = 0.01$), while the controls of sole oomycete mycelia-growing DV8 agar (Mycelia/DV8) were excluded from this comparison.

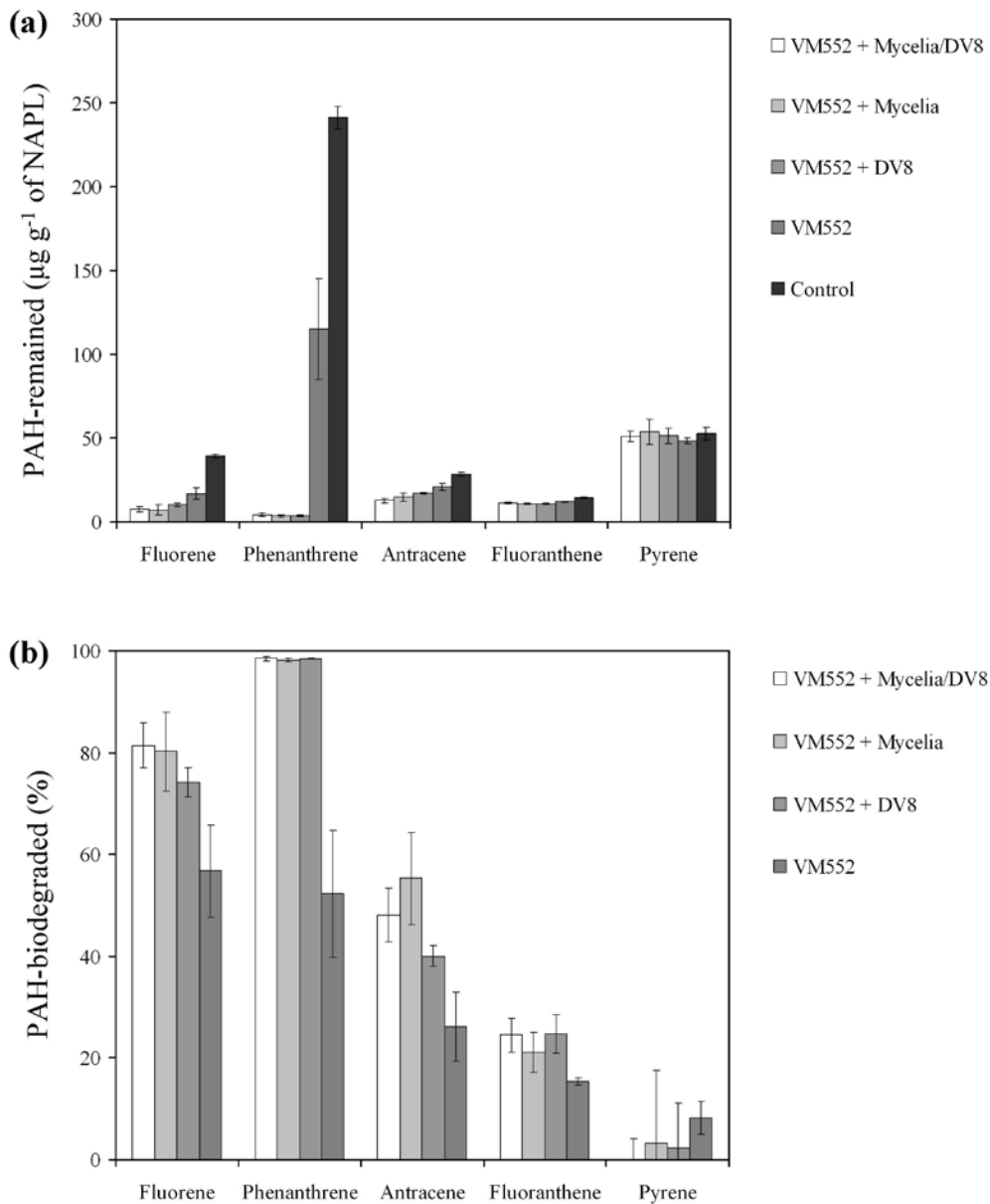


Figure 35 A set of PAHs found in NAPL residuals collected at the end of mineralization experiments under aerated conditions, using the mycelia of *Py. oligandrum*. Control is an untreated mixture of NAPL (fuel:HMN, 1:1 (w/v)). The concentrations of PAHs remained in NAPL residuals were reported in μg per g of NAPL (a), while the percentages of PAHs mineralized by *M. gilvum* VM552 were calculated (b). The analysis was done in triplicate.

4.2.3 Evolution of NAPL-water contact angle

The NAPL-water contact angle (θ_{nw}) was measured by a protractor using the side view photographs from mineralization experiments (**Fig. 18**). At the starting day of the experiments, the NAPL in all treatments exhibited a convex shape with a range of 110-120° for θ_{nw} (**Fig. 36a**). Values of θ_{nw} measured in the presence of *M. gilvum* VM552 increased gradually with the incubation period, and reached 180° at the end of the experiments (**Fig. 36b**). However, θ_{nw} at the end of the experiments measured in the controls without bacteria (only oomycete mycelia growing on DV8 agar) was within a range of 120-140° (**Fig. 36b**), what suggests that the change of θ_{nw} was strongly affected in the presence of *M. gilvum* VM552 cells. Interestingly, we observed that the evolution of θ_{nw} with time was in accordance to the mineralization activity. This was supported by the sharp increase of θ_{nw} observed at the end of lag phases in mineralization experiments. This change was observed faster during the experiments carried out under aerated conditions (**Fig. 29**), as compared with static conditions (**Fig. 30**). In addition, the evolution of θ_{nw} in the presence of *M. gilvum* VM552 cells alone under aerated conditions (**Fig. 29**) occurred gradually throughout the experimental period, to reach a final value of 180° at the end of the experiments. It seems that such changes in θ_{nw} indicated the starting point of exponential mineralization rate, suggesting that the bacterial cells could settle at the NAPL-water interface and established on-site biodegrading activity. Subsequently, this θ_{nw} evolution was a result of the microbial activity at the NAPL-water interface. It is also conceivable that the gradual change of θ_{nw} was in accordance to the increase of biofilm density formed at the NAPL-water interface (**Fig. 36b**).

4.2.4 Biofilm formation at NAPL-water interface

Microbial biofilms were observed at the NAPL-water interface (**Fig. 36**). These biofilm structures developed more densely under static conditions as compared to aerated conditions. The densest biofilms were found in the presence of *Py. aphanidermatum* mycelia under static conditions and in the presence of *Py. oligandrum* mycelia under aerated conditions (**Fig. 36b**). However, these structures were microscopically similar under both aerated (**Fig. 37**) and static (**Fig. 38**) conditions. Interestingly, the presence of oomycete mycelia in the biofilm was observed only in the experiments supplemented with *Py. aphanidermatum* grown on DV8 agar under static conditions (**Fig. 38**). Most biofilm structures were constituted by a clump of older bacterial cells (identified as red cells due to RNA labelling by acridine orange), surrounded by young cells (labelled green due to DNA). These biofilms

were often observed in the presence of exopolysaccharide (EPS) visible as a light yellow thin layer that surrounded bacterial cells (Figs. 37 and 38).

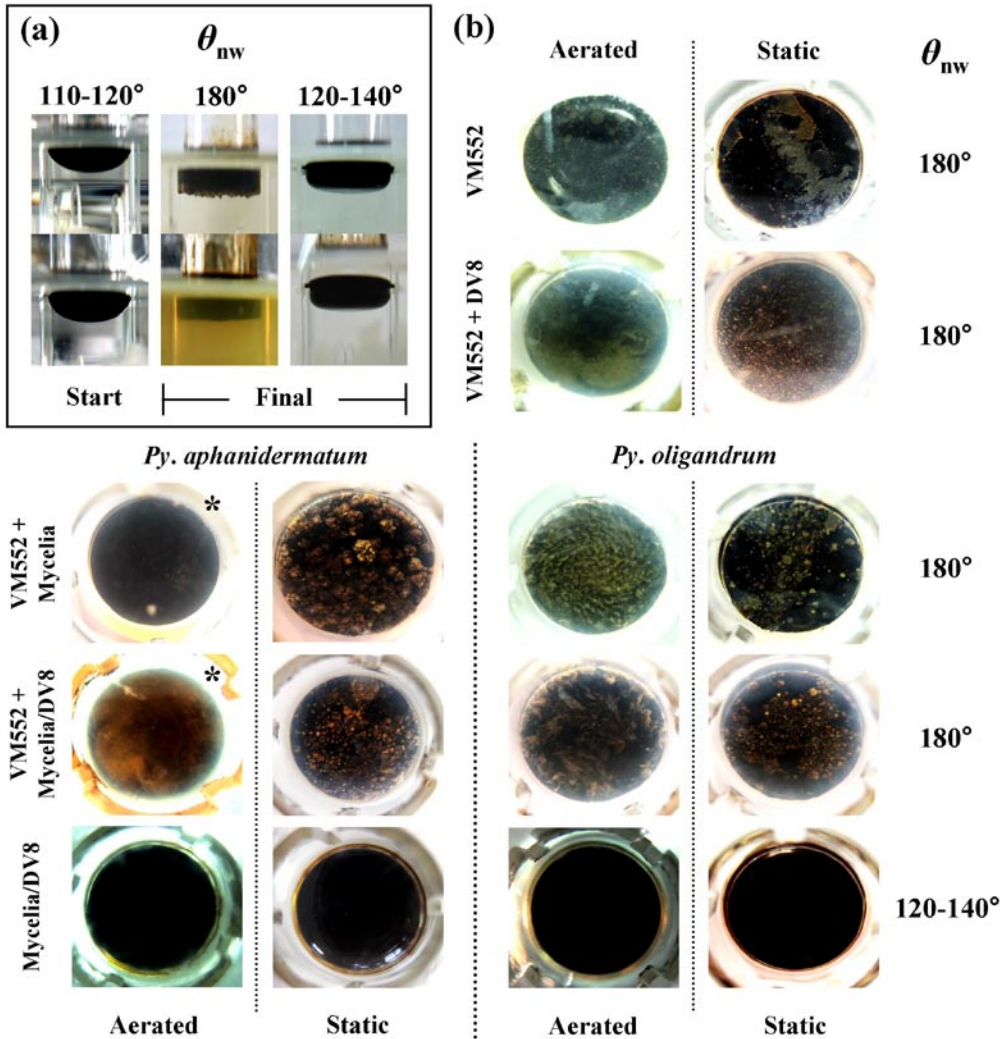


Figure 36 Evolution of NAPL-water contact angle (θ_{nw}) and its relevance in biofilm formation at the NAPL-water interface under aerated and static conditions of mineralization experiments. The θ_{nw} is used as a criterion for topographical changes of the NAPL-water interface. The value of θ_{nw} is compared at the end of mineralization experiments (Final) with that one observed at the start (Start) (a). The biofilms developed at the NAPL-water interface were observed at the end of mineralization experiments, and their θ_{nw} was also determined (b). Asterisks in (b) refer to the dense growth of bacterial cells in the biometric systems that prevented the observation of biofilms.

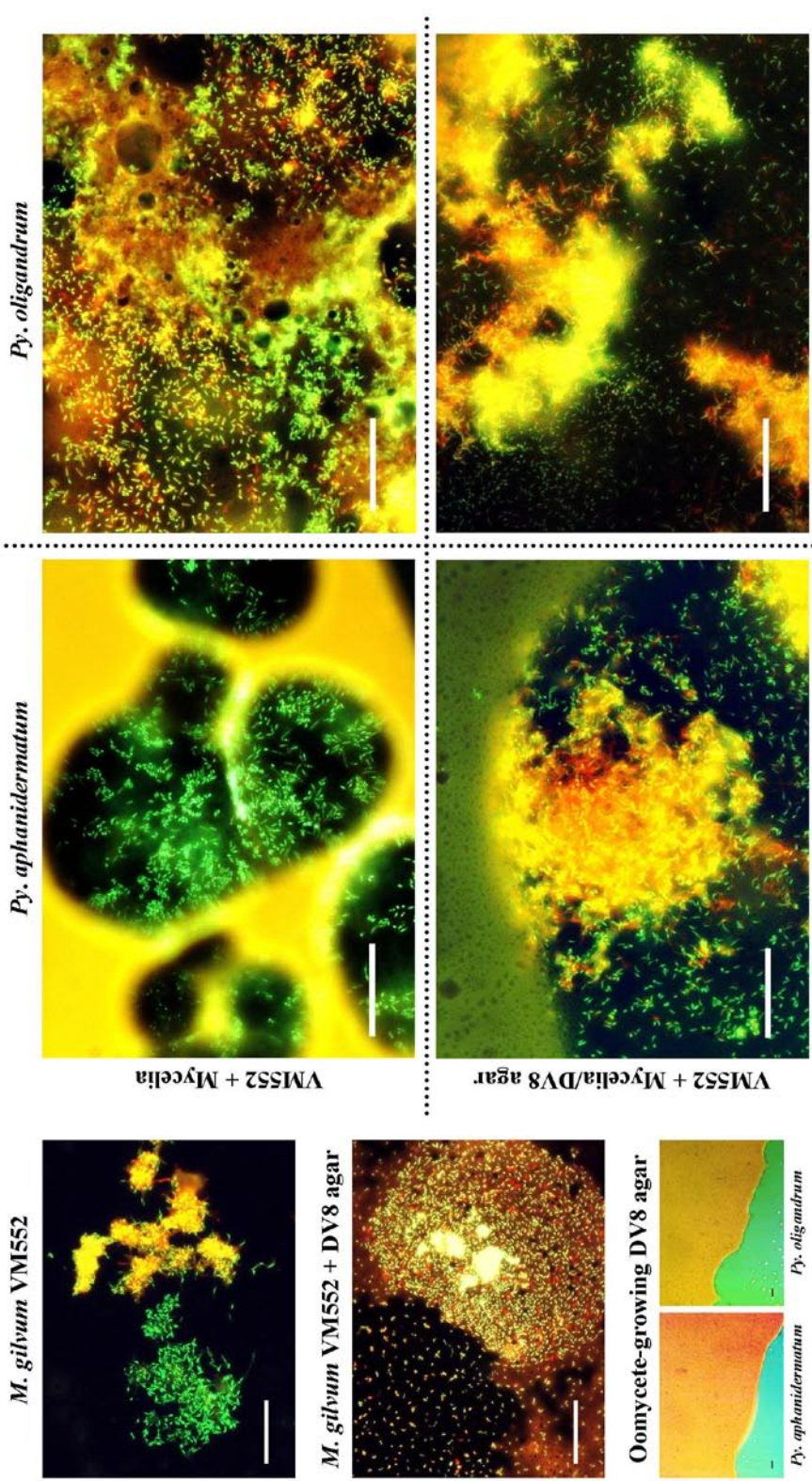


Figure 37 Microbial lifes at NAPL-water interfaces developed in the mineralization experiments under aerated conditions. Biofilms formed at the NAPL-water interface were sampled at the end of the mineralization experiments by a transfer loop and stained with 0.02% (w/v) acridine orange, then observed with a fluorescence microscope. The bars = 30 μ m.

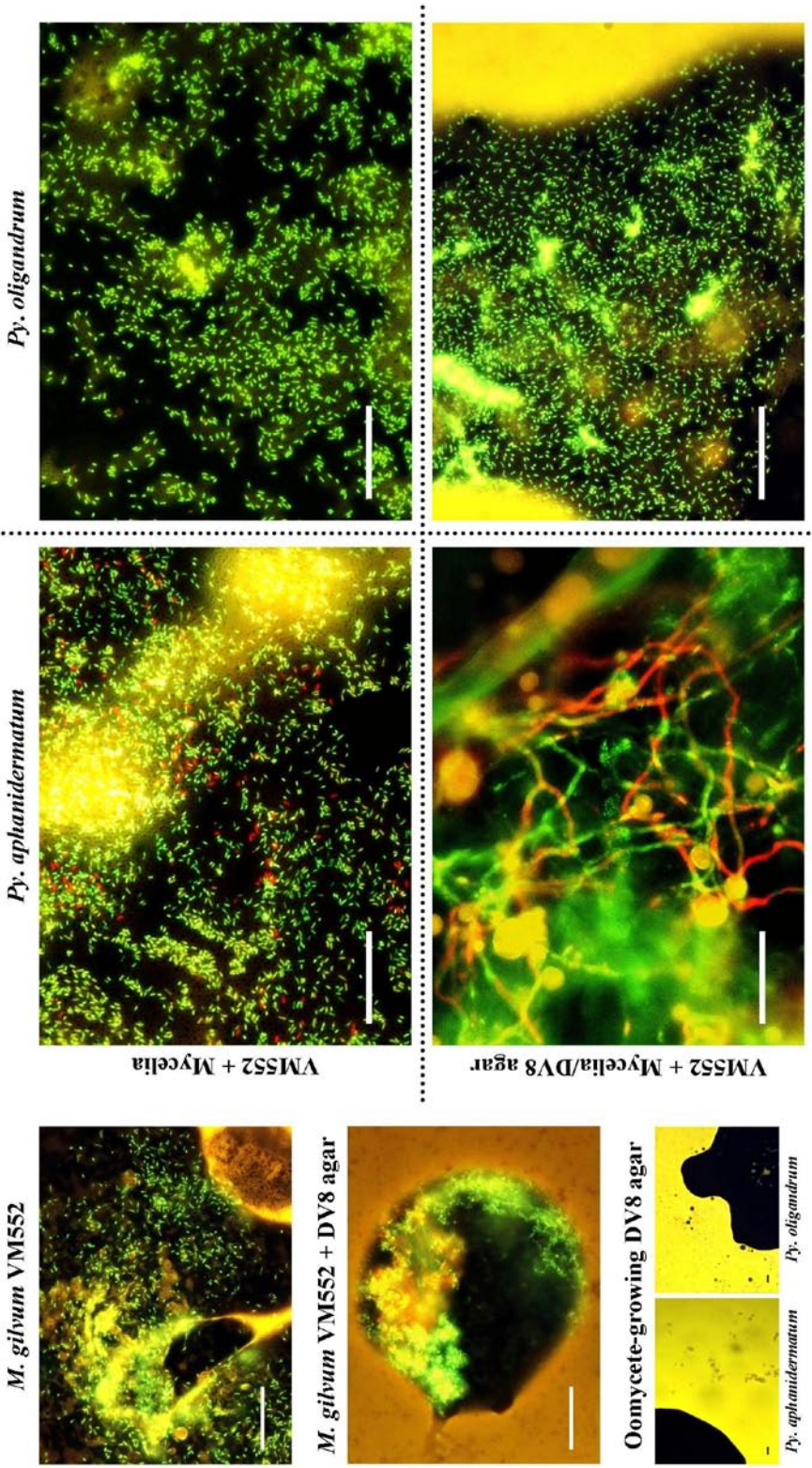


Figure 38 Microbial lifes at NAPL-water interfaces developed in the mineralization experiments under static conditions. Biofilms formed at the NAPL-water interface were sampled at the end of the mineralization experiments by a transfer loop and stained with 0.02% (w/v) acridine orange, then observed with a fluorescence microscope. The bars = 30 µm.

4.2.5 Influences of DO and DOC variations on mineralization kinetics

To discriminate the chemical influences on the mineralization activity of *M. gilvum* VM552 from the biological and physical influences, we determined the variation of dissolved oxygen (DO) and dissolved organic carbon (DOC). A set of experiments that imitated mineralization experiments (but without NAPL) were performed, and DO was measured (**Fig. 39**). Under aerated conditions (**Fig. 39a**), the values of DO were stable at approximately 6 mg L⁻¹, suggesting that physical aeration could supply dissolved oxygen from the atmosphere into the water phase at a sufficient level for microbial growth. Also, it was observed that oomycete mycelia affected DO only at the initial 300 h in the experiments under static conditions (**Fig. 39b**). The concentrations of DO detected were, however, still high and excluded that the lag phase observed in bacterial mineralization was due to competition between the bacterium and oomycete. Nevertheless, it was clear that the rich biomass of *Py. aphanidermatum* mycelia was the greatest reducer of DO during the initial 100 h of the experiments under static conditions.

For the variations of DOC during the mineralization experiments (**Fig. 40**), it can be concluded that DOC found mainly in the aqueous phase derived from DV8 agar. This observation was supported by the significant differences between the treatments supplemented solely with oomycete mycelia and in the presence of DV8 agar or oomycete grown on DV8 agar. Moreover, DOC in the presence of DV8 agar as a sole supplement was found with the highest concentration compared to the other treatments in both aerated and static conditions. It was also found that mycelia of both oomycetes did not contribute DOC from their biomass. However, it seemed that both oomycete mycelia could increase slightly the concentration of DOC in the presence of NAPL under aerated conditions (**Fig. 40b**). In addition, the results suggested that oomycete mycelia played an important role as a nutrient exchanger within biometric systems of the mineralization experiment. This observation was supported by the significantly higher DOC concentrations in all treatments supplemented with oomycete-growing DV8 agar, compared to the treatments supplemented with solely oomycete mycelia either under aerated or static conditions. Although oomycete mycelia could increase DOC in the aqueous phase, the concentrations of DOC were lower than the treatments supplemented solely with DV8 agar, suggesting that the rate of DOC actively dissolved from solid agar caused by the growth of oomycetes was faster than their rate of nutrient uptake.

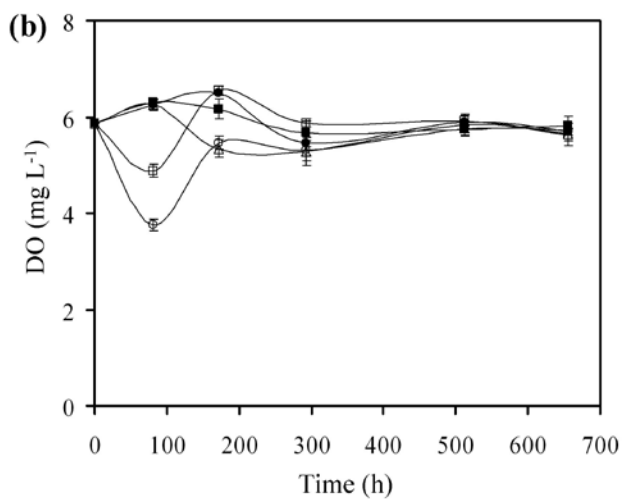
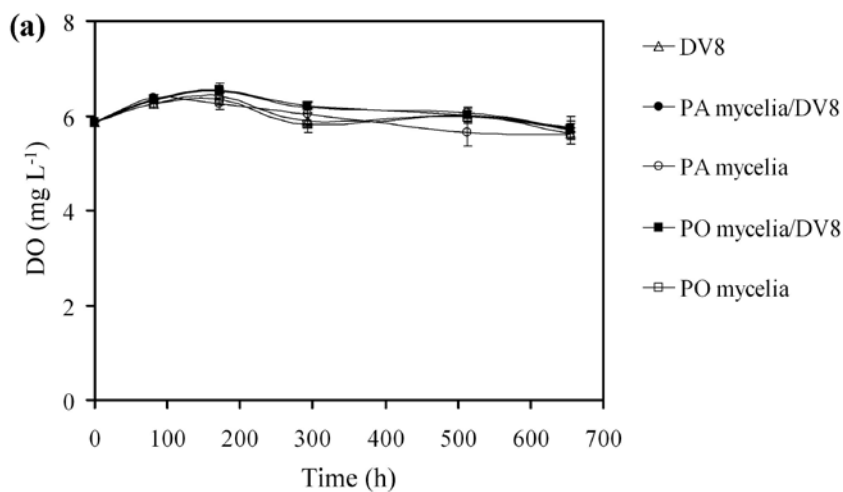


Figure 39 Variations of DO in the aqueous phase of mineralization experiments. The measurement was done in the absence of NAPL and bacterial inoculum, while the experimental sets were performed as same as the mineralization experiments under aerated (a) and static conditions (b). Two oomycetes (*Py. aphanidermatum* (PA) and *Py. oligandrum* (PO)) were used, while five treatments supplemented with DV8 agar (DV8), oomycete mycelia grown on DV8 (PA or PO mycelia/DV8) and solely oomycete mycelia (PA or PO mycelia) were constructed. Do was measured from a duplicate experimental set, by using an oxygen meter.

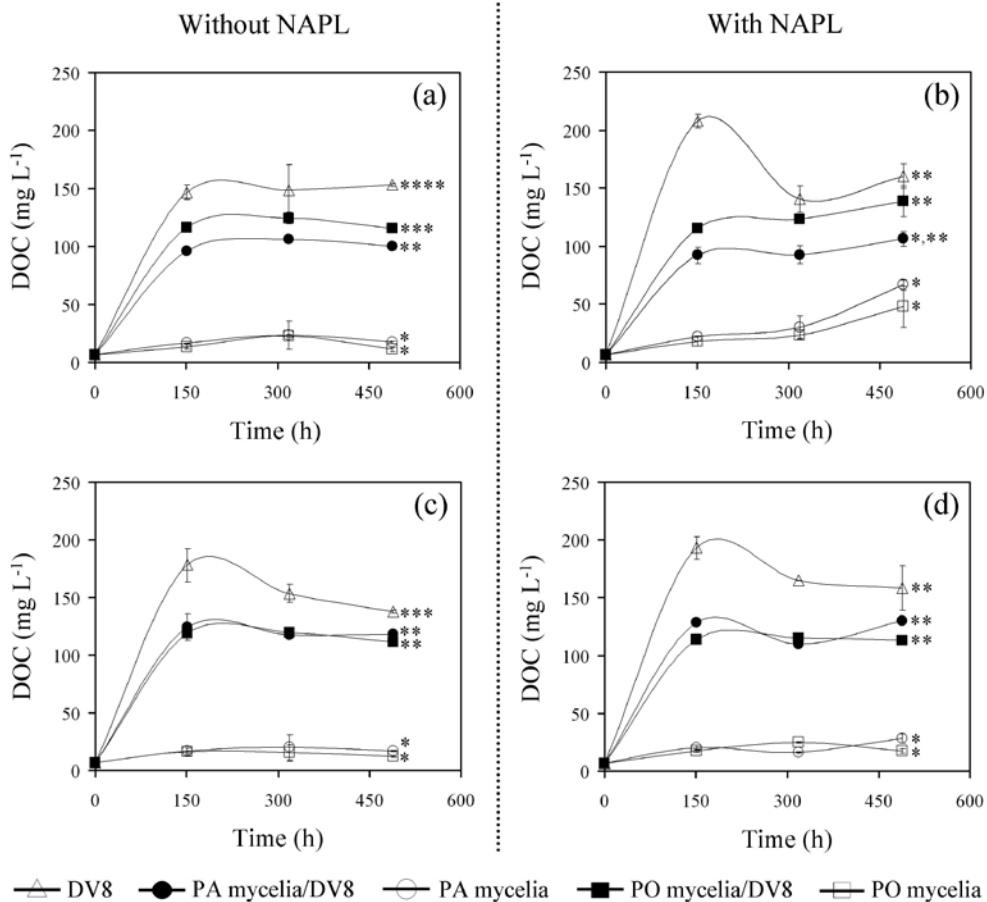


Figure 40 Variations of DOC in the aqueous phase of mineralization experiments. The measurement was done in the absence of bacterial inoculum either without or with NAPL, while the experimental sets were performed as same as the mineralization experiments under aerated (a, b) and static conditions (c, d). Two oomycetes (*Py. aphanidermatum* (PA) and *Py. oligandrum* (PO)) were used, while five treatments supplemented with DV8 agar (DV8), oomycete mycelia grown on DV8 (PA or PO mycelia/DV8) and solely oomycete mycelia (PA or PO mycelia) were constructed. The concentration of DOC was assumed by the analysis of TOC, which was measured using a Shimadzu TOC-VCSH equipment with ASI-V auto sampler after filtration through Whatman® No. 1 (pore size, $\varnothing = 11 \mu\text{m}$). The experiments were done in duplicate, while the analysis of TOC was performed twice per each sample.

4.3 Biomobilization of pollutant-degrading bacteria by chemotaxis of eukaryotic zoospores

4.3.1 Chemotaxis of zoospores and bacterial mobilization

Zoospore chemotaxis was carried out using a modified chemical-in-capillary method (Fig. 19) with ethanol as a zoospore attractant. After zoospores were allowed to perform the chemotactic reaction, the number of encysted zoospores found inside the chemotactic capillary tubes increased with the concentrations of ethanol, but it was inversely correlated with the travelling distance of zoospores along the capillary tubes (Fig. 41). It was found that the lowest concentration (5% (v/v) ethanol) of zoospore attractant was optimal for biomobilization assays, in accordance with the absence of any negative influences on bacterial viability (Fig. 42a) and bacterial chemotaxis towards this chemical dose (Fig. 43). Therefore, this concentration of ethanol was chosen for biomobilization assays.

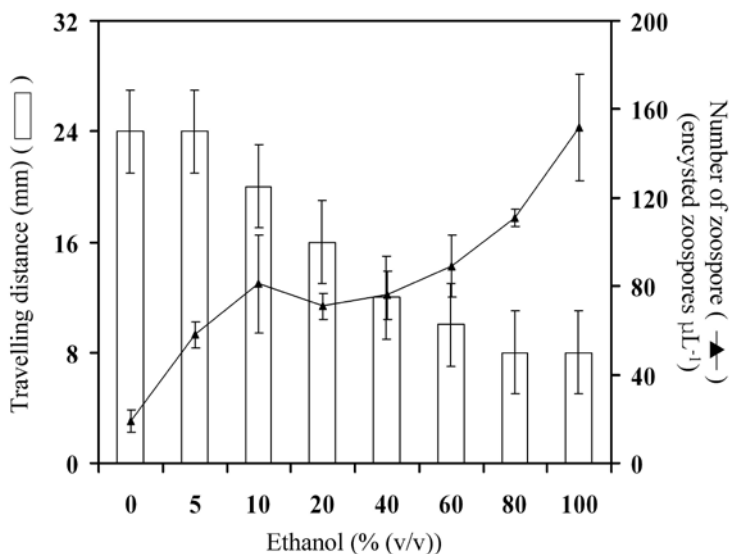


Figure 41 Zoospore chemotaxis towards different concentrations of ethanol (a zoospore attractant, diluted with sterilized lake water). This investigation was carried out using modified chemical-in-capillary method (Fig. 19), aiming to search for the optimal concentration of zoospore attractant for biomobilization assay. The travelling distance of zoospores entering into the capillary tubes filled with different concentrations of ethanol (bar graph) was estimated by wherever zoospores encysted. The error bars show an approximate variation of ± 3 mm in each observation. The number of encysted zoospores per the whole volume ($1 \mu\text{L}^{-1}$) of the capillary tube (line graph) was counted. The plots were derived from at least four-replication of each test, while the error bars refer to SD.

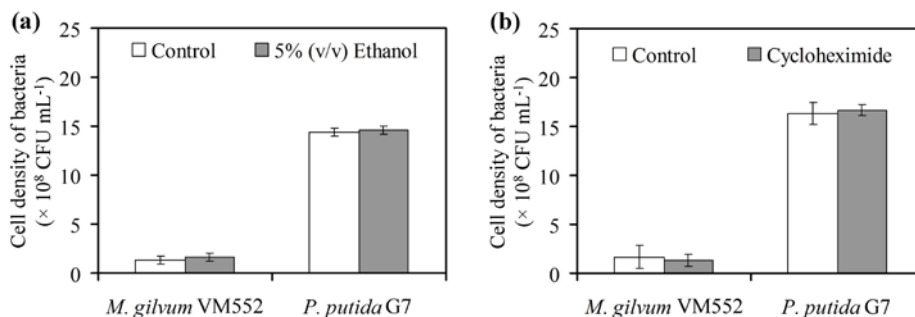


Figure 42 Bacterial development in the presence of zoospore attractant (5% (v/v) ethanol) or cycloheximide. Bacterial cells (96 h of incubation) at the initial OD_{600 nm} of 1.5 were used. No significant difference of bacterial counts compared between control and in the presence of either zoospore attractant ($F_{(3, 8)} = 684.336$, $P = 0.001$) (a) or cycloheximide ($F_{(3, 8)} = 55.129$, $P = 0.001$) (b).

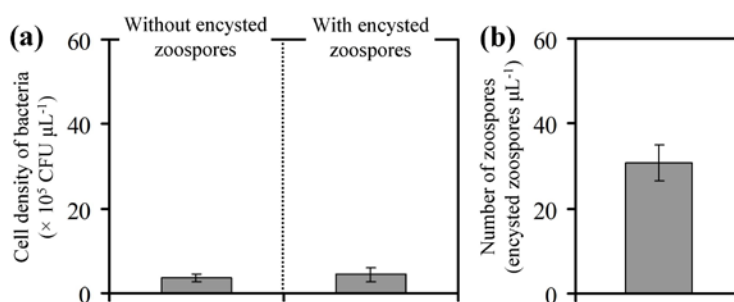


Figure 43 Chemotaxis of *P. putida* G7 towards zoospores encysted chemotactically towards their attractant (5% (v/v) ethanol). The experiment was evaluated by 2 steps of a modified chemical-in-capillary method (Fig. 19). At the first step, the chamber was filled either with zoospore suspension or sterilized lake water (control, without encysted zoospores) (a), where capillary tubes filled with the zoospore attractant (5% (v/v) ethanol) were inserted into the chamber and incubated at 25 °C for 1 h. Zoospores were allowed to respond chemotactically to their attractant and to encyst inside the capillary tube, where the number of encysted zoospores was counted (b). Afterwards, the capillary tubes tested at the first step were transferred into the second chamber filled with bacterial suspension of highly motile cells of *P. putida* G7 (a 10-fold dilution of the initial cell density at OD_{600 nm} = 1.5). The experiment was incubated at the same conditions as in the first step. Bacterial cells entering into the capillary tubes (a) were quantified by CFU developed on TSA supplemented with 0.3 g L⁻¹ cycloheximide. The graphical results are means of at least triplicate experiments, where the error bars represent the SDs of those respective means.

Bacterial cells with three different motility levels were used for biomobilization assay (Table 7). *M. gilvum* VM552 was used as a representative non-motile PAH-degrading bacterium. The motility of *P. putida* G7 cells was determined through their global speeds as computed by the CellTrak program. We found that stationary phase cells exhibited a lower level of

motility than exponentially growing cells. The lengths and L/B ratios of bacterial cells were also different, as the highly motile cells of *P. putida* G7 were 2-time bigger than those other bacterial cells (**Table 7**).

Table 7 Motility and cell size determinations of PAH-degrading bacteria

PAH-degrading bacteria	Age (h)	Cell motility ^a	Cell characteristics ^b		
			Length (µm)	Breadth (µm)	L/B ratio
<i>M. gilvum</i> VM552	96	Non-motile	1.52 ± 0.46	1.03 ± 0.11	1.48 ± 0.45 (N = 51)
		Slightly motile			
	96	(global speed = 40.82 µm s ⁻¹ , SE = 2.42, N = 85)	1.73 ± 0.40	1.02 ± 0.10	1.70 ± 0.36 (N = 50)
<i>P. putida</i> G7		Highly motile			
	12	(global speed = 82.81 µm s ⁻¹ , SE = 2.80, N = 91)	3.36 ± 0.83*	1.09 ± 0.11	3.12 ± 0.82* (N = 50)

^aMotility of bacterial cells suspended in sterilized lake water was determined into three levels, while the global speeds of motile bacterial cells were computed with the CellTrak program (see also **CHAPTER III**). SE is standard error and N is population number of measured cells. ^bLength, breadth and L/B ratio are shown with mean ± SD. Asterisks represent significant difference of means among lengths ($F_{(2, 148)} = 144.130, P = 0.001$) or L/B ratios ($F_{(2, 148)} = 119.221, P = 0.001$), while without asterisk of breadth is not different significantly ($F_{(2, 148)} = 6.484, P = 0.001$).

The mobilization of bacterial cells by zoospore chemotaxis was tested using the modified capillary assay as described previously. In the presence of zoospores, the number of *M. gilvum* VM552 cells (**Fig. 44a**) entering into the capillary tubes filled with zoospore attractant was significantly highest ($F_{(3, 10)} = 37.492, P = 0.001$), revealing that the bacterial mobilization was enhanced by zoospore chemotaxis. This chemotactic response of zoospores was confirmed by a significant higher number of encysted zoospores in the capillary tubes filled with zoospore attractant ($F_{(5, 17)} = 34.861, P = 0.001$) (**Fig. 44b, d and f**). A similar trend of results was also observed with slightly motile cells of *P. putida* G7 ($F_{(3, 10)} = 139.456, P = 0.001$) (**Fig. 44c**). However, the enhanced biomobilization was not observed when highly motile cells of *P. putida* G7 were applied ($F_{(3, 16)} = 2.210, P = 0.001$) (**Fig. 44e**), although the chemotactic response of zoospores remained unchanged as compared with other conditions tested (**Fig. 44b, d and f**).

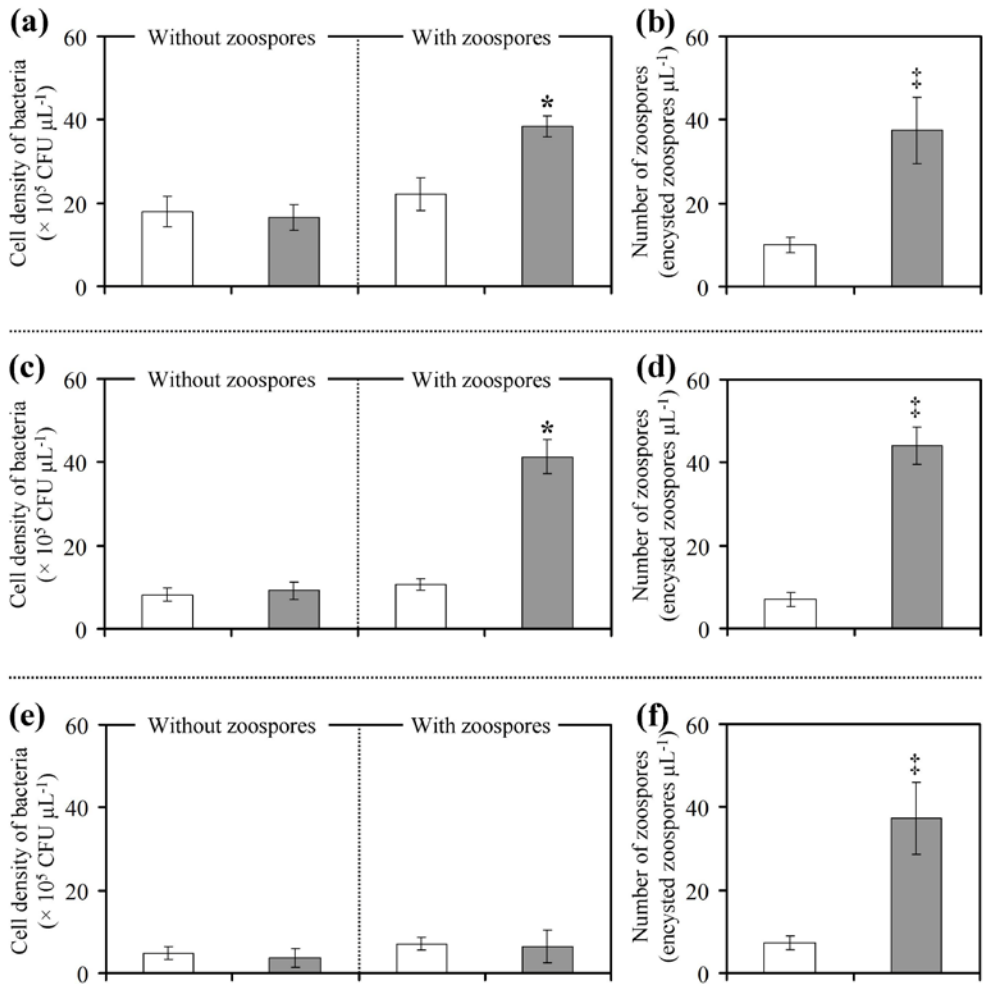


Figure 44 Mobilization of PAH-degrading bacteria by zoospore chemotaxis. *M. gilvum* VM552 cells (a) and slightly (c) or highly (e) motile cells of *P. putida* G7 were used for this investigation, which was evaluated by modified chemical-in-capillary method (Fig. 19). Bacterial suspension (without zoospores) or a microbial mixture of bacterial cells and zoospores (with zoospores) was filled in the chamber. Sterilized lake water (control, empty bars) or zoospore attractant (5% (v/v) ethanol, filled bars) was filled in the capillary tubes, which was further inserted into the prepared chamber. The chemotactic response of zoospores in each assay was confirmed by counting the number of zoospores encysted inside the capillary tubes either absence (empty bars) or presence (filled bars) of their attractant (b, d and f). The results are means of at least triplicate experiment, where the error bars represent the SD. Asterisks refer to a significant difference of means compared within a, c and e, while double daggers refer to a significant difference across b, d and f.

4.3.2 Possible mechanisms of bacterial mobilization by zoospore chemotaxis

Based on the motion records of the biomobilization assays and the microscopic observations of the microbial mixture, we could not observe any direct association between bacterial cells and zoospores. The absence of these direct associations was confirmed by unchanged L/B ratios of zoospores either in the presence or absence of bacterial cells (**Table 8** and **Fig. 45**). Moreover, there was no bacterial chemotaxis towards encysted zoospores (**Fig. 43**). Therefore, the bacterial mobilization could happen through other mechanisms caused mainly by chemotactic response of zoospores. We hypothesized that a key mechanism was a change in fluid dynamics due to the chemotactic responses and/or swimming behaviour of zoospores.

Table 8 Influence of bacterial cells on zoospore sizes

PAH-degrading bacteria	Zoospores characteristics ^a		
	Length (µm)	Breadth (µm)	L/B ratio
None	20.16 ± 1.75***	14.16 ± 2.32***	1.45 ± 0.20 (N = 50)
<i>M. gilvum</i> VM552	17.27 ± 1.70**	12.64 ± 1.83**	1.39 ± 0.19 (N = 33)
<i>P. putida</i> G7 (stationary)	19.47 ± 1.84***	13.36 ± 1.98*** **	1.48 ± 0.18 (N = 55)
<i>P. putida</i> G7 (exponential)	14.24 ± 1.17*	10.35 ± 0.91*	1.38 ± 0.13 (N = 55)

^aLength, breadth and L/B ratio are shown with mean ± SD. Sizes of zoospores swimming in sterilized lake water with the absence (none) or presence of bacterial cells, were measured, while the number of measured zoospores (N) is indicated. Initial density of bacterial cells was prepared at OD_{600 nm} = 1.5 (see also **CHAPTER III**). Asterisks represent significant difference of means among lengths ($F_{(3, 189)} = 143.204$, $P = 0.001$) or breadths ($F_{(3, 189)} = 43.471$, $P = 0.001$), while no asterisk indicated among L/B ratios was no significant difference ($F_{(3, 189)} = 3.383$, $P = 0.001$).

A difference in biomass flow velocities of bacteria in the absence and presence of zoospores was an influencing factor proposed here for describing the mobilizing mechanism caused by zoospores. In the absence of zoospores but presence of their attractant, *M. gilvum* VM552 cells was mobilized spontaneously by the fluid flow through the capillary tubes due to the capillary force and aqueous evaporation (**Fig. 44** and **Vid. 5(4.3)**, this video and the others that support section **4.3** are available at <http://digital.csic.es/handle/10261/96015>). Under the same condition, either slightly (**Fig. 44c**) or highly (**Fig. 44e**) motile cells of *P. putida* G7 could swim either inwards or outwards the capillary tubes (**Vid. 6(4.3)**).

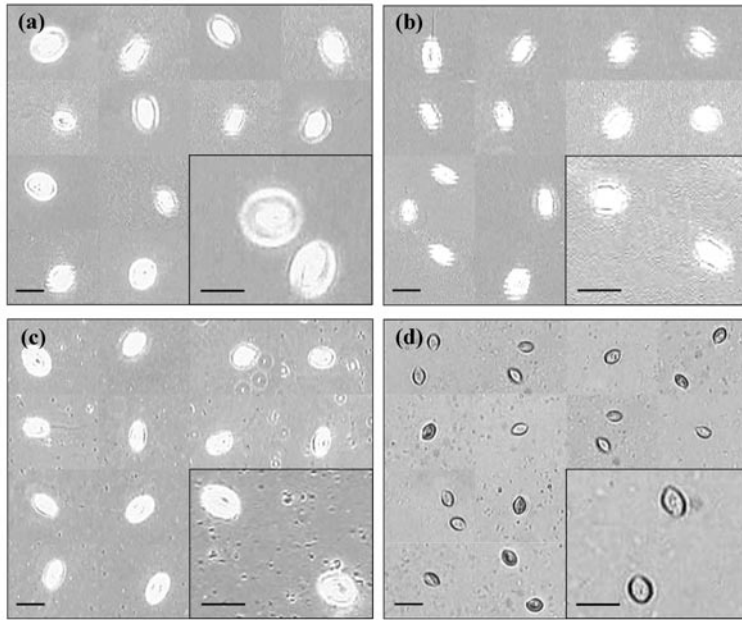


Figure 45 Morphology of swimming zoospores either in the absence or presence of bacterial cells. Initial cell density of bacterial suspensions was prepared at $OD_{600\text{ nm}} = 1.5$ (see also **CHAPTER III**). The micrographs of zoospores were taken during their freely swimming in sterilized lake water (a) or in bacterial suspension of *M. gilvum* VM552 cells (b) or slightly (c) and highly (d) motile cells of *P. putida* G7, where the bars = 20 μm .

The flow velocities of *M. gilvum* VM552 cells flowing through the chemotactic capillary tubes in the absence of zoospores were determined with the CellTrak program at different time periods. A linear correlation, $y = 0.0003x + 19.51$ between the flow velocities and time periods was computed (**Fig. 46** and **Vid. 5(4.3)**). The slope of the linear correlation was nearly zero, what suggests that the flow velocity was not changed according to the time frame as described with equation (v). This demonstrated that the flow velocities of *M. gilvum* VM552 cells were due to the spontaneous flow velocity (u_0) of the fluid body, which was a constant derived from the linear correlation that was steady at $19.51\ \mu\text{m s}^{-1}$. When we compared different bacterial cells mobilized at this u_0 (**Fig. 44a, c and e**), the bacterial cell densities mobilized in most conditions except in the presence of zoospores and their attractant were diminished according to the motility of bacterial cells. This suggested that slightly and highly motile cells of *P. putida* G7 were free to swim either inwards or outwards the capillary tubes (**Vid. 6(4.3)**), which was supported by relative higher speeds of cell

motility (**Table 7**) than u_0 . Interestingly, the mobilizing rate calculated by equation (vi) of *M. gilvum* VM552 cells caused by zoospore chemotaxis (**Fig. 44a**) was equal to 22 cells $\mu\text{L}^{-1} \text{s}^{-1}$, indicating that a zoospore could mobilize 22 cells of non-motile bacteria per second. The calculation was likely the same with slightly motile cells of *P. putida* G7 (**Fig. 44c**), which gave a rate of 24 cells $\mu\text{L}^{-1} \text{s}^{-1}$, while both mobilization rates were approximately seven-eight times higher than the case of highly motile cells with a rate of 3 cells $\mu\text{L}^{-1} \text{s}^{-1}$ (**Fig. 44e**). Although non- and slightly motile cells possessed similar mobilizing rates of 22-24 cells $\mu\text{L}^{-1} \text{s}^{-1}$, their mass flow velocities in the presence of zoospores were different. Zoospore chemotaxis increased mass flow velocities of bacterial cells, calculated by equation (vii) and subtracted with u_0 . This increase was higher with slightly motile cells of *P. putida* G7 ($68.38 \mu\text{m s}^{-1}$) than with *M. gilvum* VM552 cells ($25.85 \mu\text{m s}^{-1}$), and much greater than highly motile cells of *P. putida* G7 ($14.82 \mu\text{m s}^{-1}$).

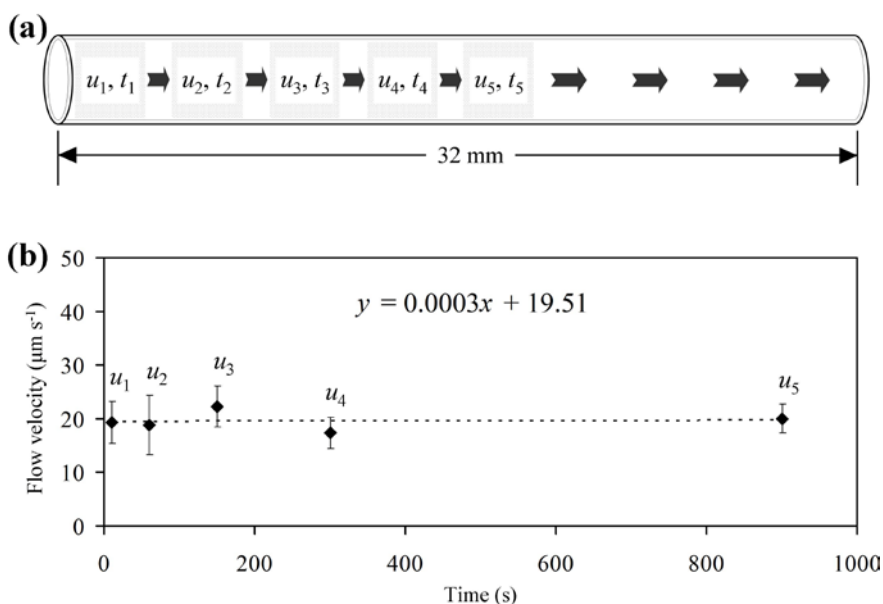


Figure 46 Flow velocity (u) of fluid flowing through capillary tube filled with zoospore attractant (5% (v/v) ethanol). *M. gilvum* VM552 cells were used as detecting particles for computing the flow velocity by the CellTrak program (see also **CHAPTER III**). A study model shows the detecting locations of bacterial cells inside a capillary tube with 32 mm of a total length (a). The flow velocities of bacterial cells were computed and graphed (b). The results were plotted with means of ten speeds derived from ten bacterial cells detected at the same time, while the error bars represent the SD. A linear correlation between the flow velocity and detecting time was computed.

We also observed that the chemotactic response of zoospores towards their attractant was often found to create advection flows (**Vid. 7(4.3)**). Zoospores performed circular or helical movements inside the chemotactic capillary tubes, which could create vortical flows of fluid (**Fig. 47** and **Vid. 7(4.3)**). These advection and vortical flows could either enhance or induce short-path movements for bacterial translocation, forwarding cells into the capillary tubes.

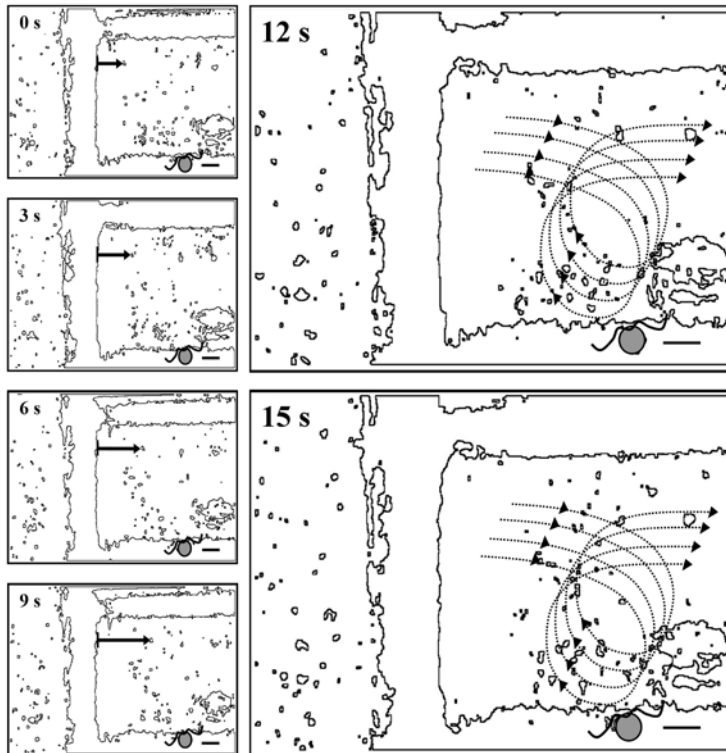


Figure 47 Influence of circular movement of zoospores on mobilization of *M. gilvum* VM552 cells. The images at different time frames (from 0 to 15 s) were tracked from the motion records of biomobilization assay (in the presence of zoospores and their attractant) using the CellTrak program (see also **CHAPTER III**). The arrows with different lengths shown in frames 0 to 9 s refer to the spontaneous flows of bacterial cells moving into the capillary tube, while the dash arrows in frames 12 to 15 s show the vortical flows of bacterial cells due to the circular movement of zoospore (see also **Vid. 7(4.3)**). The position of a zoospore performing the circular movement in each image was indicated with grey circle with two flagella, while the scale bars are 20 μm .

4.3.3 Swimming behaviour and interactive motility of zoospores and bacteria

Besides the change of fluid dynamics by zoospore chemotaxis, the swimming behaviour of zoospores and their interactive motility with different bacterial cells were also likely a key

factor influencing effectiveness of biomobilization. The spontaneous behaviour of zoospores swimming in sterilized lake water was investigated by the CellTrak program. The swimming behaviour of zoospores was categorized into four typical patterns including (I) linear, (II) circular, (III) sine wave and (IV) freestyle (**Fig. 48**). The ratios of these swimming patterns is shown in **Fig. 49a** (control, N = 59). There was no significant difference among the average speeds of every swimming patterns in **Fig. 48** ($F_{(3, 55)} = 11.277$, $P = 0.001$), where the global speed ($82.59 \mu\text{m s}^{-1}$, SE = 2.46, N = 59) of all zoospores was computed (**Fig. 49a**, control). In contrary, RCDIs derived from individual swimming patterns in **Fig. 48** were significantly different ($F_{(3, 55)} = 10.067$, $P = 0.001$), where pattern III (**Fig. 48k**) was more similar to pattern I (**Fig. 48i**). These two patterns were more different to pattern II (**Fig. 48j**) that was more similar to pattern IV (**Fig. 48l**). The global RCDI ($772.90 \text{ deg s}^{-1}$, SE = 41.73, N = 59) of all zoospores was computed (**Fig. 49c**, control). Based on the motion records, we observed that most zoospores often performed the circular swimming pattern (II) at the initial period before releasing their flagella for encystment (**Vid. 8(4.3)**).

The swimming behaviour of zoospores in the presence of bacterial cells is summed up in **Fig. 49**. Cells of *M. gilvum* VM552 exerted an obvious influence on the swimming patterns of zoospores (**Fig. 49a**), by increasing the circular swimming pattern (II) from 15.25% (in the control) to 47.46%. Moreover, only three swimming patterns (I, II and IV) of zoospores were observed in this condition. Both slightly and highly motile cells of *P. putida* G7 had less influence on the swimming pattern of zoospores, but only highly motile cells increased the sine wave swimming pattern (III) approximately two times higher than the control and in the presence of slightly motile cells. Randomly selected swimming trajectories (10 trajectories) derived from each pattern shown in **Fig. 49a**, are displayed in **Fig. 50**. The statistical comparison of global speeds of zoospores in either absence or presence of bacterial cells (**Fig. 49b**), indicated that only highly motile cells of *P. putida* G7 reduced significantly the global speed of zoospores ($74.06 \mu\text{m s}^{-1}$, SE = 2.08 N = 79) ($F_{(3, 249)} = 9.926$, $P = 0.05$). However, the presence of bacterial cells reduced significantly the global RCDIs of zoospores (**Fig. 49c**). The greatest reduction was caused by highly motile cells of *P. putida* G7 ($256.28 \text{ deg s}^{-1}$, SE = 12.55, N = 79), followed by *M. gilvum* VM552 cells ($464.62 \text{ deg s}^{-1}$, SE = 34.21, N = 59) and slightly motile cells of *P. putida* G7 ($634.06 \text{ deg s}^{-1}$, SE = 33.18, N = 54), respectively ($F_{(2, 249)} = 60.243$, $P = 0.05$).

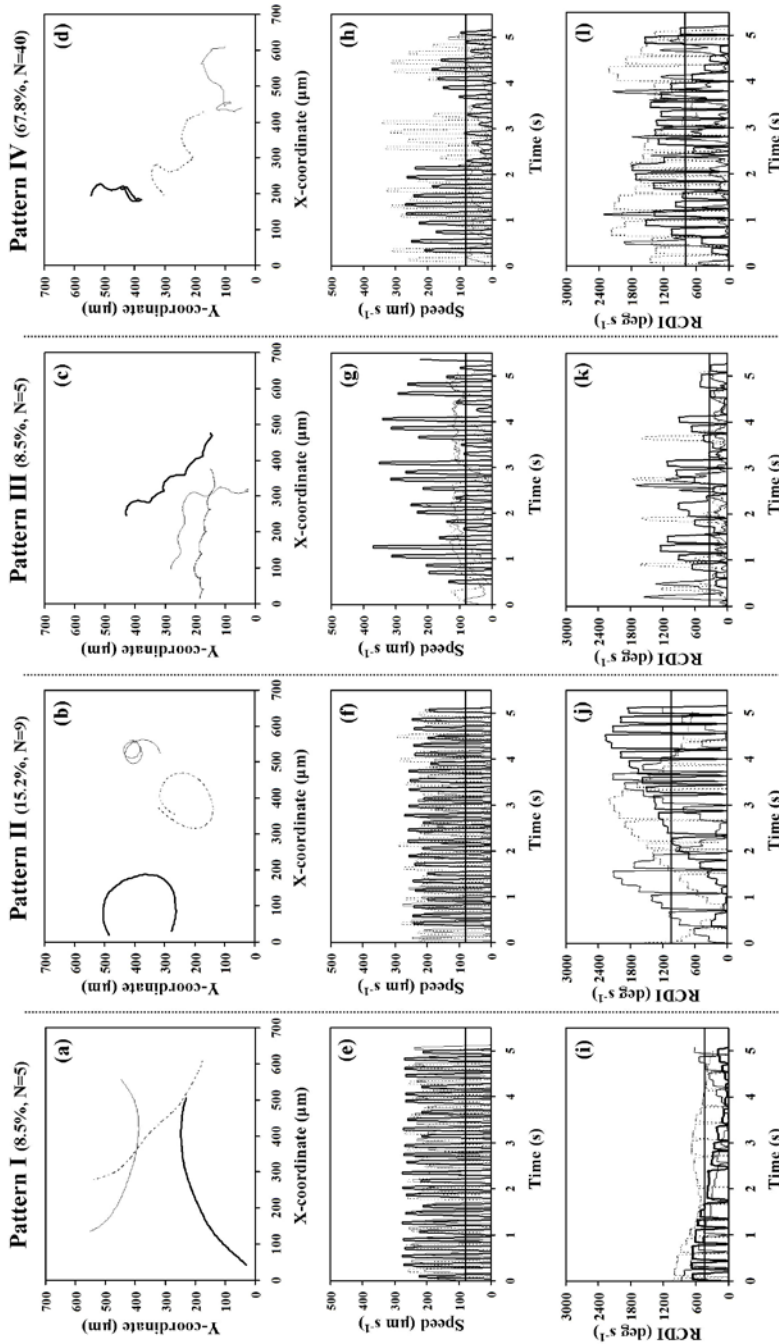


Figure 48 Swimming behaviour of zoospores in sterilized lake water. Three swimming parameters including swimming trajectory (a-d), speed (e-h) and RCDI (i-l) were analyzed by the CellTrak program (see also **CHAPTER III**). The swimming trajectory of zoospores ($N = 59$) was used to determine their swimming patterns, which could be observed with four different patterns comprised of pattern I linear (a), pattern II circular (b), pattern III sine wave (c) and pattern IV freestyle (d). Three representative zoospores were randomly selected to show their swimming trajectories in each swimming pattern, indicating with different line formats (normal, thick and dash lines) (a-d). These swimming trajectories are corresponded to their speeds (e-h) and RCDIs (i-l). The horizontal lines in graphs (e-l) represent the average of means derived from the three representative zoospores shown in each swimming pattern. The population numbers (N) and percentages of zoospores observed in each swimming pattern were determined.

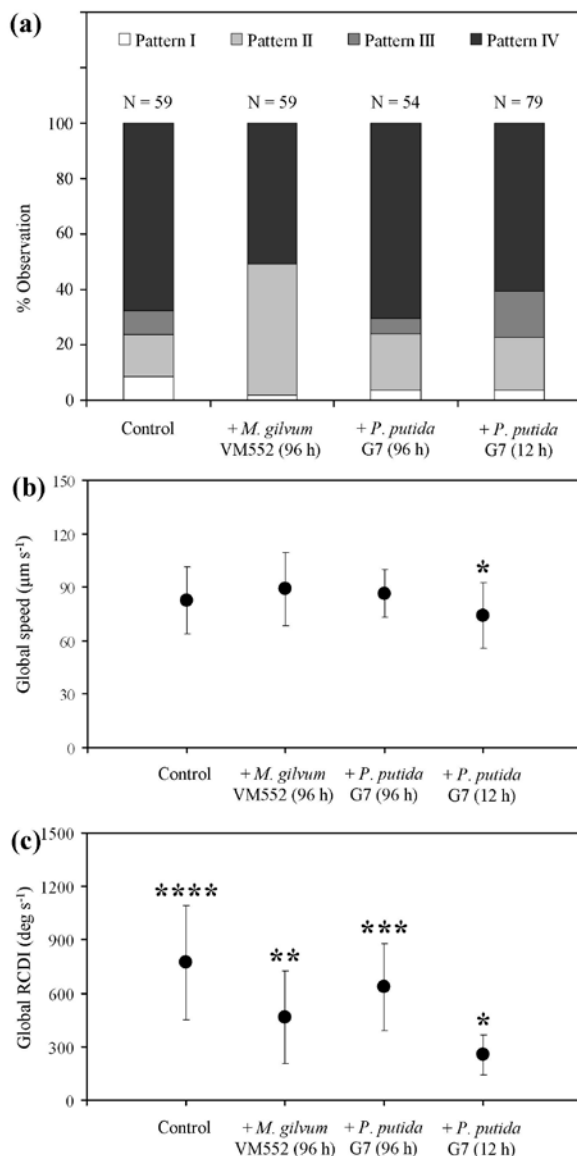


Figure 49 Influence of bacterial cells on swimming behaviour of zoospores. Bacterial cells with different motility levels of *M. gilvum* VM552 and *P. putida* G7 (indicated with the culture ages in the parentheses) were used for evaluation of their influence on swimming behaviour of zoospores, analyzed by the CellTrak program (see also **Table 7** and **CHAPTER III**). The swimming patterns (a), global speeds (b) and global RCDIs (c) were summed up, while the population number (N) of zoospores analyzed in the absence (control) and presence (+) of bacterial cells were indicated in (a). The percent observation of each swimming pattern derived from zoospores analyzed within the same condition was accounted (a). The results of global speeds (b) and global RCDIs (c) were plotted by the average of means derived from zoospores analyzed within the same condition, while the error bars represent the SD. Asterisks and their number refer to a significant difference of means within (b) or (c).

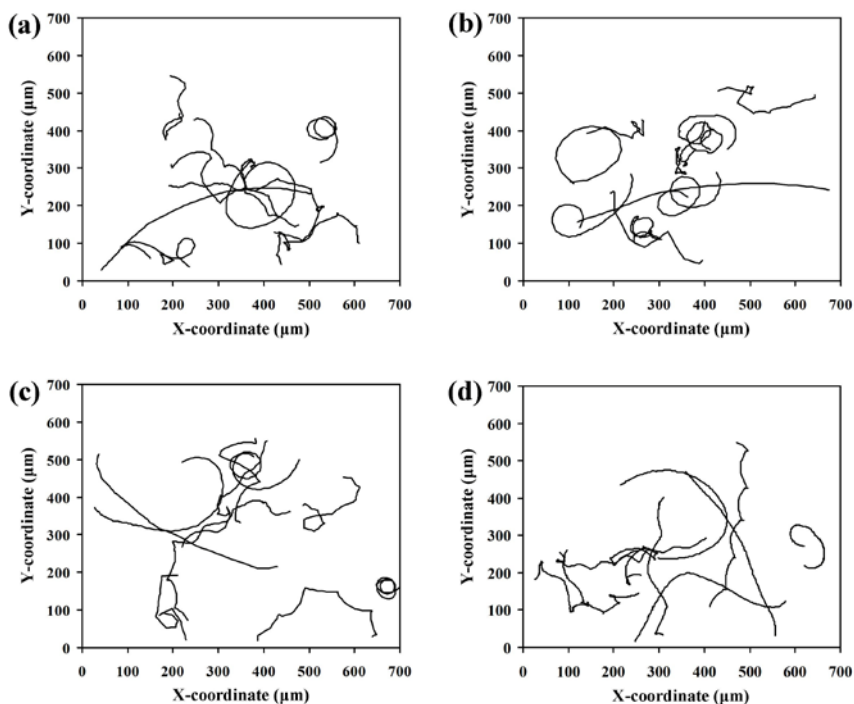


Figure 50 Swimming trajectory of zoospores in the absence and presence of bacterial cells. The trajectories of ten representative swimming zoospores either in sterilized lake water (a) or in the presence of *M. gilvum* VM552 (b), and slightly (c) or highly (d) motile cells of *P. putida* G7 were randomly selected and graphed (see also **Table 7** and **CHAPTER III**).

On the other hand, the influence of zoospores on the swimming behaviour of bacterial cells was also evaluated and summed up in **Fig. 51**. The criteria used for evaluating the swimming behaviour of zoospores were also applied for studying bacterial swimming behaviour. Obviously, only cells from the motile bacterium (*P. putida* G7) were included in this study. Zoospores exhibited an obvious influence on swimming patterns of either slightly (96 h) or highly (12 h) motile cells of *P. putida* G7 (**Fig. 51a**) by increasing the freestyle swimming pattern (IV) from 35.30-37.40% in control to 85.30-97.60%, respectively. Moreover, the sine wave swimming pattern (III) of its slightly motile cells was vanished by zoospores, while both linear (I) and sine wave swimming patterns (III) of its highly motile cells were vanished. Bacterial cells themselves also showed different ratios of swimming patterns in the absence of zoospores (control). Highly motile cells preferred to swim with the circular pattern (II) (40.60%), while slightly motile cells preferred to swim with linear pattern (I).

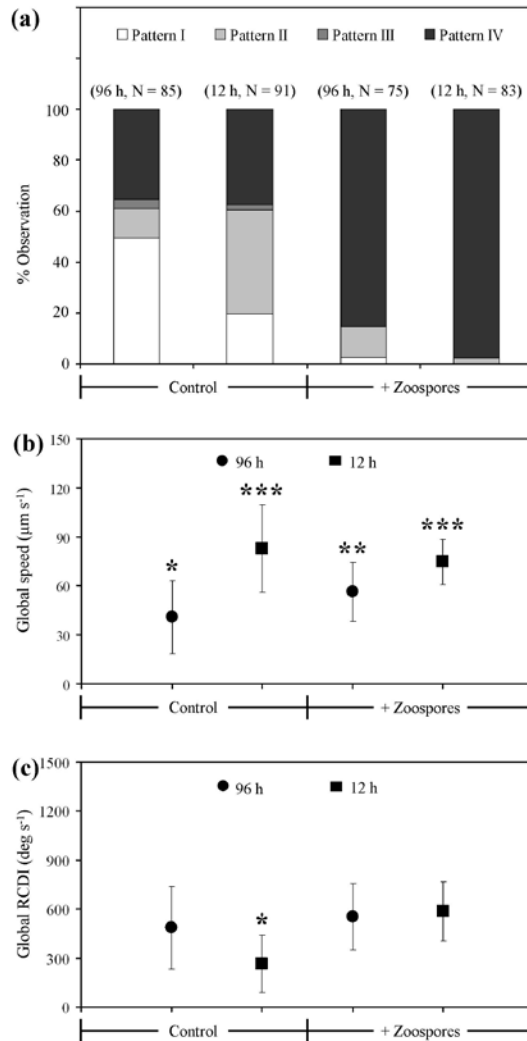


Figure 51 Influence of zoospores on swimming behaviours of *P. putida* G7 cells. The swimming behaviours of slightly (96 h) and highly (12 h) motile cells of *P. putida* G7 (see also **Table 7**) were observed either in the absence (control) or presence (+) of zoospores. The swimming patterns (a), global speeds (b) and global RCDIs (c) of bacterial cells were analyzed by the CellTrak program (see also **CHAPTER III**) and summed up, while the population number (N) of bacterial cells analyzed within the same condition were indicated in (a). The percent observation of each swimming pattern derived from all bacterial cells detected in each condition was accounted (a). The percent observation of each swimming pattern derived from bacterial cells analyzed within the same condition was accounted (a). The results of global speeds (b) and global RCDIs (c) were plotted by the average of means derived from bacterial cells analyzed within the same condition, while the error bars represent the SD. Asterisks and their number refer to a significant difference of means within (b) or (c).

Randomly selected swimming trajectories (10 trajectories) derived from each pattern shown in **Fig. 51a**, are displayed in **Fig. 52**. When the statistical comparison of the global speeds of

bacterial cells either in the absence or presence of zoospores was performed (**Fig. 51b**), we determined that zoospores increased significantly only the global speed of slightly motile cells of *P. putida* G7 up to $56.37 \mu\text{m s}^{-1}$ (SE = 2.09 N = 75) ($F_{(3, 330)} = 68.597$, $P = 0.001$). However, zoospores did significantly increase only the global RCDIs (**Fig. 7C**) of its highly motile cells up to $586.41 \text{ deg s}^{-1}$ (SE = 19.84, N = 83) ($F_{(3, 330)} = 43.511$, $P = 0.001$).

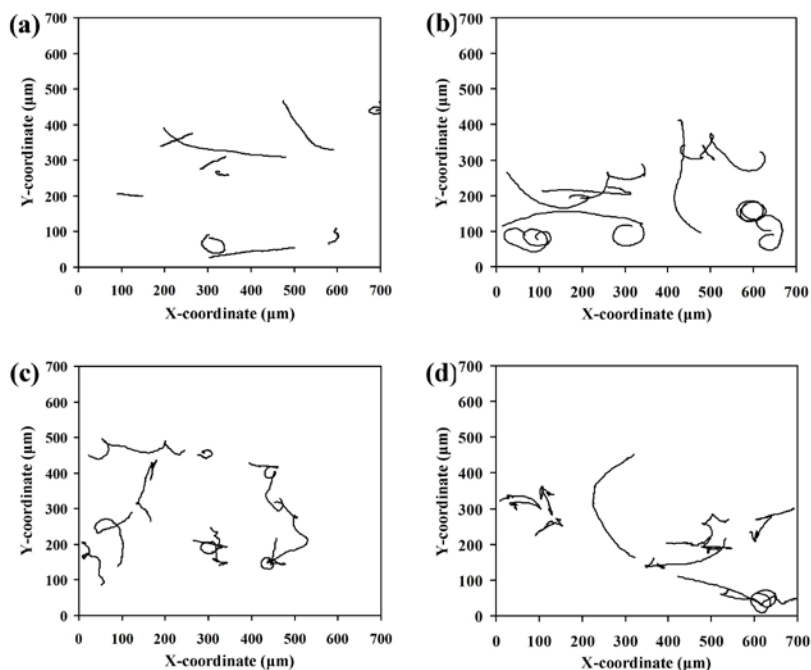


Figure 52 Swimming trajectory of *P. putida* G7 in the absence and presence of zoospores. The trajectories of ten representative bacterial cells swimming either in sterilized lake water (a,b) or in the presence of zoospores (c,d) were randomly selected and graphed (see also **Table 7** and **CHAPTER III**).

CHAPTER V: DISCUSSION

5.1 Ecological interaction between eukaryotic zoospores and PAH-degrading bacteria

Recent studies revealed that mycelia of zoospore-producing oomycetes could mobilize PAH-degrading bacteria and/or PAHs, what later promoted biodegradation of these pollutants (Furuno *et al.*, 2010; 2012; Wick *et al.*, 2007a). The mobilization of motile cells of *P. putida* G7 through the mycelial surfaces of *Py. aphanidermatum* and *Py. oligandrum* was observed in the antagonism tests carried out in this study. These mobilizing phenomena were observed only on a rich medium (TSA, 2% (w/v) of total carbon and energy source), what suggests that the bacterium might have been mobilized effectively by the oomycete as a result of its chemotaxis and growth on nutrients mobilized along the mycelia. Moreover, the dense mycelial growth of the oomycete was found only on the biomass of *M. gilvum* VM552 grown on limited medium (DV8 agar, 0.2% (w/v) of total carbon and energy source). Thus, the nutrient exchange between bacterial cells and oomycetes could occur selectively, depending on either bacterial species or carbon and energy source. Given the lack of knowledge on how eukaryotic zoospores live and respond within polluted environments, we first examined here the development of these zoospores in different exposure regimes of PAHs and expanded the idea on how these zoospores could interact with PAH-degrading bacteria.

For the assessment of the potential of eukaryotic zoospores in biodegradation and bioremediation of PAHs, a fundamental understanding of zoospore formation in the presence of PAHs is needed. It was conceived that the toxic influence of PAHs on zoospore formation was dependent on either C_{exp} that exhibited a strong connection with the aqueous solubility of PAHs or on the unique chemical structure of each PAH. It is already known that PAHs possessing bay or fjord regions in their chemical structures are the most potent carcinogens to eukaryotic cells than those lacking these regions (Sundberg *et al.*, 1997). Therefore, the strong toxic influence of low-water-solubility PAHs, such as phenanthrene and fluoranthene, may concern to the bay region within their chemical structures, while phenanthrene showed a higher influence as its C_{exp} was 3-time higher than fluoranthene. Also, with the rest PAHs

that have no either bay or fjord regions, the toxic influences could be described in accordance to their C_{exp} , where naphthalene and fluorene, possessing higher C_{exp} , showed a greater toxic influence than those others with a lower C_{exp} . Interestingly, PAH-degrading bacteria suppressed the toxic influence of most PAHs tested, as evidenced by a significant enhancement of zoospore formation. The detoxification mechanisms of PAHs were somewhat species-dependent and might be connected with either sorption of PAHs to bacterial biomass (Stringfellow and Alvarez-Cohen, 1999) or to the removal of the existing PAHs through bacterial metabolism. Some studies have evidenced that microbial degradation of PAHs could reduce their toxicity (Gandolfi *et al.*, 2010; Pagnout *et al.*, 2006). This is in agreement with our results, which show that the naphthalene-degrading bacterium *P. putida* G7 detoxified naphthalene more efficiently than *M. gilvum* VM552, while the latter could better detoxify phenanthrene than naphthalene.

In this thesis, we explored how eukaryotic zoospores reacted to diverse chemical effectors typically found in PAH-polluted scenarios. Zoospores possess at least a flagellum for translocation purposes. The swimming period and travelling distance of zoospores vary dependent on each species and the surrounding microenvironment (Blanco and Judelson, 2005; Fan *et al.*, 2002; Gleason and Lilje, 2009; Heungens and Perke, 2000). Swimming can be maintained up to 2 days in some fungal zoospores (Gleason and Lilje, 2009). The swimming capacity of zoospores constitutes an efficient dispersal tool for their homing, settlement and colonization on target locations, and it is mainly regulated through chemotactic mechanisms. Chemotaxis of rhizosphere zoospores, known so far, occurs towards a set of attractants excreted from plant roots. We first found here that *Festuca* root exudates are a potent attractant for *Py. aphanidermatum* zoospores, while the chemotactic response of the zoospores towards this attractant was not interrupted by PAHs or PAH-degrading bacteria. Some organic solvents like alcohols are known also as an attractant of diverse zoospores (Cameron and Carlile, 1978; Fan *et al.*, 2002). Here we also found that acetone is one of these attracting solvents for *Py. aphanidermatum* zoospores. It is conceivable that exposure to PAHs at a maximum C_{exp} , (i.e., dissolved in the solvents) diminished zoospore chemotaxis due to toxicity. However, zoospore chemotaxis towards *Helianthus* root exudates was enhanced when they were co-exposed with PAHs. The exact reason for this enhancement remains uncertain, but it may be related to possible chemoattraction to DOC-associated PAHs. Interestingly, *P. putida* G7 cells also caused an enhancement of zoospore chemotaxis towards *Helianthus* root exudates, and this

enhancement was not affected by PAHs. This bacterium-mediated enhancement can be understood by postulating toxic suppression mechanisms (biosorption or biodegradation) for specific components in root exudates driven by bacterial biomass. It is also possible that fluid advection during interactive motility of both zoospores and bacterial cells promoted zoospore mobilization towards such root exudates.

The settlement behaviour was evaluated as an interesting lifestyle in zoospore development that could be relevant in PAH-polluted scenarios. PAHs are often found in the environment associated to hydrophobic materials, such as liquid hydrocarbons, which causes a low bioavailability for microbial degradation and further limits the efficiency of bioremediation. The development of interface microbial communities with PAH-degrading capabilities is often required for effective biodegradation (García-Junco *et al.*, 2001; Ortega-Calvo and Alexander, 1994; Tejeda-Agredano *et al.*, 2011). However, the formation of these communities has been found to be limited by diverse factors, such as limited bacterial dispersion in subsurface environments and nutrient limitations at interfaces. Based on the settlement behaviour of zoospores in our pollutant-water interface model, we observed that zoospores settled at the HD-water interface. This settlement was not influenced by PAHs and PAH-degrading bacteria but it seemed to occur through selective sensing toward HD, because the methyl-branched chemical HMN was not recognized by *Py. aphanidermatum* zoospores. In addition, neither HD nor HMN was a carbon and/or energy source for growth of this zoospore-producing oomycete (**Fig. 27**). Thus, substratum sensing was probably related to the population community of the zoospores themselves and the surface topography of such substratum. This observation agrees with a set of studies on the selective settlement behaviour of marine fouling zoospores (Greer *et al.*, 2003; Heydt *et al.*, 2012; Schumacher *et al.*, 2007). Moreover, a recent study evidenced that the spontaneous settlement of oomycete zoospores, known as auto-aggregation behaviour, was regulated through chemotaxis and bioconvection mechanisms (Savory *et al.*, 2014). After settlement, zoospores could germinate their germ tubes into the hydrophobic layer of HD. This may cause an increase of pollutant-water interfacial area and an enhancement of chemical partitioning from the substratum into the aqueous phase, which may subsequently increase bioavailability of the pollutants for bacterial degradation. We also found, at the settlement areas, the co-existence with numerous cells of PAH-degrading bacteria which could well be a starting point of biofilm formation at the HD-water interface. The potential of biofilm as a promoting strategy in bioremediation of diverse pollutants is well documented (Singh *et al.*, 2006). A number of

studies have revealed that algal zoospores react chemotactically towards quorum sensing compounds produced by bacterial biofilms, what lead to complex eukaryote-prokaryote communities on wet solid surfaces within marine environments (Joint *et al.*, 2002; Patel *et al.*, 2003).

5.2 Roles of oomycetes/bacteria interaction in biodegradation of PAHs

With the aim to evaluate the influence of oomycetes on the biodegradation activity of *M. gilvum* VM552, we confirmed that mineralization of phenanthrene by oomycetes was negligible either under aerated or static conditions. Under aerated conditions and absence of any supplements (oomycetes and/or DV8 agar), bacterial mineralization of phenanthrene was linear during the entire experimental period. This linear kinetics of mineralization activity of phenanthrene associated with the same NAPL (fuel/HMN) and under the same aerated conditions also occurred in a previous study from our group, and it was consistent with bioavailability-limited biodegradation (Tejeda-Agredano *et al.*, 2011). In addition, the different element composition found in the medium solutions (lake water (**Fig. 14**) for this work and mineral salt medium (Tejeda-Agredano *et al.*, 2011) for the previous study) used in the biometric system did not influence such linear kinetics. Other physicochemical properties of lake water with a little amount of DOC ($9.00 \pm 0.12 \text{ mg L}^{-1}$) and slightly basic pH (7.8 ± 0.14) (**Table 2**) are also different to the ones of the mineral salt medium (without DOC and acidic pH (5.4)). These observations suggested that *M. gilvum* VM552 can metabolize NAPL-associated phenanthrene with a constant rate ($0.29 \pm 0.04 \text{ ng mL}^{-1} \text{ h}^{-1}$) under aerated conditions, although it was introduced in different ecological niches. This constant rate was not different significantly to the previous work at $0.11 \text{ ng mL}^{-1} \text{ h}^{-1}$, but it was slightly higher than the partitioning rate ($0.18 \text{ ng mL}^{-1} \text{ h}^{-1}$) of phenanthrene derived from NAPL into the aqueous phase (Tejeda-Agredano *et al.*, 2011). It seemed that a low concentration of DOC in lake water could enhance bacterial mineralization by increasing 3-time higher in mineralization rate than the use of mineral salt medium. This was in agreement with a recent study, revealing that in the presence of humic acid as a common dissolved organic matter could enhance bacterial uptake of PAHs (Tejeda-Agredano *et al.*, 2014). Surprisingly, we first found that *M. gilvum* VM552 exhibited an exponential mineralization (logistic kinetics with S-shaped curve) in the absence of any supplements under static conditions. It was supported by the percent mineralization of phenanthrene compared at the same experimental

period, where the extent of phenanthrene mineralization was 50% under static conditions, while under aerated conditions it was 25%. This would be a breakthrough of the commonly assumed concept that physical aeration often promotes bacterial mineralization.

It was conceived that oomycetes and/or DV8 agar could enhance bacterial mineralization either under aerated or static conditions. The difference between these two conditions resulted in dissimilar mineralization kinetics, where the aerated conditions could reach to the stationary phases with shorter time from zero-order compared to the static conditions. We assumed initially that the availability of nutrients in the aqueous phase of mineralization experiments, enhanced by either oomycete growth or physical aeration, was a primary reason influencing bacterial mineralization. However, the access amount of nutrients was not a major factor enhancing bacterial mineralization, as in the presence of oomycete mycelia as the only supplement, the logistic kinetics, with maximum mineralization rates still above the predictions from partitioning rate, was still observed. Such observation was supported by the significant different concentrations of DOC quantified during the mineralization experiments, where the lowest concentrations of DOC were found in the treatments supplemented solely with oomycete mycelia (**Fig. 40**). The role of DO exhibited also a slight effect on bacterial mineralization because the variations of DO were observed only during the initial 200 h (**Fig. 39**), a period in which phenanthrene mineralization was still in the lag phase. Therefore, we propose that the major factor in the enhancement of bacterial mineralization is the improvement of conditions for promoting microbial life at the interface between NAPL and water. It was found that the treatments implemented with oomycetes grown on DV8 caused the highest rates of mineralization, even when the mineralization experiments were performed under aerated or static conditions. The reason of such results could be explained by the mutual subsistence of oomycetes within the aqueous phase of the biometric systems, where they might provide nutrients, initially bound in the solid phase but dissolved passively into the aqueous phase, and/or reduce the shear force of the aqueous microenvironment caused by aeration. An evidence of oomycete development in the formation of zoospores was also revealed, while this developmental stage was species-dependent but independent from any treatments and experimental conditions (**Fig. 32**). The proposed effects by oomycetes and/or DV8 agar would promote bacterial colonization at the NAPL-water interface, which subsequently enhance onsite biodegradation activity of bacteria. Diverse studies of bacterial mineralization of organic chemicals dissolved either in single- or multiple-component NAPLs revealed that logistic kinetics has been commonly observed in

relevant to the attribution of attached bacteria at the NAPL-water interface (Garcia-Junco *et al.*, 2003; Ortega-Calvo and Alexander, 1994; Tejeda-Agredano *et al.*, 2011). However, the exact mechanisms and influencing factors of such bacterial attachment is still unknown.

Within this study, we observed an interesting correlation between the microbial settlement at the NAPL-water interface and the evolution of NAPL surface topography, in connection with bacterial mineralization of phenanthrene. It was observed that the shape of the NAPL surface in contact with the water phase changed along the entire period of the mineralization experiments, but it experienced a more rapid change in the presence of *M. gilvum* VM552. This may relate to the surface wettability of the NAPL drop in contact with the water phase. Therefore, the bacterium seemed to enhance the wettability after it attached at the surface of NAPL. The study by Grate *et al.* (2012) revealed that the oil-water contact angle increased in accordance to the surface wettability of the oil drop, which at an intermediate wet stage had a range of contact angles between 80-120°, but it could reach up to a range of 120-160° at the full wet conditions. Our observations were in agreement with this study, and suggested that the activity of *M. gilvum* VM552 cells and their settlement at the NAPL-water interface caused a faster change of the NAPL-water contact angle than it happened spontaneously in the absence of bacteria. This change may also involve the simultaneous biodegradation of substrates present in fuel (PAHs, their alkyl derivatives, and alkanes) by the attached bacteria. Moreover, the interface colonization by bacteria may not only increase the evolution of such surface topography, but may also reduce the viscosity of the NAPL. We observed a clear change of colour in the aqueous phase in the presence of *M. gilvum* VM552, turning from clear transparent at the starting day to yellowish solutions at the end of experiments. The correlation of NAPL viscosity and chemical partitioning from it into aqueous phase has been well documented (Chen *et al.*, 1994). However, this colour might also have been caused by the release of PAH metabolites into the aqueous medium. We also observed that the evolution of NAPL-water contact angle showed a strong connection with biofilm formation at the NAPL-water interface. The impacts of biofilms in bioremediation technology have been well documented (Singh *et al.*, 2006). Although dense biofilms were observed in all treatments inoculated with *M. gilvum* VM552, it was interesting that only the biofilms formed in the presence of *Py. aphanidermatum* grown on DV8 agar under static conditions, had oomycete mycelia as a component in the biofilm structure. With these findings, we concluded that the biofilms could be initiated spontaneously through bacterial colonization, but further biofilm development was mediated through an ecological interaction with

oomycetes. The mechanisms on how oomycetes behaved in the biofilm structure are still unknown, but we postulate that the formation of zoospores could play a role. Therefore, the static conditions caused greater enhancements of bacterial colonization on the NAPL-water interface and zoospore formation by the oomycete, and they can be proposed as an optimal system for integrating the positive oomycete traits in an enhanced pollutant biodegradation of *Mycobacterium* spp. in low bioavailability regimes. Moreover, the coexistence, within the biofilm structure, of bacterial cells and oomycete zoospores, may allow cross-kingdom interactions, where the metabolites released by bacterial biofilms settled initially at the NAPL-water interface may act as attractive compounds inducing zoospore chemotaxis towards such bacterial biofilm. There are some studies revealed that eukaryotic zoospores of marine algae showed a chemotactic response toward signalling molecules produced by bacterial populations, which leads to complex biofilm formation of this eukaryote-prokaryote consortium (Joint *et al.*, 2002; Patel *et al.*, 2003; Twigg *et al.*, 2014). The coexistence of bacteria and oomycetes in the biofilm structure could allow functional interactions at the community level, which may further expand the interface exchange of chemicals (enhanced pollutant bioavailability) and/or the bacterial mineralization activity (enhanced biodegradation). The determination of the roles of oomycetes on the synergistic formation of microbial biofilm at the pollutant-water interfaces and the mechanical interaction between these two microbes within aqueous microenvironments are essential in order to sustain the microbial degrading activity in development of bioremediation.

5.3 Biomobilization of pollutant-degrading bacteria by chemotaxis of eukaryotic zoospores

Ecological interactions between zoospores and other microorganisms have been studied mostly in connection with the biological control of zoospore invasion and pathogenicity (Heungens and Parke 2000; Timmusk *et al.*, 2009). A set of studies evidenced that some algal zoospores performed a mutual lifestyle with bacterial biofilm dwelling at the solid surfaces in marine environment (Joint *et al.*, 2002; Tait *et al.*, 2005; 2009; Twigg *et al.*, 2014). The key mechanism through which zoospores interact with their targets is chemotaxis and electrotaxis (Hosseini *et al.*, 2014; van West *et al.*, 2002). Here, we aim to employ the swimming activity of zoospore chemotaxis for mobilization of pollutant-degrading bacteria. A set of organic solvents like alcohols is known so far to be attractant for chemotaxis of

oomycete zoospores (Allen and Newhook, 1973; Cameron and Carlile, 1978). The chemotactic reaction of *Phytophthora* zoospores towards a set of alcohols within water-saturated soil pores has been proposed as an infection mechanism of these zoospores towards their host plants (Allen and Newhook 1973). This reaction correlated with the concentration of alcohols, although the different concentrations of alcohols tested did not influence the speed and RCDI of the zoospores. We observed in our study that zoospores of *Py. aphanidermatum* could respond chemotactically towards a wide range (5-100%) of ethanol concentrations. The lowest concentration of this zoospore attractant was selected to assess bacterial mobilization.

We first evidenced here that eukaryotic zoospores caused the mobilization of PAH-degrading bacteria through chemotaxis. The effectiveness of this mobilization was highly dependent on the motility and the physiology of bacterial cells. It was conceived that non-flagellated or slightly motile and smaller cells of bacteria were more effectively mobilized by zoospores. This might be related to the changes of fluid dynamics caused by the swimming behaviour and chemotaxis of zoospores, what would have a higher influence on the translocation of immotile particles suspended in their swimming trajectories. Some evidences revealed that micro-swimmers (motile bacteria and green algae) could reduce the viscosity of suspensions, and this reduction was dependent on cell density and swimming speed (Gyrya *et al.*, 2011; Sokolov and Aranson, 2009). It was probably due to the reduced viscosity of bacterial suspension caused by swimming zoospores, which further promoted bacterial mobilization. In addition, a recent study on auto-aggregation of oomycete zoospores revealed that this zoospore behaviour can occur only through a combination of chemotaxis and bioconvection mechanisms (Savory *et al.*, 2014). Interestingly, the authors evidenced that such swimming phenomenon causes dramatic changes in the fluid dynamics of aqueous microenvironments. On the basis of our study, we observed two possible mechanisms, including bioadvection and microbial vortex, appeared when zoospores performed chemotactically towards their attractant. The bioadvection could be observed when zoospores entering into the capillary tubes, which further created advection flows as a hydraulic force moving bacterial cells at a short-path translocation, along their swimming trajectories. There are some studies revealed that bioadvection caused by diverse benthos can create a fluid flow through capillary pores in sediments, where the nutrient and oxygen exchange has been proposed to take place (Matsui *et al.*, 2011; Volkenborn *et al.*, 2010). The microbial vortex caused by circular movement of zoospores was proposed first here to be a biological factor influencing the hydraulic activity

of their microhabitat. This mechanism was observed as an effective tool in mobilization of bacterial cells. Some studies evidenced that vortical flows within aqueous microenvironments could affect microbial motility, aggregation and biofilm formation (Marcos and Stocker, 2006; Yazdi and Ardekani, 2012). The two mechanisms proposed here were strongly connected with the swimming behaviour and chemotactic response of zoospores, because we found that zoospores spontaneously performed circular movement either during their swimming periods or before their encystment. Hence, the mobilizing efficiency may be reflected by either a unique swimming behaviour of zoospores or their interactive motility in the presence of PAH-degrading bacteria.

Four swimming patterns of zoospores were reported here. The freestyle swimming pattern was found abundantly in either absence or presence of PAH-degrading bacteria. This observation differs from a previous report, where the sine wave swimming pattern was found typically in *Py. aphanidermatum* zoospores (Appiah *et al.*, 2005). It might be due to undetermined differences in the zoospore-producing conditions used. The global speed of zoospores detected in this work ($82.59 \mu\text{m s}^{-1}$, SE = 2.46, N = 59) was more constant across different swimming patterns, but it was much faster ($180\text{-}210 \mu\text{m s}^{-1}$, N = 30) when a 2 mM sodium phosphate buffer (Appiah *et al.*, 2005) was used instead of sterilized lake water (our study). It was clear that RCDI is a parameter used for categorizing the swimming pattern of zoospores, because it changed across the different swimming patterns. Interestingly, the swimming behaviour of zoospores was influenced by the presence of PAH-degrading bacteria. For example, *M. gilvum* VM552 cells reduced the RCDIs and induced a circular movement in the zoospores. On the other hand, zoospores themselves influenced clearly the motility of *P. putida* G7 (both slightly and highly motile cells). The speeds of highly motile cells were constant either in absence or presence of zoospores, which were most likely the same as a previous report of this bacterium swimming in the presence of glucose, where the speed above $60 \mu\text{m s}^{-1}$ was defined as an active motility (Jimenez-Sanchez *et al.*, 2012). However, the RCDI of highly motile cells of *P. putida* G7 was increased in the presence of zoospores, what caused a shift in their swimming patterns, in a similar way as the zoospore RCDIs. This influence by zoospores on bacterial swimming might be part of an interactive motility between these two microorganisms. These observations extend previous findings that the swimming behaviour of *P. putida* G7 can be modified by chemical effectors present within its aqueous microhabitats, like carbon and energy sources such as glucose (Jimenez-Sanchez *et al.*, 2012) or repellents like silver nanoparticles (Jimenez-Sanchez *et al.*, 2012;

Ortega-Calvo *et al.*, 2011). Besides, we suppose that nutrient scarcity in this aquatic microenvironment would be a reason for competition, which could further influence the swimming physiology of both microorganisms.

CHAPTER VI: CONCLUSIONS

The most relevant conclusions from this PhD thesis are:

- 1. Oomycetes provide a set of potential benefits for bioremediation of PAHs based on their ecological lifestyles, both in the filamentous and mobile modes of their life cycle.** Mycelial growth at interfaces and zoospore development (production, chemotaxis and settlement) could further increase the efficiency of PAH-degrading bacteria during bioremediation.
- 2. There was no antagonism between oomycetes and PAH-degrading bacteria.** Although an abundant cell density of PAH-degrading bacteria diminished zoospore formation, this cell density is much higher than the density of bacterial populations typically found in natural and polluted soils.
- 3. Zoospore development within PAH-polluted scenarios was sensitive to pollutant bioavailability and bacterial activity.** The toxic effects of contaminants towards zoospores were diminished by PAH-degrading bacteria through biodegradation and biosorption. Furthermore, PAH-degrading bacteria enhanced the positive chemotactic reaction of zoospores to specific chemicals simulating PAH-polluted scenarios, such as plant root exudates. Zoospore settlement on NAPLs provided a facility for localization of bacteria at the interface.
- 4. Oomycete mycelia enhanced bacterial biodegradation of PAHs under bioavailability restrictions.** Within PAH-polluted scenarios, sparingly available PAHs were transformed faster by specialized bacteria in the presence of oomycetes. Oomycetes could support the exchange of nutrients and sustain biofilm formation at the pollutant-water interface, therefore supporting the mineralization activity of PAH-degrading bacteria at these specific niches. Moreover, the coexistence of oomycetes in this scenario could also reduce the shear interferences caused by aeration, and further facilitated bacterial biofilm formation. This bacterial biofilm was found to be a key factor influencing the biodegrading capacity of bacteria and phase-partitioning of PAHs, because the mineralization rate of phenanthrene was higher than the partitioning rate of

the chemical into the aqueous phase. Zoospore development within this scenario was observed, which further proposed as a mobile tool for dispersion of bacteria toward the pollutant-water interface, where a complex microbial community could take place and expand onsite biodegradation of active bacteria.

- 5. Oomycete zoospores mobilized directionally PAH-degrading bacteria through their chemotactic behaviour.** This behaviour together with their intrinsic mode of swimming influenced the hydraulic activity of aqueous microenvironments, which later created a fluid flow that enhanced bacterial mobilization. Two possible mechanisms caused by the chemotactic reaction of zoospores, advection and vortical flows, were identified. However, the mobilization through these mechanisms was depended on bacterial cell size and motility. In addition, we observed an interactive swimming between zoospores and PAH-degrading bacteria that may facilitate bacterial mobilization.

CHAPTER VII: CONCLUSIONES (Conclusions in Spanish)

Las conclusiones más importantes de esta tesis doctoral son:

- 1. Los oomicetos proporcionan una serie de beneficios potenciales para la biorremediación de HAPs basados en sus estilos ecológicos de vida, tanto en el modo filamentosos como en el modo móvil de su ciclo de vida.** El crecimiento micelial en las interfases y el desarrollo de zoosporas (producción, quimiotaxis y asentamiento) podrían incrementar la eficiencia de las bacterias degradadoras de HAPs durante la biorremediación.
- 2. No hubo antagonismo entre las bacterias degradadoras de HAPs y los oomicetos.** Aunque una alta densidad de células bacterianas podría disminuir la formación de zoosporas, esta densidad celular es mucho mayor que la densidad típica de las poblaciones bacterianas que se encuentran en suelos naturales y contaminados.
- 3. El desarrollo de las zoosporas en escenarios de contaminación por HAPs fue sensible a la biodisponibilidad de los contaminantes y a la actividad bacteriana.** Las bacterias degradadoras de HAPs disminuyeron los efectos tóxicos de los contaminantes a través de biodegradación y bioadsorción. Además, las bacterias aumentaron la reacción quimiotáctica positiva de las zoosporas frente a compuestos específicos que simulaban escenarios contaminados por HAPs, tales como exudados de raíces de plantas. El asentamiento de las zoosporas sobre el NAPL proporcionó sitios para la colonización bacteriana de la interfase.
- 4. Los micelios de los oomicetos causaron un aumento de la biodegradación bacteriana de HAPs bajo restricciones de biodisponibilidad.** En escenarios de contaminación por HAPs, los contaminantes fueron transformados más rápidamente por bacterias especializadas en presencia de los oomicetos. Los oomicetos pudieron promover el intercambio de nutrientes y mantener la formación de biofilms en la interfase entre el contaminante y el agua, por tanto promoviendo la mineralización de los contaminantes por parte las bacterias degradadoras de HAPs en estos nichos específicos. Además, la coexistencia con los oomicetos en este escenario podría también reducir las

interferencias de cizalla causadas por la aeración, facilitando así la formación de biofilms por las bacterias. Estos biofilms bacterianos se identificaron como un factor clave en la capacidad degradadora de las bacterias y en el reparto de los HAPs, dado que la tasa de mineralización de fenantreno fue mucho mayor que la tasa de reparto del compuesto hacia la fase acuosa. Se observó en este escenario el desarrollo de las zoosporas, por lo que se propone que las mismas suponen una herramienta móvil para la dispersión de las bacterias hacia la interfase entre el contaminante y la fase acuosa, donde se podría desarrollar una comunidad microbiana compleja, y expandir la biodegradación por parte de las bacterias activas.

- 5. Las zoosporas de los oomicetos movilizaron direccionalmente a las bacterias degradadoras de HAPs a través de su comportamiento quimiotáctico.** Este comportamiento junto a su modo intrínseco de natación influyeron sobre la actividad hidráulica de los microambientes acuosos, lo que subsecuentemente creó un flujo de fluido que promovió la movilización bacteriana. Se identificaron dos mecanismos posibles causados por la reacción quimiotáctica de las zoosporas, a través de los flujos por advección y por vórtice. No obstante, la movilización a través de estos mecanismos fue dependiente del tamaño celular y de la movilidad de las bacterias. Además, observamos la natación interactiva entre zoosporas y bacterias, lo cual puede facilitar la movilización bacteriana.

CHAPTER VIII: REFERENCES

Adl SM, Simpson AG, Farmer MA, et al. (2005) The new higher level classification of eukaryotes with emphasis on the taxonomy of protists. *J Eukaryot Microbiol* 52:399-451

Allen RN, Newhook FJ (1973) Chemotaxis of zoospores of *Phytophthora cinnamomi* to ethanol in capillaries of soil pore dimensions. *Trans Br Mycol Soc* 61:287-302

Alexander M (2000) Aging, bioavailability, and overestimation of risk from environmental pollutants. *Environ Sci Technol* 34:4259-4265

Ambrosoli R, Petruzzelli L, Luis Minati J, Ajmone Marsan F (2005) Anaerobic PAH degradation in soil by a mixed bacterial consortium under denitrifying conditions. *Chemosphere* 60:1231-1236

Appiah AA, van West P, Osborne MC, Gow NAR (2005) Potassium homeostasis influences the locomotion and encystment of zoospores of plant pathogenic oomycetes. *Fungal Genet Biol* 42:213-223

Aßmann C, Nechwatal J, Rinke K, von Elert E (2010) The impact of axenic strains of fungi and oomycetes on the preference of *Gammarus roeselii* for leaf litter. *Fundam Appl Limnol, Arch Hydrobiol* 176:235-248

Aßmann C, Rinke K, Nechwatal J, von Elert E (2011) Consequences of the colonisation of leaves by fungi and oomycetes for leaf consumption by a gammarid shredder. *Freshwater Biol* 56:839-852

Bellas J, Saco-Álvarez L, Nieto Ó, Beiras R (2008) Ecotoxicological evaluation of polycyclic aromatic hydrocarbons using marine invertebrate embryo-larval bioassays. *Mar Poll Bull* 57:493-502

Bengtsson G, Zerhouni P (2003) Effects of carbon substrate enrichment and DOC concentration on biodegradation of PAHs in soil. *J Appl Microbiol* 94:608-617

Benhamou N, le Floch G, Vallance J, Gerbore J, Grizard D, Rey P (2012) *Pythium oligandrum*: an example of opportunistic success. *Microbiol* 158:2679-2694

Blanco FA, Judelson HS (2005) A bZIP transcription factor from *Phytophthora* interacts with a protein kinase and is required for zoospore motility and plant infection. *Mol Microbiol* 56:638-648

Bogan BW, Sullivan WR (2003) Physicochemical soil parameters affecting sequestration and mycobacterial biodegradation of polycyclic aromatic hydrocarbons in soil. *Chemosphere* 52:1717-1726

Cerniglia CE (1992) Biodegradation of polycyclic aromatic hydrocarbons. *Biodegradation* 3:351-368

Cameron JN, Carlile MJ (1978) Fatty acids, aldehydes and alcohols as attractants for zoospores of *Phytophthora palmivora*. *Nature* 271:448-449

Chen C, Delfino JJ, Rao PSC (1994) Partitioning of organic and inorganic components from motor oil into water. *Chemosphere* 28:1385-1400

Desai JD, Banat IM (1997) Microbial production of surfactants and their commercial potential. *Microbiol Mol Biol Rev* 61:47-64

Dick MW (2001) Straminipilous fungi: systematics of the Peronosporomycetes including accounts of the marine straminipilous protists, the plasmodiophorids and similar organisms. Springer, Germany

Eaton RW, Chapman PJ (1992) Bacterial metabolism of naphthalene: construction and use of recombinant bacteria to study ring cleavage of 1,2-dihydroxynaphthalene and subsequent reactions. *J Bacteriol* 174:7542-7554

Ellis B, Harold P, Kronberg H (1991) Bioremediation of a creosote contaminated site. *Environ Technol* 12:447-459

Elskens F, Harmsen J (2007) Costs of treatment chains. In: Bortone G, Palumbo L (eds), Sustainable management of sediment resources: sediment and dredged material treatment, Elsevier, Amsterdam, The Netherlands, pp. 185-192

Fan KW, Vrijmoed LLP, Jones EBG (2002) Zoospore chemotaxis of mangrove thraustochytrids from Hong Kong. *Mycologia* 94:569-578

Fester T, Giebler J, Wick LY, Schlosser D, Kästner M (2014) Plant-microbe interactions as drivers of ecosystem functions relevant for the biodegradation of organic contaminants. *Curr Opin Biotechnol* 27:168-175

Fredslund L, Sniegowski K, Wick LY, Jacobsen CS, De Mot R, Springael D (2008) Surface motility of polycyclic aromatic hydrocarbon (PAH)-degrading mycobacteria. *Res Microbiol* 159:255-262

Furuno S, Foss S, Wild E, Jones KC, Semple KT, Harms H, Wick LY (2012) Mycelia promote active transport and spatial dispersion of polycyclic aromatic hydrocarbons. *Environ Sci Technol* 46:5463-5470

Furuno S, Pätzolt K, Rabe C, Neu TR, Harms H, Wick LY (2010) Fungal mycelia allow chemotactic dispersal of polycyclic aromatic hydrocarbon-degrading bacteria in water-unsaturated systems. *Environ Microbiol* 12:1391-1398

Gandolfi I, Sicolo M, Franzetti A, Fontanarosa E, Santagostino A, Bestetti G (2010) Influence of compost amendment on microbial community and ecotoxicity of hydrocarbon-contaminated soils. *Biores Technol* 101:568-575

Gan S, Lau EV, Ng HK (2009) Remediation of soils contaminated with polycyclic aromatic hydrocarbons (PAHs). *J Hazard Mater* 172:532-549

García-Junco M, De Olmedo E, Ortega-Calvo JJ (2001) Bioavailability of solid and non-aqueous phase liquid (NAPL)-dissolved phenanthrene to the biosurfactant-producing bacterium *Pseudomonas aeruginosa* 19SJ. *Environ Microbiol* 3:561-569

Garcia-Junco M, Gomez-Lahoz C, Niqui-Arroyo JL, Ortega-Calvo JJ (2003) Biodegradation- and biosurfactant-enhanced partitioning of polycyclic aromatic hydrocarbons from nonaqueous-phase liquids. *Environ Sci Technol* 37:2988-2996

Garon D, Sage L, Wouessidjewe D, Seigle-Murandi F (2004) Enhanced degradation of fluorene in soil slurry by *Absidia cylindrospora* and maltosyl-cyclodextrin. *Chemosphere* 56:159-166

Gleason FH, Lilje O (2009) Structure and function of fungal zoospores: ecological implications. *Fungal Ecol* 2:53-59

Grate JW, Dehoff KJ, Warner MG, Pittman JW, Wietsma TW, Zhang C, Oostrom M (2012) Correlation of oil-water and air-water contact angles of diverse silanized surfaces and relationship to fluid interfacial tensions. *Langmuir* 28:7182-7188

Greer SP, Iken KB, McClintock JB, Amsler CD (2003) Individual and coupled effects of echinoderm extracts and surface hydrophobicity on spore settlement and germination in the brown alga *Hinckesia irregularis*. *Biofouling* 19:315-326

Grimm AC, Harwood CS (1997) Chemotaxis of *Pseudomonas* spp. to the polyaromatic hydrocarbon naphthalene. *Appl Environ Microbiol* 63:4111-4115

Grimm AC, Harwood CS (1999) NahY, a catabolic plasmid-encoded receptor required for chemotaxis of *Pseudomonas putida* to the aromatic hydrocarbon naphthalene. *J Bacteriol* 181:3310-3316

Gyrya V, Lipnikov K, Aranson IS, Berlyand L (2011) Effective shear viscosity and dynamics of suspensions of micro-swimmers from small to moderate concentrations. *J Math Biol* 62:707-740

Haderlein A, Legros R, Ramsay B (2001) Enhancing pyrene mineralization in contaminated soil by the addition of humic acids or composted contaminated soil. *Appl Microbiol Biotechnol* 56:555-559

Haftka JJH, Parsons JR, Govers HAJ, Ortega-Calvo JJ (2008) Enhanced kinetics of solid-phase microextraction and biodegradation of polycyclic aromatic hydrocarbons in the presence of dissolved organic matter. *Environ Toxicol Chem* 27:1526-1532

Hanzel J, Harms H, Wick LY (2010) Bacterial chemotaxis along vapor-phase gradients of naphthalene. *Environ Sci Technol* 44:9304-9310

Haritash AK, Kaushik CP (2009) Biodegradation aspects of polycyclic aromatic hydrocarbons (PAHs): A review. *J Hazard Mater* 169:1-15

Harms H, Schlosser D, Wick LY (2011) Untapped potential: exploiting fungi in bioremediation of hazardous chemicals. *Nat Rev Microbiol* 9:177-192

- Harvey S, Elashvili I, Valdes JJ, Kamely D, Chakrabarty AM (1990)** Enhanced removal of Exxon Valdez spilled oil from Alaskan gravel by a microbial surfactant. *Biotechnol* 8:228-230
- Hawkins AC, Harwood CS (2002)** Chemotaxis of *Ralstonia eutropha* JMP134(pJP4) to the herbicide 2,4-dichlorophenoxyacetate. *Appl Environ Microbiol* 68:968-972
- Herman DC, Artiola JF, Miller RM (1995)** Removal of cadmium, lead, and zinc from soil by a rhamnolipid biosurfactant. *Environ Sci Technol* 29:2280-2285
- Heungens K, Parke JL (2000)** Zoospore homing and infection events: effects of the biocontrol bacterium *Burkholderia cepacia* AMMDR1 on two oomycete pathogens of pea (*Pisum sativum* L.). *Appl Environ Microbiol* 66:5192-5200
- Heydt M, Pettitt ME, Cao X, Callow ME, Callow JA, Grunze M, Rosenhahn A (2012)** Settlement behavior of zoospores of *Ulva linza* during surface selection studied by digital holographic microscopy. *Biointerphases* 7:33
- Hosseini S, Heyman F, Olsson U, Broberg A, Funck Jensen D, Karlsson M (2014)** Zoospore chemotaxis of closely related legume-root infecting *Phytophthora* species towards host isoflavones. *Plant Pathol* 63:708-714
- Hulvey J, Telle S, Nigrelli L, Lamour K, Thines M (2010)** *Salisapiliaceae* - a new family of oomycetes from marsh grass litter of southeastern North America. *Persoonia* 25:109-116
- Husain S (2008)** Literature overview: Microbial metabolism of high molecular weight polycyclic aromatic hydrocarbons. *Remediation* 18:131-161
- Hyman M, Dupont R (2001)** Groundwater and soil remediation: process design and cost estimating. ASCE Press, Reston, Virginia (USA)
- James TY, Letcher PM, Longcore JE, Mozley-Standridge SE, Porter D, Powell MJ, Griffith GW, Vilgalys R (2006)** A molecular phylogeny of the flagellated fungi (Chytridiomycota) and description of a new phylum (Blastocladiomycota). *Mycologia* 98:860-871
- Jimenez-Sanchez C, Wick LY, Ortega-Calvo J-J (2012)** Chemical effectors cause different motile behavior and deposition of bacteria in porous media. *Environ Sci Technol* 46:6790-6797
- Joint I, Tait K, Callow ME, Callow JA, Milton D, Williams P, Cámara M (2002)** Cell-to-cell communication across the prokaryote-eukaryote boundary. *Science* 298:1207-1207
- Kanaly RA, Harayama S (2000)** Biodegradation of high-molecular-weight polycyclic aromatic hydrocarbons by bacteria. *J Bacteriol* 182:2059-2067
- Kanaly RA, Harayama S (2010)** Advances in the field of high-molecular-weight polycyclic aromatic hydrocarbon biodegradation by bacteria. *Microb Biotechnol* 3:136-164
- Keith LH, Telliard WA (1979)** ES&T special report-priority pollutants: I - a perspective view. *Environ Sci Technol* 13:416-423

- Kerwin JL (2007)** Oomycetes: *Lagenidium giganteum*. J Am Mosq Control Assoc 23:50-57
- Kohlmeier S, Smits THM, Ford RM, Keel C, Harms H, Wick LY (2005)** Taking the fungal highway: mobilization of pollutant-degrading bacteria by fungi. Environ Sci Technol 39:4640-4646
- Kostecki PT, Calabrese EJ (1992)** Contaminated soils. In: Diesel fuel contamination, Lewis Publishers Inc, Chelsea, Michigan (USA)
- Krell T, Lacal J, Reyes-Darias JA, Jimenez-Sanchez C, Sungthong R, Ortega-Calvo JJ (2013)** Bioavailability of pollutants and chemotaxis. Curr Opin Biotechnol 24:451-456
- Lahlou M, Harms H, Springael D, Ortega-Calvo JJ (2000)** Influence of soil components on the transport of polycyclic aromatic hydrocarbon-degrading bacteria through saturated porous media. Environ Sci Technol 34:3649-3656
- Lahlou M, Ortega-Calvo JJ (1999)** Bioavailability of labile and desorption-resistant phenanthrene sorbed to montmorillonite clay containing humic fractions. Environ Toxicol Chem 18:2729-2735
- Lang S, Wullbrandt D (1999)** Rhamnose lipids - biosynthesis, microbial production and application potential. Appl Microbiol Biotechnol 51:22-32
- Latijnhouwers M, Ligterink W, Vleeshouwers VGAA, van West P, Govers F (2004)** A *Ga* subunit controls zoospore motility and virulence in the potato late blight pathogen *Phytophthora infestans*. Mol Microbiol 51:925-936
- Law AM, Aitken MD (2003)** Bacterial chemotaxis to naphthalene desorbing from a nonaqueous liquid. Appl Environ Microbiol 69:5968-5973
- Liang YN, Britt DW, McLean JE, Sorensen DL, Sims RC (2007)** Humic acid effect on pyrene degradation: finding an optimal range for pyrene solubility and mineralization enhancement. Appl Microbiol Biotechnol 74:1368-1375
- Lopez Z, Vila J, Ortega-Calvo JJ, Grifoll M (2008)** Simultaneous biodegradation of creosote-polycyclic aromatic hydrocarbons by a pyrene-degrading *Mycobacterium*. Appl Microbiol Biotechnol 78:165-172
- Mackay D, Shiu WY, Ma K-C, Lee SC (2006)** Handbook of physical-chemical properties and environmental fate for organic chemicals, 2nd edn. CRC Press, Boca Raton, Florida (USA)
- Maier RM, Soberon-Chavez G (2000)** *Pseudomonas aeruginosa* rhamnolipids: biosynthesis and potential applications. Appl Microbiol Biotechnol 54:625-633
- Marcos, Stocker R (2006)** Microorganisms in vortices: a microfluidic setup. Limnol Oceanogr Meth 4:392-398

Martínez-Lladó X, Gibert O, Martí V, Díez S, Romo J, Bayona JM, de Pablo J (2007) Distribution of polycyclic aromatic hydrocarbons (PAHs) and tributyltin (TBT) in Barcelona harbour sediments and their impact on benthic communities. *Environ Poll* 149:104-113

Marx RB, Aitken MD (2000) Bacterial chemotaxis enhances naphthalene degradation in a heterogeneous aqueous system. *Environ Sci Technol* 34:3379-3383

Matsui GY, Volkenborn N, Polerecky L, Henne U, Wetthey DS, Lovell CR, Woodin SA (2011) Mechanical imitation of bidirectional bioadvection in aquatic sediments. *Limnol Oceanogr Meth* 9:84-96

McCray JE, Bai G, Maier RM, Brusseau ML (2001) Biosurfactant-enhanced solubilization of NAPL mixtures. *J Contam Hydrol* 48:45-68

Moody JD, Freeman JP, Doerge DR, Cerniglia CE (2001) Degradation of phenanthrene and anthracene by cell suspensions of *Mycobacterium* sp. strain PYR-1. *Appl Environ Microbiol* 67:1476-1483

Mueller JG, Lantz SE, Blattmann BO, Chapman PJ (1991) Bench-scale evaluation of alternative biological treatment processes for the remediation of pentachlorophenol-and creosote-contaminated materials. Solid-phase bioremediation. *Environ Sci Technol* 25:1045-1055

Mulligan CN, Yong RN, Gibbs BF, James S, Bennett HPJ (1999) Metal removal from contaminated soil and sediments by the biosurfactant surfactin. *Environ Sci Technol* 33:3812-3820

Niqui-Arroyo JL, Bueno-Montes M, Ortega-Calvo JJ (2011) Biodegradation of anthropogenic organic compounds in natural environments. In: B. Xing, Senesi N, Huang PM (eds), *Biophysico-chemical processes of anthropogenic organic compounds in environmental systems*. IUPAC Series on Biophysico-Chemical Processes in Environmental Systems, vol 3. John Wiley & Sons Ltd, Chichester (UK)

Niqui-Arroyo JL, Bueno-Montes M, Posada-Baquero R, Ortega-Calvo JJ (2006) Electrokinetic enhancement of phenanthrene biodegradation in creosote-polluted clay soil. *Environ Pollut* 142:326-332

Ortega-Calvo JJ, Alexander M (1994) Roles of bacterial attachment and spontaneous partitioning in the biodegradation of naphthalene initially present in nonaqueous-phase liquids. *Appl Environ Microbiol* 60:2643-2646

Ortega-Calvo JJ, Birman I, Alexander M (1995) Effect of varying the rate of partitioning of phenanthrene in nonaqueous-phase liquids on biodegradation in soil slurries. *Environ Sci Technol* 29:2222-2225

Ortega-Calvo JJ, Fesch C, Harms H (1999) Biodegradation of sorbed 2,4-dinitrotoluene in a clay-rich, aggregated porous medium. *Environ Sci Technol* 33:3737-3742

Ortega-Calvo J-J, Gschwend PM (2010) Influence of low oxygen tensions and sorption to sediment black carbon on biodegradation of pyrene. *Appl Environ Microbiol* 76:4430-4437

Ortega-Calvo JJ, Marchenko AI, Vorobyov AV, Borovick RV (2003) Chemotaxis in polycyclic aromatic hydrocarbon-degrading bacteria isolated from coal-tar- and oil-polluted rhizospheres. *FEMS Microbiol Ecol* 44:373-381

Ortega-Calvo JJ, Molina R, Jimenez-Sanchez C, Dobson PJ, Thompson IP (2011) Bacterial tactic response to silver nanoparticles. *Environ Microbiol Rep* 3:526-534

Ortega-Calvo JJ, Saiz-Jimenez C (1998) Effect of humic fractions and clay on biodegradation of phenanthrene by a *Pseudomonas fluorescens* strain isolated from soil. *Appl Environ Microbiol* 64:3123-3126

Ortega-Calvo JJ, Tejeda-Agredano MC, Jimenez-Sanchez C, Congiu E, Sungthong R, Niqui-Arroyo JL, Cantos M (2013) Is it possible to increase bioavailability but not environmental risk of PAHs in bioremediation? *J Hazard Mater* 261:733-745

O'Toole GA, Kolter R (1998) Flagellar and twitching motility are necessary for *Pseudomonas aeruginosa* biofilm development. *Mol Microbiol* 30:295-304

Pagnout C, Rast C, Veber A-M, Poupin P, Férard J-F (2006) Ecotoxicological assessment of PAHs and their dead-end metabolites after degradation by *Mycobacterium* sp. strain SNP11. *Ecotoxicol Environ Saf* 65:151-158

Pandey J, Sharma NK, Khan F, Ghosh A, Oakeshott JG, Jain RK, Pandey G (2012) Chemotaxis of *Burkholderia* sp. Strain SJ98 towards chloronitroaromatic compounds that it can metabolise. *BMC Microbiol* 12:19. doi: 10.1186/1471-2180-12-19

Parales RE, Ditty JL, Harwood CS (2000) Toluene-degrading bacteria are chemotactic towards the environmental pollutants benzene, toluene, and trichloroethylene. *Appl Environ Microbiol* 66:4098-4104

Patel P, Callow ME, Joint I, Callow JA (2003) Specificity in the settlement-modifying response of bacterial biofilms towards zoospores of the marine alga *Enteromorpha*. *Environ Microbiol* 5:338-349

Peng RH, Xiong AS, Xue Y, Fu XY, Gao F, Zhao W, Tian YS, Yao QH (2008) Microbial biodegradation of polyaromatic hydrocarbons. *FEMS Microbiol Rev* 32:927-955

Perumbakkam S, Hess TF, Crawford RL (2006) A bioremediation approach using natural transformation in pure-culture and mixed-population biofilms. *Biodegradation* 17:545-557

Quantin C, Joner EJ, Portal JM, Berthelin J (2005) PAH dissipation in a contaminated river sediment under oxic and anoxic conditions. *Environ Pollut* 134:315-322

Rasconi S, Niquil N, Sime-Ngando T (2012) Phytoplankton chytridiomycosis: community structure and infectivity of fungal parasites in aquatic ecosystems. *Environ Microbiol* 14:2151-2170

Reichenberg F, Mayer P (2006) Two complementary sides of bioavailability: Accessibility and chemical activity of organic contaminants in sediments and soils. *Environ Toxicol Chem* 25:1239-1245

Resina-Pelfort O, García-Junco M, Ortega-Calvo JJ, Comas-Riu J, Vives-Rego J (2003) Flow cytometry discrimination between bacteria and clay humic acid particles during growth-linked biodegradation of phenanthrene by *Pseudomonas aeruginosa* 19SJ. FEMS Microbiol Ecol 43:55-61

Rothermich MM, Hayes LA, Lovley DR (2002) Anaerobic, sulfate-dependent degradation of polycyclic aromatic hydrocarbons in petroleum-contaminated harbor sediment. Environ Sci Technol 36:4811-4817

Samanta SK, Bhushan B, Chauhan A, Jain RK (2000) Chemotaxis of a *Ralstonia* sp. SJ98 toward different nitroaromatic compounds and their degradation. Biochem Biophys Res Commun 269:117-123

Šašek V, Bhatt M, Cajthaml T, Malachova K, Lednicka D (2003) Compost-mediated removal of polycyclic aromatic hydrocarbons from contaminated soil. Arch Environ Contam Toxicol 44:336-342

Savory AIM, Grenville-Briggs LJ, Wawra S, van West P, Davidson FA (2014) Auto-aggregation in zoospores of *Phytophthora infestans*: the cooperative roles of bioconvection and chemotaxis. J R Soc Interface 11:2140017. doi:10.1098/rsif.2014.0017

Schumacher JF, Aldred N, Callow ME, Finlay JA, Callow JA, Clare AS, Brennan AB (2007) Species-specific engineered antifouling topographies: correlations between the settlement of algal zoospores and barnacle cyprids. Biofouling 23:307-317

Schwarzenbach RP, Gschwend PM, Imboden DM (2003) Environmental organic chemistry, 2nd edn. John Wiley & Sons, Hoboken, New Jersey (USA)

Semple KT, Cain RB, Schmidt S (1999) Biodegradation of aromatic compounds by microalgae. FEMS Microbiol Lett 170:291-300

Semple KT, Doick KJ, Wick LY, Harms H (2007) Microbial interactions with organic contaminants in soil: Definitions, processes and measurement. Environ Pollut 150:166-176

Singh R, Paul D, Jain RK (2006) Biofilms: implications in bioremediation. Trends Microbiol 14:389-397

Sokolov A, Aranson IS (2009) Reduction of viscosity in suspension of swimming bacteria. Phys Rev Lett 103:148101

Steffen KT, Hofrichter M, Hatakka A (2000) Mineralisation of ¹⁴C-labelled synthetic lignin and ligninolytic enzyme activities of litter-decomposing basidiomycetous fungi. Appl Microbiol Biotechnol 54:819-825

Stringfellow WT, Alvarez-Cohen L (1999) Evaluating the relationship between the sorption of PAHs to bacterial biomass and biodegradation. Wat Res 33:2535-2544

Sundberg K, Widersten M, Seidel A, Mannervik B, Jernström B (1997) Glutathione coconjugation of bay- and fjord-region diol epoxides of polycyclic aromatic hydrocarbons by glutathione transferases M1-1 and P1-1. Chem Res Toxicol 10:1221-1227

Su YH, Yang XY (2009) Interactions between selected PAHs and the microbial community in rhizosphere of a paddy soil. *Sci Total Environ* 407:1027-1034

Tait K, Joint I, Daykin M, Milton DL, Williams P, Cámara M (2005) Disruption of quorum sensing in seawater abolishes attraction of zoospores of the green alga *Ulva* to bacterial biofilms. *Environ Microbiol* 7:229-240

Tait K, Williamson H, Atkinson S, Williams P, Cámara M, Joint I (2009) Turnover of quorum sensing signal molecules modulates cross-kingdom signalling. *Environ Microbiol* 11:1792-1802

Tejeda-Agredano MC, Gallego S, Niqui-Arroyo JL, Vila J, Grifoll M, Ortega-Calvo JJ (2011) Effect of interface fertilization on biodegradation of polycyclic aromatic hydrocarbons present in nonaqueous phase liquids. *Environ Sci Technol* 45:1074-1081

Tejeda-Agredano MC, Gallego S, Vila J, Grifoll M, Ortega-Calvo JJ, Cantos M (2013) Influence of the sunflower rhizosphere on the biodegradation of PAHs in soil. *Soil Biol Biochem* 57:830-840

Tejeda-Agredano MC, Mayer P, Ortega-Calvo JJ (2014) The effect of humic acids on biodegradation of polycyclic aromatic hydrocarbons depends on the exposure regime. *Environ Pollut* 184:435-442

Timmusk S, van West P, Gow NAR, Paul Huffstutler R (2009) *Paenibacillus polymyxa* antagonizes oomycete plant pathogens *Phytophthora palmivora* and *Pythium aphanidermatum*. *J Appl Microbiol* 106:1473-1481

Twigg MS, Tait K, Williams P, Atkinson S, Cámara M (2014) Interference with the germination and growth of *Ulva* zoospores by quorum sensing molecules from *Ulva*-associated epiphytic bacteria. *Environ Microbiol* 16:445-453

Uyttebroek M, Breugelmans P, Janssen M, Wattiau P, Joffe B, Karlson U, Ortega-Calvo JJ, Bastiaens L, Ryngaert A, Hausner M, Springael D (2006) Distribution of the *Mycobacterium* community and polycyclic aromatic hydrocarbons (PAHs) among different size fractions of a long-term PAH-contaminated soil. *Environ Microbiol* 8:836-847

van West P, Appiah AA, Gow NAR (2003) Advances in research on oomycete root pathogens. *Physiol Mol Plant Pathol* 62:99-113

van West P, Morris BM, Reid B, Appiah AA, Osborne MC, Campbell TA, Shepherd SJ, Gow NAR (2002) Oomycete plant pathogens use electric fields to target roots. *Mol Plant Microbe In* 15:790-798

Velasco-Casal P, Wick LY, Ortega-Calvo JJ (2008) Chemoeffectors decrease the deposition of chemotactic bacteria during transport in porous media. *Environ Sci Technol* 42:1131-1137

Vergnoux A, Malleret L, Asia L, Doumenq P, Theraulaz F (2011) Impact of forest fires on PAH level and distribution in soils. *Environ Res* 111:193-198

Verrhiest G, Clement B, Blake G (2001) Single and combined effects of sediment-associated PAHs on three species of freshwater macroinvertebrates. *Ecotoxicol* 10:363-372

Vila J, Grifoll M (2009) Actions of *Mycobacterium* sp. AP1 on the saturated- and aromatic-hydrocarbon fractions of fuel oil in a marine medium. *Appl Environ Microbiol* 75:6232-6239

Volkenborn N, Polerecky L, Wethey DS, Woodin SA (2010) Oscillatory porewater bioadvection in marine sediments induced by hydraulic activities of *Arenicola marina*. *Limnol Oceanogr* 55:1231-1247

Walker CA, van West P (2007) Zoospore development in the oomycetes. *Fungal Biol Rev* 21:10-18

Wang X, Yu X, Bartha R (1990) Effect of bioremediation on polycyclic aromatic hydrocarbon residues in soil. *Environ Sci Technol* 24:1086-1089

Wick LY, Mattle PA, Wattiau P, Harms H (2004) Electrokinetic transport of PAH-degrading bacteria in model aquifers and soil. *Environ Sci Technol* 38:4596-4602

Wick LY, Remer R, Würz B, Reichenbach J, Braun S, Schäfer F, Harms H (2007a) Effect of fungal hyphae on the access of bacteria to phenanthrene in soil. *Environ Sci Technol* 41:500-505

Wick LY, Shi L, Harms H (2007b) Electro-bioremediation of hydrophobic organic soil-contaminants: A review of fundamental interactions. *Electrochim Acta* 52:3441-3448

Witt ME, Dybas MJ, Worden RM, Criddle CS (1999) Motility-enhanced bioremediation of carbon tetrachloride-contaminated aquifer sediments. *Environ Sci Technol* 33:2958-2964

Yazdi S, Ardekani AM (2012) Bacterial aggregation and biofilm formation in a vortical flow. *Biomicrofluidics* 6:044114

Yi H, Crowley DE (2007) Biostimulation of PAH degradation with plants containing high concentrations of linoleic acid. *Environ Sci Technol* 41:4382-4388

About the author

- 2014 This Academic Dissertation is in fulfilment of
Ph. D. in Environmental Biotechnology & Environmental Engineering**
Doctoral Program in Natural Resources and Environment,
Department of Crystallography, Mineralogy and Agricultural Chemistry,
Faculty of Chemistry, University of Seville, **Seville, SPAIN**
Director: Dr. Jose Julio ORTEGA-CALVO
- 2012 Guest Researcher**
Department of Forest Mycology and Pathology,
Faculty of Natural Resources and Agricultural Sciences,
Swedish University of Agricultural Sciences, **Uppsala, SWEDEN**
Advisor: Prof. Dr. Dan Funck JENSEN
- 2011 Guest Researcher**
Department of Biology, Faculty of Science, Chiang Mai University, **Chiang Mai, THAILAND**
Advisor: Prof. Dr. Saisamorn LUMYONG
- 2010 Ph.D. Research Scholar**
Department of Agrochemistry and Soil Conservation,
Institute of Natural Resources and Agrobiolology of Seville (IRNAS-CSIC), **Seville, SPAIN**
Director: Dr. Jose Julio ORTEGA-CALVO
- JAE PREDOC Scholarships Program (2010-2014)**
By the Spanish National Research Council (CSIC) and the European Social Fund (ESF), **SPAIN**
- 2009 Research Assistant**
Department of Biology, Faculty of Science, Chiang Mai University, **Chiang Mai, THAILAND**
Advisor: Prof. Dr. Saisamorn LUMYONG
- Master of Engineering in Applied Chemistry & Biotechnology**
Ritsumeikan University, **Kyoto, JAPAN**
Advisor: Prof. Dr. Motoki KUBO
- 2007 Japanese Government (MEXT) Monbukagakusho Scholarships (2007-2009)**
By the Japanese Ministry of Education, Culture, Sports, Science, and Technology (MEXT),
Tokyo, JAPAN
- Thailand Outstanding Student Award in Microbiology' 2007**
By the Professor Dr. Tab Nelanidhi Foundation, **Bangkok, THAILAND**
- Bachelor of Science (1st Hons.) in Microbiology**
Department of Biology, Faculty of Science, Chiang Mai University, **Chiang Mai, THAILAND**
Advisors: Assist. Prof. Dr. Yingmanee TRAGOOLPUA & Prof. Dr. Saisamorn LUMYONG
- 2003 High School Graduation** at Chonkanyanukoon School, **Chon Buri, THAILAND**
- 2000 Junior High School Graduation** at Phanthong School, **Chon Buri, THAILAND**
- 1997 Primary School Graduation** at Napamanorot School, **Chon Buri, THAILAND**